Title
MECHANICS OF MICROCRACK TOUGHENING IN CERAMICS

Author
Fu, Y.

Publication Date
1983-09-01

Lawrence Berkeley Laboratory
UNIVERSITY OF CALIFORNIA

Materials & Molecular Research Division

MECHANICS OF MICROCRACK TOUGHENING IN CERAMICS

Y. Fu
(Ph.D. Thesis)

September 1983

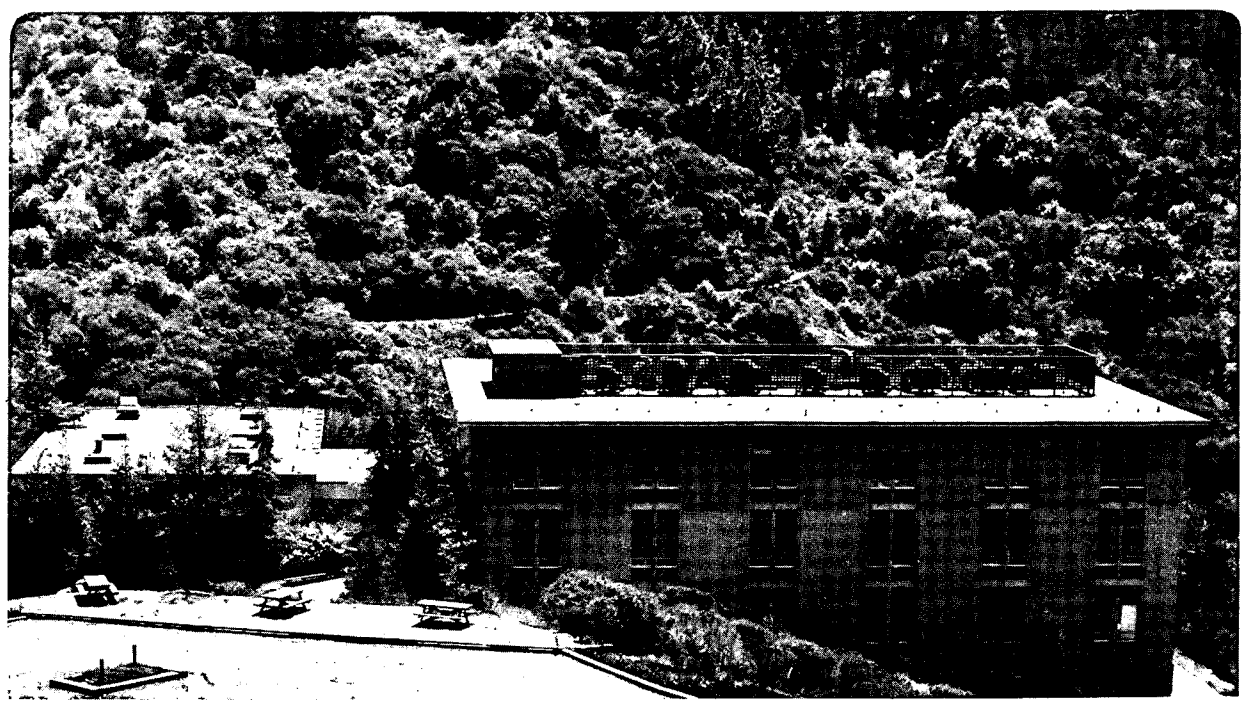

Prepared for the U.S. Department of Energy under Contract DE-AC03-76SF00098

DISCLAIMER

LBL-16839

MECHANICS OF MICROCRACK TOUGHENING IN CERAMICS

Yen Fu
(Ph.D. Thesis)

Lawrence Berkeley Laboratory
University of California
Berkeley, California 94720

September 1983

This work was supported by the Director, Office of Energy Research, Office of Basic Energy Sciences, Materials Science Division of the U.S. Department of Energy under Contract Number DE-AC03-76SF00098 and Office of Naval Research, Contract Number N00014-81-0362.

Mechanics of Microcrack Toughening in Ceramics

Yen Fu

Doctor of Philosophy in Engineering

Materials Science and Mineral Engineering Departmant

Sponsors: Department of Energy
Naval Research Center

Professor Anthony G. Evans
Chairman of Committee

ABSTRACT

The formation of a crack tip process zone consisting of stress induced microcracks has been observed to modify the fracture toughness of a material. In single phase polycrystalline ceramics with microstructural residual stresses due to thermal contraction anisotropy, the grain size dependence of fracture toughness is attributed to the microcrack toughening effect. Associated with the process are several unique features; namely, the microstructural threshold for the onset of microcrack toughening and an R-curve characteristic. A theoretical analysis of the mechanics of microcrack toughening, parallel to that conducted by Budiansky et al for transformation toughening, is conducted, whereupon the basis of these unique features are established.

The mechanics approach of modeling the toughening process is essentially based on the stress/strain characteristics of a microcracking medium. Below the microstructural threshold for spontaneous microcracking, the microcracking medium exhibits a nonlinear strain response to loading above the induced microcracking threshold, by virtue of the elastic moduli decrease. During unloading, a linear strain response resumes and a hysteresis derives from the

irreversible cycle, which cooresponds to a strain energy dissipation mode.

The microstructural configuration for the onset of microcrack toughening originates from the nucleation of discrete microcracks. The calculations of the residual stress field around the primary crack show preferential orientations and sites for discrete microcrack formation. The driving force for such a cracking system is compared with that of primary crack extension to determine the onset configuration. It is found that microcrack zone formation is fully suppressed below a critical grain size, ~40% of the critical grain size for spontaneous microcracking.

The theoretical analysis of the mechanics of microcrack toughening invokes both linear and nonlinear fracture mechanics concepts. The fracture energies at the initiation of crack propagation subject to a frontal microcrack zone and at the steady-state cracking stage subject to an extended microcrack zone are calculated, corresponding to the two exttremities on the R-curve. It is found that the toughening effect derives from the nonlinear characteristics of the microcrack zone; specifically, the R-curve originates from the hysteresis associated with the gradual unloading of the microcrack zone wake. Additionally, characteristics of the grain size dependence of the fracture toughness at different stages of crack evolution vary significantly, due to the existence of the R-curve. The predicted results of the fracture energies correlate quite well with experimental observations.

ACKNOWLEDGMENT

Many people have contributed to the achievement of this work. Among them, my deepest appreciation is for Professor Anthony G. Evans whose continuous guidance and encouragement have supported me throughout the course. Working with him has been the most precious and pleasant experience. Most importantly, his ingenuity and enthusiasm in research set a good example for me.

I would like also to thank Professor Iain Finnie whose excellent instructions in several courses lead me into the exciting new field of fracture mechanics. I am grateful to him, as well as Professor Robert O. Ritchie, for their review and advice on this work.

My gratitude is further extended to my friends and colleages Dr. S. S. Chiang and Dr. C. H. Hsueh for first introducing me into this career and constantly providing fruitful suggestions and discussions.

Finally, I would love to thank my parents and my wife for their love and support. My wife, Jen, in particular, has helped me in preparing this thesis.

This work was supported by the Director, Office of Energy Research, Office of Basic Energy Sciences, Materials Science Division of the U.S. Department of Energy under Contract Number DE-AC03-76SF00098 and Office of Naval Research, Contract Number N00014-81-0362.

TABLE OF CONTENTS

1. Introduction

As science and technology improve, ceramics are emerging as a prospective category of materials for novel applications [1]. Among the superior properties with practical applications of ceramics are hardness (abrasives), corrosion resistance (ceramic coatings), radiation resistance (nuclear fuels), high temperature strength (engine components, refractories), etc.. In particular, many advanced technologies rely on the use of ceramics uniquely endowed with certain optical (wave guides, filters), electrical (semiconductors, ferroelectrics, insulators) or magnetic (ferromagnetics) properties. However, in these situations, brittleness often presents a serious problem both in terms of the limitation in toughness and of the unpredictability in strength [2]. Therefore, it is extremely desirable to understand the failure processes as well as the possible toughening mechanisms. Very often, these two efforts support each other.

In room temperature regime, several categories of mechanisms have been observed to enhance fracture toughness [3]; namely, crack bridging, crack interaction and crack shielding. The unique example of crack bridging is the WC/Co composite [4] in which the ductile Co phase is introduced into the brittle ceramic phase, WC, and some plasticity is restored. The crack interaction includes mechanisms as crack deflection and crack bowing where the crack plane or crack front is distorted by certain microstructural features and thus the crack propagation is hindered [5]. The interest of the present work is in the crack shielding mechanisms; specifically, the microcrack toughening process.

The concept of crack shielding is that, during fracture, a crack tip process zone is induced which counteracts the applied stress intensity and relaxes the crack tip singularity; a process similar to plastic zone formation [6]. Presently, stress induced microcracking at microstructural stress sites [7-12] and mar-

tensitic transformation of partially stabilized ZrO_2 inclusions [13] are the major mechanisms to accomplish this purpose. Specifically, in single phase anisotropic polycrystalline materials, grain size dependence of fracture energy has been observed and attributed to the microcrack toughening effect [14-25]. Hubner et al [16] and Knehans et al [17] have reported observations of an R-curve. Several other observations [14,18,24,25] suggested a microstructural threshold for onset of microcrack toughening. However, the basis of these unique features have not been well established. In particular, experimental measurements of fracture toughness with different tests (e.g. notch beam and cantilever beam) yield conflicting trends of the grain size dependence [14,15, 26,18-25]. Hence, the need is apparent to construct a theoretical analysis to understand the basis of the toughening effect and the special features associated.

The theoretical analysis of the microcrack toughening process presents several complexities. Specifically, the event of microcracking is random by virtue of the orientations of the facets in the crack tip stress field and the crystallographic orientations of adjacet grains dictating the microstructural stresses. Moreover, the microcracks would interact with each other as well as the macrocrack to modify the applied stress field, and the exact fracture criterion in the presence of a microcrack zone is not well established. Hence, many theoretical approaches have been attempted to model the process but often only a few of the complexities could be tackled. More importantly, either one or both of the unique features (the microstructural threshold and the R-curve) were excluded in these studies. For example, the energy approach by Lange [27] and Kreher et al [28] established a Griffith-type energy balance fracture criterion and attributed the toughening effect to an energy dissipation mode of induced microcracking. On the other hand, the analyses of Buresch [29] and Claussen

et al [15,26] used a crack tip radius fracture criterion where toughening originated from a larger crack tip radius, essentially equivalent to the microcrack zone radius. Yet, both approaches excluded the randomness factor, the interaction effect and, more importantly, the associated features*. Hoagland et al [30] conducted a more rigorous analysis using a computer simulation method with a random array of microcracking sites. Additionally, the interaction effect was incorporated and an R-curve was predicted. However, the randomness of the residual stresses was excluded and the fracture criterion** invoked is questionable [31,32], hence, the basis of the R-curve remains doubtful.

Recently, Budiansky et al [33] constructed a successful continuum mechanics description of martensitic transformation toughening. The analysis is essentially based on the stress/strain characteristics of a transformation medium; i.e. nonlinear strain response and hysteresis in unloading. Thereof, the complexity of the interactions is well contained in the nonlinear stress/strain behavior. Based on nonlinear fracture mechanics concepts and energy balance considerations, their analysis revealed that the toughening effect originates from the nonlinear characteristics of the transformation zone and an R-curve derives from the unoading hysteresis of the zone wake. The intent of the present work is to establish a mechanics approach for the microcrack toughening problem paralell to Budiansky et al's analysis. Additionally, the random nature of the grain facet orientation and the residual stresses are incorporated and the physical origin of the microstructural threshold are assessed.

The study is deemed preliminary and the analysis is kept simple so that an overall appreciation of the mechanics approach, a general understanding of the

*Onset of microcrack toughening and resistance(R) curve characteristic.
**that the projection of microcracks ahead of the main crack equals the crack propagation.

toughening process and the justification of the associated unique features can be achieved. Both linear and nonlinear fracture mechanics concepts are invoked in the analysis. The attention is mainly on a model simulating single phase anisotropic polycrystalline systems, although microcrack toughening is also observed in other polyphase systems [10,27]. Future refinements of the analysis are intended and encouraged.

The main body of this work is divided into five sections. Separate introductions reviewing specific, relevent background information and discussion of specific analysis methods, results and implications are provided in each section. Correlations with experimental observations are conducted whenever possible so as to substantiate the analyses and the predicted results. Sections 2 to 4 describe the general features of microcracking, followed by studies on the toughening process in sections 5 and 6. In particular, section 2 analyses the microstructural residual stresses from two approaches: the Eshelby procedure and the first order approximation. The event of spontaneous microcracking at grain facets subject to these residual stresses is examined and a generalized microcracking criterion is established in section 3. Section 4 then conludes the general description with the study of the stress/strain characteristics of a microcracking medium. In section 5, the onset condition of microcrack toughening is determined. Finally, the mechanics of toughening and R-curve behavior are studied in section 6.

REFERENCES

1. W. D. Kingery, H. K. Bowen and D. R. Uhlmann, "Introduction to Ceramics", 2nd. ed., John Wiley and Sons, N.Y. (1976).
2. A. G. Evans, J. Am. Ceram. Soc., 65, 127 (1982).
3. A. G. Evans and T. G. Langdon, "Progress in Materials Science", 19 (1976).
4. C. R. Barrett, W. D. Nix and A. S. Tetelman, "The Principles of Engineering Materials", pp.317, Prentice-Hall Inc., N.J. (1973).
5. K. T. Faber, "Toughening of Ceramic Materials by Crack Deflection Process", Ph.D. Thesis, Univ. of Calif., Berkeley (1982).
6. J. R. Rice, "Fracture", vol.2, pp.191, edited by H. Liebowitz, Academic Press, N.Y. (1968).
7. A. G. Evans, A. H. Heuer and D. L. Porter, "Fracture '77", vol.1, pp.529, edited by D. M. R. Taplin, Univ. of Waterloo Press, Waterloo, Ontario, Canada (1977).
8. R. G. Hoagland, C. W. Marschall, A. R. Rosenfield, G. Hollenberg and R. Ruh, Mater. Sci. Eng., 15, 51 (1974).
9. C. C. Wu, S. W. Freiman, R. W. Rice and J. J. Mecholsky, J. Mater. Sci., 13, 2659 (1978).
10. R. G. Hoagland, G. T. Hahn and A. R. Rosenfield, Rock Mech., 5, 2, 77 (1973).
11. R. G. Hoagland, J. D. Embury and D. J. Green, Scr. Metall., 9, 9, 907 (1975).
12. A. G. Evans, ibid., 10, 1, 93 (1976).
13. A. G. Evans and A. H. Heuer, J. Am. Ceram Soc., 63, 241 (1980).
14. R. W. Rice, S. W. Freiman and P. F. Becher, ibid., 64, 6, 345 (1981).

15. N. Claussen, B. Mussler and M. V. Swain, ibid., 65, 1, C-14 (1982).

16. H. Hubner and J. Jillek, J. Mater. Sci., 12, 117 (1977).

17. R. Krehans and R. Steinbrech, J. Mater. Sci. Letters, 1, 327 (1982).

18. L. A. Simpson, J. Am. Ceram. Soc., 56, 11, 610 (1973).

19. B. J. Dalgleish, P. L. Pratt and J. Sanford, "Science of Ceramics", vol.8, pp.659, edited by P. Popper, The British Ceramic Soc., Stoke-on-Trent, England (1976).

20. P. L. Pratt,"Fracture '77", vol.3, pp.909, edited by D. M. R. Taplin, Univ. of Waterloo Press, Waterloo, Canada (1977).

21. A. G. Evans and G Tappin, Proc. Br. Ceram. Soc., 20, 275 (1972).

22. N. Claussen, P. Pabst and C. P. Lahrmann, ibid., 25, 139 (1975).

23. R. F. Pabst, "Fracture Mechanics of Ceramics", vol.2, pp.556, edited by R. C. Bradt, D. P. H. Hasselman and F. F. Lange, Plenum Press, N.Y. (1974).

24. G. D. Swanson, J. Am. Ceram. Soc., 55, 1, 48 (1972).

25. S. W. Freiman, K. R. McKinney and H. L. Smith, pp.659 in Ref. 27.

26. B. Musller, M. V. Swain and N. Claussen, J. Am. Ceram. Soc., 65, 11, 566 (1982).

27. F. F. Lange, J. Mater. Sci., 17, 225 (1982).

28. W. Kreher and W. Pompe, ibid, 16, 3, 694 (1981).

29. F. E. Buresch, "Fracture Mechanics of Ceramics", vol.4, pp.835, edited by R. C. Bradt, D. P. H. Hasselman and F. F. Lange, Plenum Press, N.Y. (1978). 16, 3, 694 (1981).

30. R. G. Hoagland and J. D. Embury, J. Am. Ceram. Soc., 63, 7, 404 (1980).

31. W. Kreher and W. Pompe, ibid, 65, 7, C-117 (1982).

32. R. G. Hoagland and J. D. Embury, C-118 in Ref.31.

33. B. Budiansky, J. Hutchinson and J. Lambropolous, Int. J. Solids & Structure, 19, 337 (1983).

2. Microstructural Residual Stresses

2.1. Introduction

In a solid body, residual stresses often exist in the absence of an external load. The occurrence of these stresses originates from a mismatch in permanent strain among regions in the body. The range of the stresses created in plastic deformation or welding is often on a macroscopic scale comparable to the size of the body. However, residual stresses localized in a microstructural region, such as a grain, also occur. The thermal contraction (expansion) associated with a temperature change is one major mechanism which can create such microstructural residual stresses. In a heterogeneous system, each homogeneous part, such as a single phase region, possesses a unique thermal expansion property. When the temperature changes, each part undergoes a different thermal contraction (expansion) strain and microstructural stresses can then be created. Microstructural residual stresses can also occur in a single phase material if the thermal expansion property of the single crystal is anisotropic and each grain is randomly oriented [1]. Phase transformation is another common mechanism which can create microstructural residual stresses [1].

Most of the important effects attributed to microstructural residual stresses, especially in brittle materials, are caused by microcracks, initiated by these stresses*. However, microstructural residual stresses can also influence other properties of a material. In metal, it has been observed that these stresses can lead to thermal fatigue [2], irreversible changes in shape and creep [3]. The high dielectric constant of fine grain $BaTiO_3$ has also been explained by residual stresses [4].

The study of microstructural residual stresses in anisotropic polycrystal

*see section 3

due to thermal contraction mismatch was initiated by Boas and Honeycombe [2], and an order-of-magnitude estimate to the stresses was given. Likhachev then established a more rigorous analysis using matrix algebra and variational principles [3]. The basic approach he used was to embed an anisotropic grain into an isotropic rigid medium, having the same thermal expansion coefficient α_0 as the polycrystalline body. The residual stresses $(\sigma_{ij})_0$ developed in the grain after a temperature change ΔT are,

$$(\sigma_{ij})_0 = C_{ijkk}(\alpha_0 - \alpha_k)\Delta T \tag{2.1}$$

where C_{ijkl} is the compliance tensor and α_k the thermal expansion coefficient in the k-axis of the grain. Using the variational principle, he then derived a tensor factor M_{ijkl} such that,

$$\sigma_{ij} = M_{ijkl}(\sigma_{kl})_0 \tag{2.2}$$

represents the resultant stresses in the grain after the relaxation of the medium. It is clear that the Likachev theory is useful for calculating the most prevalent residual stresses in the grains. However, it does not provide an estimate of the grain boundary stress distribution. Subsequently, Buessem and Lange [5] applied the Likhachev approach and gave an approximate analysis for the grain boundary stresses, which are more relevent to the problem of grain boundary microcracking.

The most rigorous approach for analysing microstructural residual stresses was developed by Eshelby [6]. The unique feature of the Eshelby approach is that the analysis is devoid of simplifications. However, Eshelby only conducted calculations for ellipsoidal regions in a homogeneous, isotropic medium. Subsequently, Evans [7] applied the basic three-step (cutting, straining and welding) Eshelby procedure to analyse the residual stresses in anisotropic polycrystals due to thermal contraction mismatch. Both the Eshelby procedure and the Buessem and Lange model will be described and discussed in

the next section.

2.2. Grain Boundary Residual Stress

Two methods are used to analyse the grain boundary microstructural residual stresses in single phase anisotropic polycrystals due to thermal contraction mismatch. The first uses the Eshelby procedure which is tedious but can provide a detailed distribution of the residual stress field. The second method follows Buessem and Lange's model which provides a first order approximation of the residual stresses. Although the result obtained with the second method is less accurate, it is fairly simple and permits further manipulation in latter studies.

2.2.1 Complete Solution with Eshelby Procedure

The Eshelby procedure is an imaginary three-step process of cutting,straining and welding which enables the calculation of miscrostructural residual stresses. In this procedure, the first step is to separate from the body the miscrostructual features, whose permanent strains created the major part of the miscrostructural stress of interest. To calculate the grain boundary residual stress due to thermal contraction anisotropy in a two-dimensional system (Fig. 2.1), this step of cutting corresponds to separating the four grains surrounding the grain boundary of interest, since the strains and elastic responses in these grains would determine most of the grain boundary stress. The remaining matrix is assumed to act as an isotropic medium, having the same thermal and elastic properties as the polycrystalline body. The cavity in the matrix, as well as the four separated grains, would experience some stress-free strain and remain in a stress-free state after the separation.

In the second step of straining, each separated grain is strained to fit back into the cavity in the matrix by applying surface tractions on each grain. There

are many ways to fit these grains back into the cavity; all of them will lead to the same result. So, it is simplest to strain such that homogeneous principal strains ε_k^T

$$\varepsilon_k^T=(\alpha_k-\alpha)\Delta T \quad ; \quad k=1,2 \tag{2.3}$$

are created in each grain where α is the thermal expansion coefficient of the polycrystalline body, α_k is the thermal expansion coefficient of the grain in the k-axis and ΔT is the temperature range where the residual stress accumulates*. If the body is composed of randomly oriented grains, its thermal expansion coefficient α should be,

$$\alpha=(\alpha_1+\alpha_2)/2 \tag{2.4}$$

With the definition,

$$\Delta\alpha\equiv\alpha_1-\alpha=\alpha-\alpha_2 \tag{2.5}$$

the principal strains ε_1^T and ε_2^T can be expressed as

$$\varepsilon_1^T=\Delta\alpha\Delta T \tag{2.6a}$$
$$\varepsilon_2^T=-\Delta\alpha\Delta T \tag{2.6b}$$

The homogeneous stresses σ_{ij}^T in each grain are related to the strains ε_{kl}^T by,

$$\sigma_{ij}^T=C_{ijkl}\,\varepsilon_{kl}^T \tag{2.7}$$

where C_{ijkl} is the compliance tensor of the single crystal grain. For simplicity, it is assumed that the elastic property is isotropic such that

$$\sigma_1^T=E\varepsilon_1^T/(1+\nu)=E\Delta\alpha\Delta T/(1+\nu) \tag{2.8a}$$
$$\sigma_2^T=E\varepsilon_2^T/(1+\nu)=-E\Delta\alpha\Delta T/(1+\nu) \tag{2.8b}$$

where σ_1^T, σ_2^T are the principal stresses, E is the Young's modulus and ν is the Possion ratio. With the coordinate system shown in Fig. 2.1 and ϑ_n taken to be the angle between the maximum contraction in grain n (n=1,.....,4) and the grain boundary, the stresses in each grain are,

$$(\sigma_{xx}^T)_n=E\Delta\alpha\Delta T\cos 2\vartheta_n/(1+\nu)$$
$$(\sigma_{yy}^T)_n=-E\Delta\alpha\Delta T\cos 2\vartheta_n/(1+\nu) \tag{2.9}$$

*$\Delta T = T_f - T_{ambient}$; see section 2.3.

$$(\sigma^T_{xy})_n = E\Delta\alpha\Delta T \sin 2\vartheta_n / (1+\nu)$$

The surface tractions $P_i dS$ on each grain can be obtained from the equilibrium conditions on the surface (see Fig. 2.2),

$$P_i dS = \sigma^T_{ij} dS_j \tag{2.10}$$

During this process, the matrix remains in the stress-free state.

In the last step, the separated grains are welded back to the matrix and the surface tractions $P_i dS$ relaxed. In the calculation, the surface traction relaxation is realized by replacing the surface tractions with body forces of opposite sign. These body forces would create an additional stress field σ^C_{ij} in the whole body. In the present two-dimensional problem of the grain boundary residual stresses, each infinitesimal element of the body force is treated as a point force acting on an infinite plate. The stresses σ^C_{ij} are then calculated by superposition of these point force stress fields.

The resultant residual stresses σ_{ij} of this system, due to thermal contraction anisotropy, are then given by,

$$\sigma_{ij} = \sigma^T_{ij} + \sigma^C_{ij} \tag{2.11}$$

Results of σ_{ij} along grain boundary for several different surrounding microstructures are shown in Fig. 2.3. Details of the results are given in Ref.1.

2.2.2. First Order Approximation

As shown in Fig. 2.3, the residual stresses σ_{ij} vary along the grain boundary. Additionally, the amplitude of the grain boundary stress depends upon the microstructure around the grain boundary, e.g. the crystallographic orientations of the surrounding grains. In latter work, it is necessary to use the expression of the stress field amplitude as a function of the parameters (ϑ_n) describing the facet configuration*. Although the Eshelby procedure can give a

*see section 3

complete solution of the stress field, the complexity of the result make further usage extremely difficult. Therefore, it is desirable to find a suitable simplification which can also serve as the stress field amplitude.

In the complete solution of the stress field as obtained in section 2.2.1, there is one major component $(\sigma_{ij})_M$ which originates directly from the mismatch between the two grains 1 and 2 adjacent to the grain boundary of interest. Specifically, if an average of the residual stresses in grains 1 and 2 (as given in equation (2.9)) is taken, then,

$$(\sigma_{yy})_m = -E\Delta\alpha\Delta T(\cos 2\vartheta_1 + \cos 2\vartheta_2)/2(1+\nu) \tag{2.12a}$$

$$(\sigma_{xy})_m = E\Delta\alpha\Delta T(\sin 2\vartheta_1 + \sin 2\vartheta_2)/2(1+\nu) \tag{2.12b}$$

This component predominates the grain boundary residual stress, except close to the edges where the influence of the body forces on the nearby grain boundaries becomes important. As the expressions of $(\sigma_{ij})_M$ show, the major component is constant along the grain boundary. So, it appears adequate to use this component as a first order approximation of the grain boundary stress field. The physical significance of this first order approximation can also been seen from Buessem and Lange's model of the grain boundary residual stress. In their model (Fig. 2.4), the thermal contraction of the network, formed by the lines connecting the center of gravity of all grains is assumed to conform most closely to the macroscopic contraction of the body. Also, the stresses at the center of a grain boundary are considered to be predominantly determined by the thermal and elastic properties of the two adjacent grains. Finally, the grain boundary is assumed to be perpendicular to the line connecting the centers of the two adjacent grains. Under these assumptions, they gave an expression for the grain boundary stresses σ_{ij}.

$$\sigma_{yy} = \left(\frac{\alpha_1^n + \alpha_2^n}{2} - \alpha\right) E\Delta T/(1+\nu) \tag{2.13a}$$

$$\sigma_{xy} = \left(\frac{\alpha_1^p + \alpha_2^p}{2}\right) E\Delta T/(1+\nu) \tag{2.13b}$$

where α_i^n are the thermal expansion coefficient in grain i in the normal direction to the boundary and α_i^p are the thermal expansion coefficient in grain i in the tangential direction to the boundary. From Fig. 2.1, if ϑ_i is the angle between maximum contraction (α_1) and the grain boundary, then,

$$\alpha_i^n=\alpha_1\sin^2\vartheta_i+\alpha_2\cos^2\vartheta_i \tag{2.14a}$$

$$\alpha_i^p=\alpha_1\cos^2\vartheta_i+\alpha_2\sin^2\vartheta_i \tag{2.14b}$$

Substituting these expressions into equation (2.13), yields the same expressions for $(\sigma_{ij})_M$ given in equation (2.12). Therefore, the expression for the major component $(\sigma_{ij})_M$ derives directly from the mismatch of the adjacent grains. It is a first order approximation to the grain boundary stress field in the sense that the influence of mismatch and constraint on the nearby boundaries is neglected.

2.3. Discussion

There are advantages and disadvantages associated with both the Eshelby procedure and the first order approximation. The selection between the two methods would be determined by the nature of the problem. The Eshelby procedure can, in general, provide complete solutions of the microstructural residual stress fields of complex microstructure, thus, it is possible to use this method to justify other simplified approach, e.g. the first order approximation. Furthermore, the complete solution often contains certain features of the stress field which can not be obtained in simple approaches. For instance, it shows the logarithmic stress concentration effect at the junction of facets which may be important to the microcrack nucleation process. In the latter study of the onset of microcrack toughening, we also used the Eshelby procedure because the onset condition is mainly determined by the detailed microstructural stress distribution near the main crack tip. On the other hand, the first order approximation can provide simple expressions for the residual

stresses and permits further manipulation. It is also easier to extract information about the general behavior of the residual stresses from such simple expressions. For example, from the first order approximation, the most prevalent residual stresses in the grain would be $E\Delta\alpha\Delta T/(1+\nu)$ (tension) in one principal axis and $-E\Delta\alpha\Delta T/(1+\nu)$ (compression) in the other principal axis. Furthermore, the first order approximation can be easily extended to irregular microstructures and three dimensional analysis [10] which are more pertinent to real systems.

In the practical application of the solutions of residual stresses in anisotropic polycrystals, it is necessary to choose appropriate values for the major parameters E, ν, $\Delta\alpha$ and ΔT. Whereas the values of E and ν can be obtained easily, those for $\Delta\alpha$ and ΔT should be considered more carefully. At high temperatures, the thermal contraction mismatch can be relaxed by diffusional creep. Evans and Clarke's [8] analysis showed that there is a freezing temperature T_f below which the relaxation stops and the residual stress increases linearly with $\Delta T=T_f$-T. The freezing temperature is a function of the grain boundary length l and the cooling rate T, since diffusional creep is a time-dependent process. The values of T_f can be either obtained from experimental creep data or theoretical prediction. Furthermore, the linear relation between the thermal strain ε_i and ΔT, i.e. $\varepsilon_i=-\Delta\alpha\Delta T$, is based on the simplification that $\Delta\alpha$ is constant in ΔT. A more accurate solution, if the variation of $\Delta\alpha$ in ΔT is large, for ε_i would be to integrate the differential strains $d\varepsilon_i=\alpha_i dT$ from the freezing temperature. This factor can be incorporated in the present analysis by replacing $\Delta\alpha\Delta T$ with the integrated ε_i.

It should also be noted that the present stress analysis is performed for a system prior to any stress-modifying processes such as microcracking and plastic deformation. In most ceramics, the motion of dislocation, twinning and

hence plastic deformation are limited. The analysis is then applicable. The problem of microcracking in a residual stress field is studied latter.

Experimental measurement of the residual stress is difficult. The indirect methods are to monitor certain features associated with microcracking, such as the elastic strain or the critical grain size, induced by the residual strains. The prediction of the critical grain size from the analysis based on the calculated residual strains is in good agreement with the experimental data*. The direct method of measuring residual strains as performed by Blendall and Coble [9], is to monitor the broadening of spectroscopic lines caused by the average strains in the body. From equation (2.8), the most prevalent residual stresses σ_i in the grains are

$$\sigma_1 = E\Delta\alpha\Delta T/(1+\nu) \tag{2.15a}$$

$$\sigma_2 = -E\Delta\alpha\Delta T/(1+\nu) \tag{2.15b}$$

Taking values of E=420Gpa, ν=0.22, $\Delta\alpha = 3.7\cdot10^{-7}\,^{\circ}C^{-1}$ and $\Delta T = 1500\,^{\circ}C$ which are consistent with Blendall and Coble's experimental conditions, we obtain σ_1=230Mpa and σ_2=-230Mpa, which are also in good agreement with the experimental data (~120Mpa).

For some cases, it is desirable to minimize the residual stresses. The following mehtods are possible. Slow cooling of the body from the fabrication temperature lowers the freezing temperature. Once below T_f, the body can be cooled as rapidly as the thermal shock limit allows. However, because of the exponential temperature dependence of the creep rate, the extent that T can change T_f is limited. Alternatively, a reduced randomness in grain orientations reduces the mismatch strains. For instance, in HCP materials, alignment of grains in the c-axis would reduce the thermal contraction mismatch and hence the residual strains. Finally, introducing a grain boundary glassy phase, with

*see section 3.

good wetting property allows creep relaxation through a solution -precipitation mechanism, that persists to a fairly low temperature.

REFERENCES

1. Y. Fu, "Microfracture in Brittle Solids"; M.S. Thesis, University of California, Berkeley, 1980.
2. W. Boas and R. W. K. Honeycombe, Nature, 153, 495 (1944).
3. V. A. Likhachev, Soviet Physics- Solid State, 3, 6, 1330 (1961).
4. W. R. Buessem, L. E. Cross and A. K. Goswami, J. Am. Ceram. Soc., 49, 1, (1966)
5. W. R. Buessem and F. F. Lange, Interceram, 15, 3, 229 (1966).
6. J. D. Eshelby, Proc. Roy. Soc., A241, 376 (1957).
7. A. G. Evans, Acta Met., 26, 1845 (1978).
8. A. G. Evans and D. R. Clarke, "Thermal Stresses in Severe Enviroments"(1980) D. P. H. Hasselman and R. A. Heller, eds. Plenum Publishing Co., New York.
9. J. E. Blendall and R. L. Coble, J. Am. Ceram. Soc., 65, 3, 174 (1982).
10. R. W. Davidge, Acta Met., vol. 29, 1695 (1981).

FIGURE CAPTIONS

2.1. Schematic showing of residual stresses on grain boundary caused by anisotropic contraction of nearby grains.

2.2. Schematic of surface forces needed to restore the shape of a grain after thermal contraction.

2.3. Plots of normalized residual stresses along grain boundaries vs distance from corner for four different grain facet configurations a-d.

2.4. Idealized picture of a grain with six neighbors in a plane (after Ref. 4).

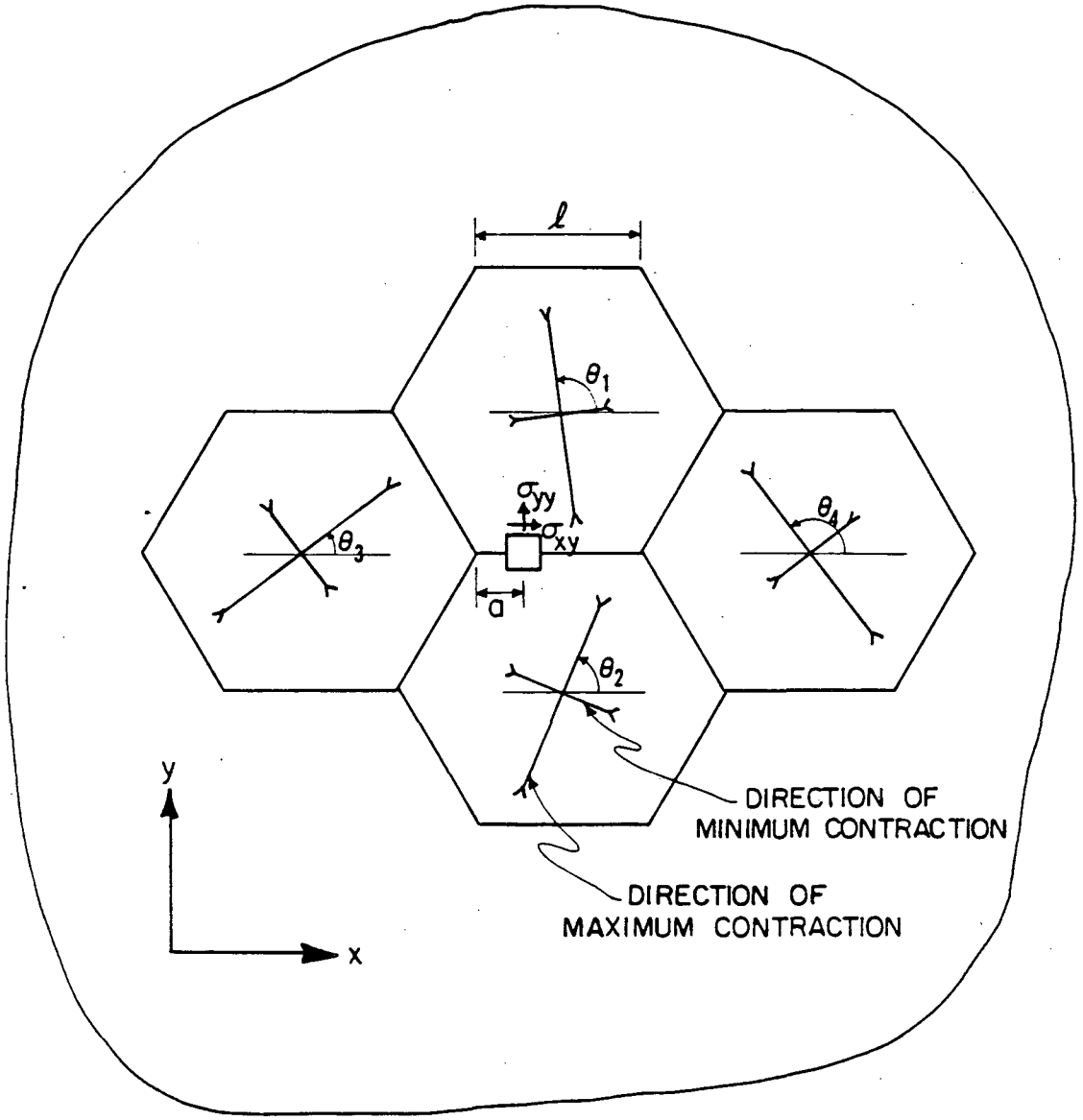

XBL 815-5841

Fig.2.1.

$$P_x = \sigma_\ell^T \sin\theta\cos\theta - \sigma_s^T \cos\theta\sin\theta$$
$$P_y = \sigma_\ell^T \sin\theta\sin\theta + \sigma_s^T \cos\theta\cos\theta$$

$$P_x = -\sigma_\ell^T \sin(\pi/3-\theta)\cos\theta - \sigma_s^T \cos(\pi/3-\theta)\sin\theta$$
$$P_y = -\sigma_\ell^T \sin(\pi/3-\theta)\sin\theta + \sigma_s^T \cos(\pi/3-\theta)\cos\theta$$

$$P_x = \sigma_\ell^T \sin(2/3\pi-\theta)\cos\theta + \sigma_s^T \cos(2/3\pi-\theta)\sin\theta$$
$$P_y = \sigma_\ell^T \sin(2/3\pi-\theta)\sin\theta - \sigma_s^T \cos(2/3\pi-\theta)\cos\theta$$

$$P_x = -\sigma_\ell^T \sin(2/3\pi-\theta)\cos\theta - \sigma_s^T \cos(2/3\pi-\theta)\sin\theta$$
$$P_y = -\sigma_\ell^T \sin(2/3\pi-\theta)\sin\theta + \sigma_s^T \cos(2/3\pi\ \ \theta)\cos\theta$$

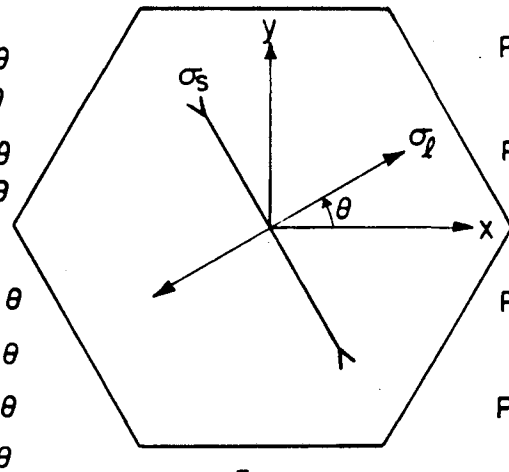

$$P_x = \sigma_\ell^T \sin(\pi/3-\theta)\cos\theta + \sigma_s^T \cos(\pi/3-\theta)\sin\theta$$
$$P_y = \sigma_\ell^T \sin(\pi/3-\theta)\sin\theta - \sigma_s^T \cos(\pi/3-\theta)\cos\theta$$

$$P_x = -\sigma_\ell^T \sin\theta\cos\theta + \sigma_s^T \cos\theta\sin\theta$$
$$P_y = -\sigma_\ell^T \sin\theta\sin\theta - \sigma_s^T \cos\theta\cos\theta$$

$$\sigma_{xx} = \sigma_\ell^T \cos^2\theta + \sigma_s^T \sin^2\theta$$

$$\sigma_{yy} = \sigma_\ell^T \sin^2\theta + \sigma_s^T \cos^2\theta$$

$$\sigma_{xy} = (\sigma_s^T - \sigma_\ell^T)\sin\theta\cos\theta$$

XBL 815-5842

Fig.2.2

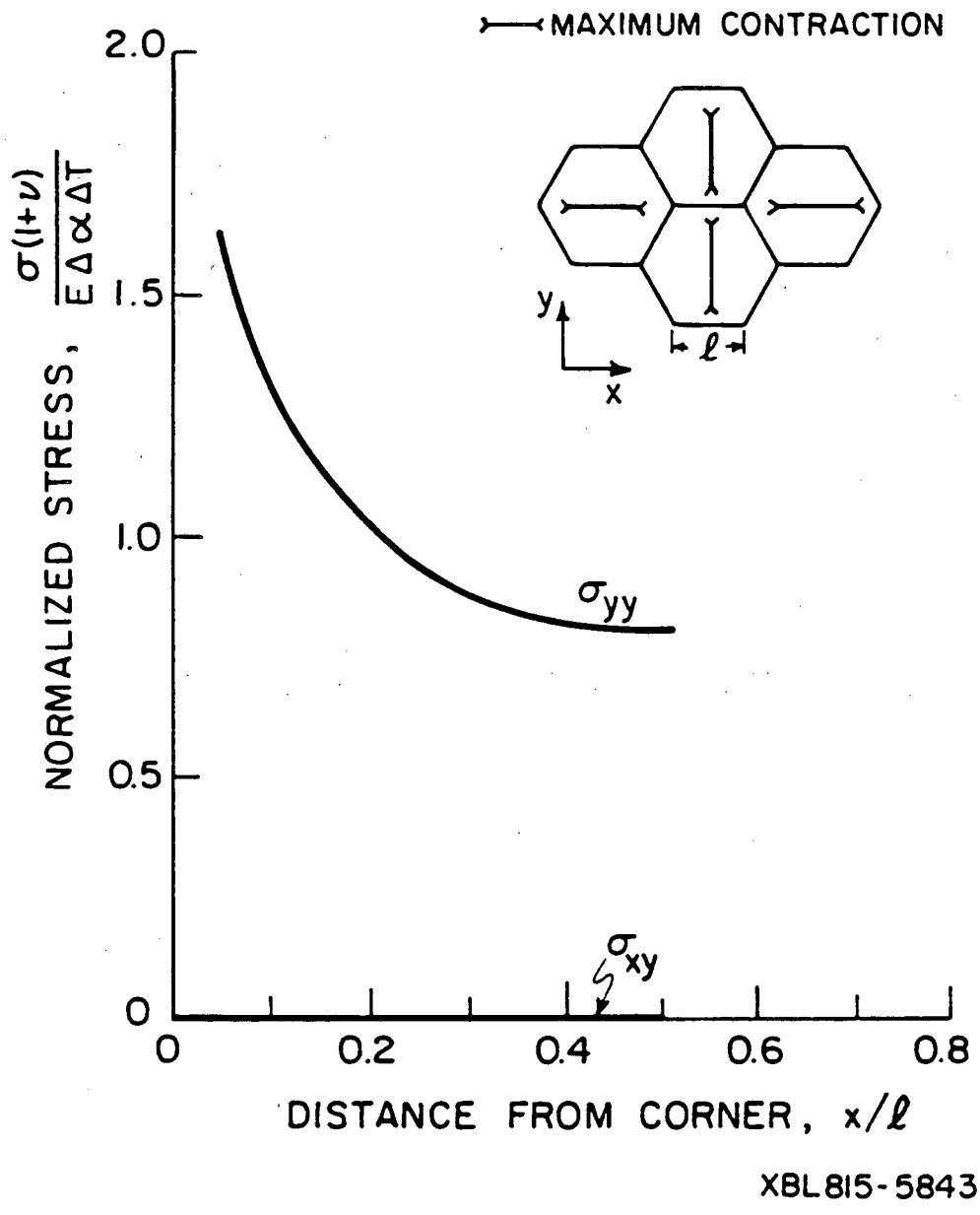
MAXIMUM CONTRACTION
2.0
1.5
1.0
0.5
0
NORMALIZED STRESS, $\frac{\sigma(1+\nu)}{E\Delta\alpha\Delta T}$
σ_{yy}
σ_{xy}
y
x
ℓ
0
0.2
0.4
0.6
0.8
DISTANCE FROM CORNER, x/ℓ
XBL815-5843

Fig.2.3a

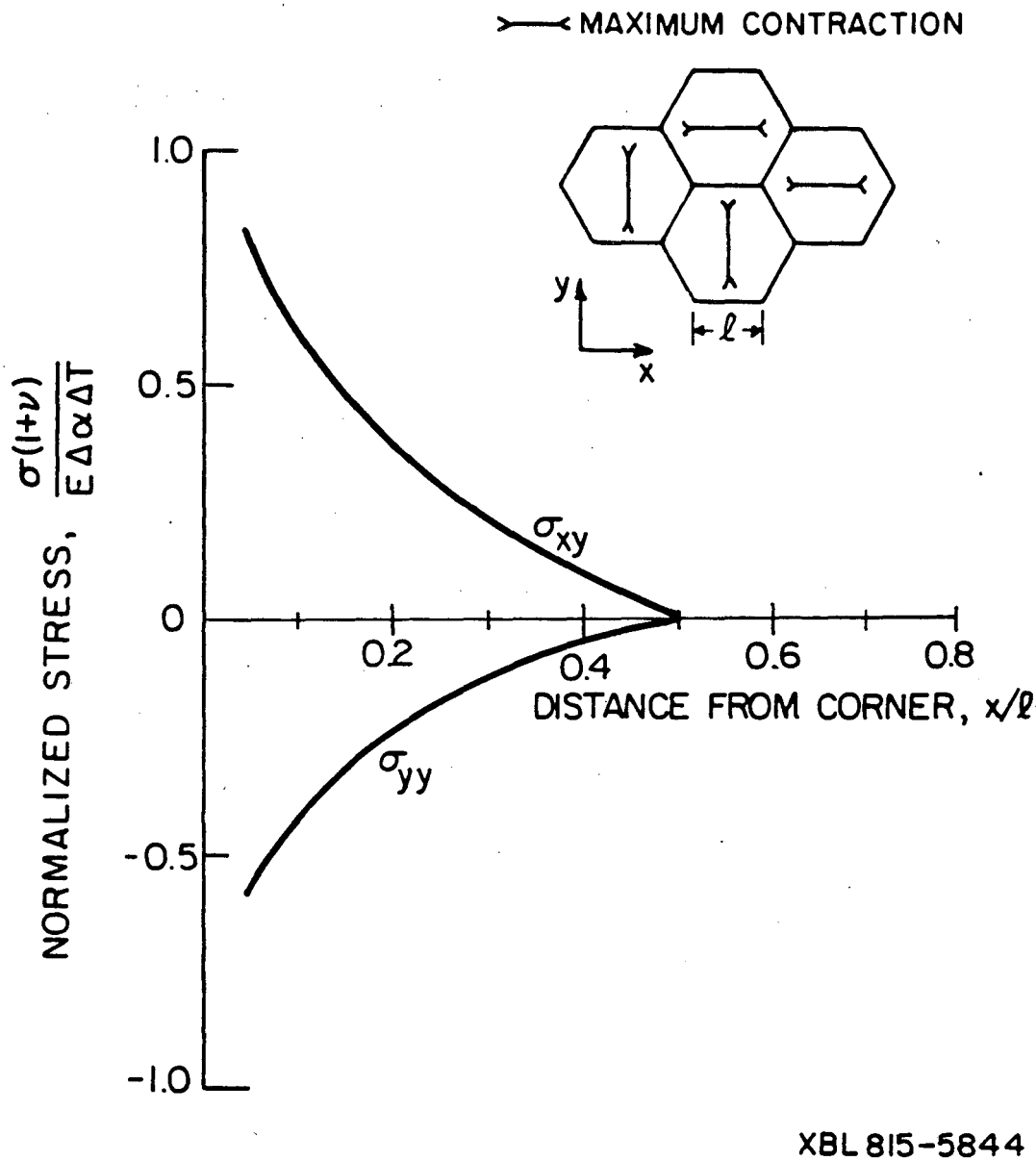
MAXIMUM CONTRACTION
y
x
ℓ
1.0
0.5
0
-0.5
-1.0
0.2
0.4
0.6
0.8
σ_{xy}
σ_{yy}
NORMALIZED STRESS, $\frac{\sigma(1+\nu)}{E\Delta\alpha\Delta T}$
DISTANCE FROM CORNER, x/ℓ
XBL 815-5844

Fig. 2.3b

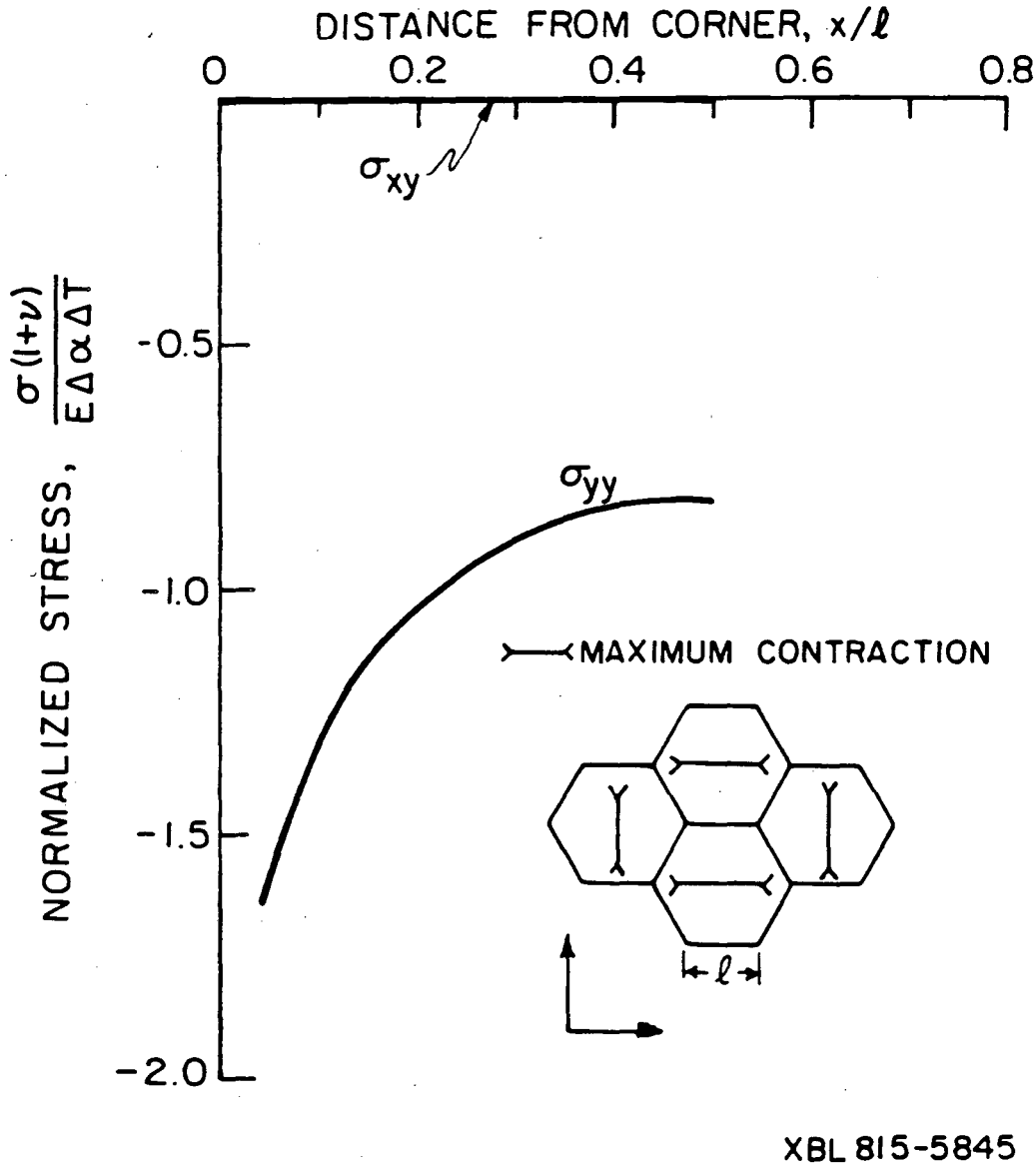
DISTANCE FROM CORNER, x/ℓ
0
0.2
0.4
0.6
0.8
σxy
NORMALIZED STRESS, σ(1+ν)/EΔαΔT
-0.5
-1.0
-1.5
-2.0
σyy
MAXIMUM CONTRACTION
ℓ
XBL 815-5845

Fig.2.3c

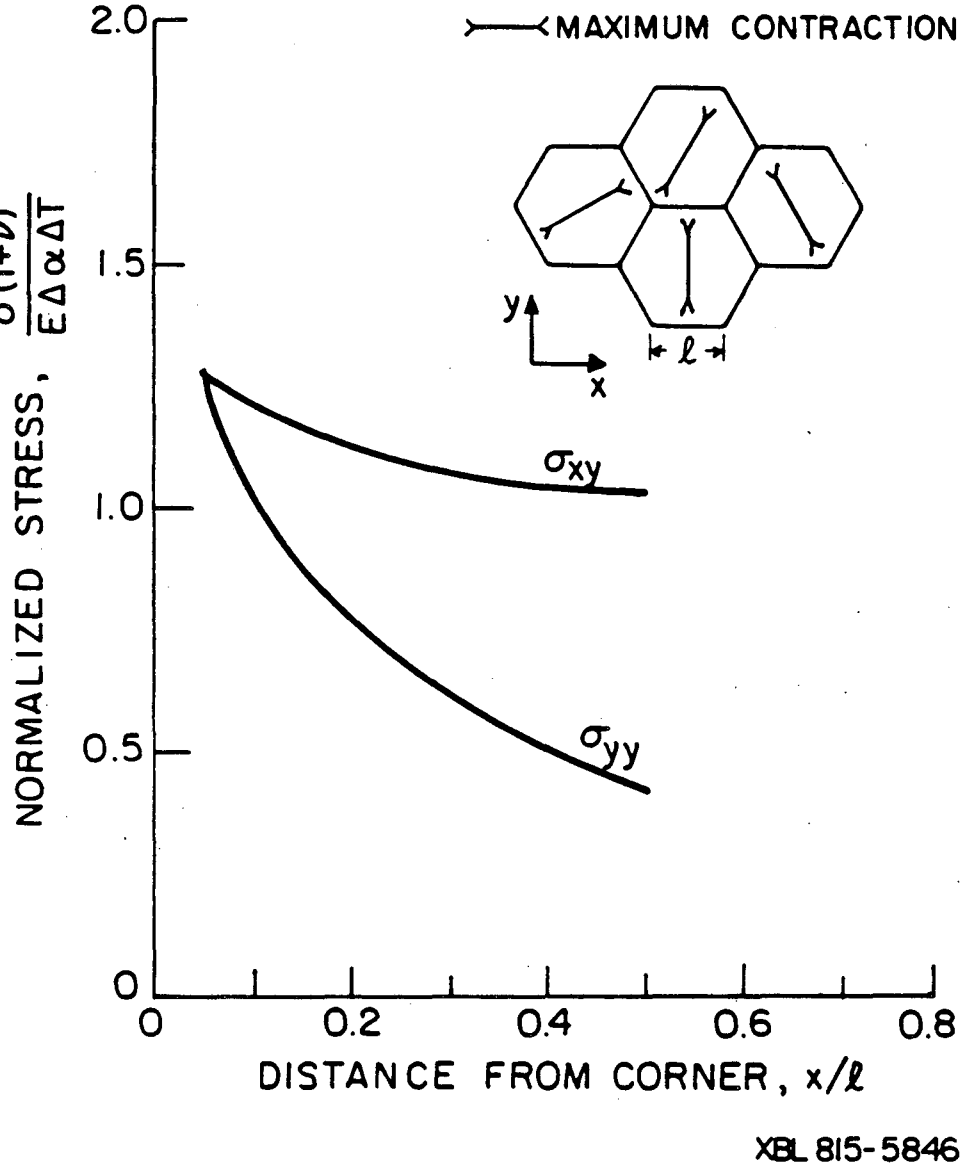
MAXIMUM CONTRACTION
2.0
1.5
1.0
0.5
0
NORMALIZED STRESS, $\frac{\sigma(1+\nu)}{E\Delta\alpha\Delta T}$
σ_{xy}
σ_{yy}
y
x
ℓ
0
0.2
0.4
0.6
0.8
DISTANCE FROM CORNER, x/ℓ
XBL 815-5846

Fig.2.3d

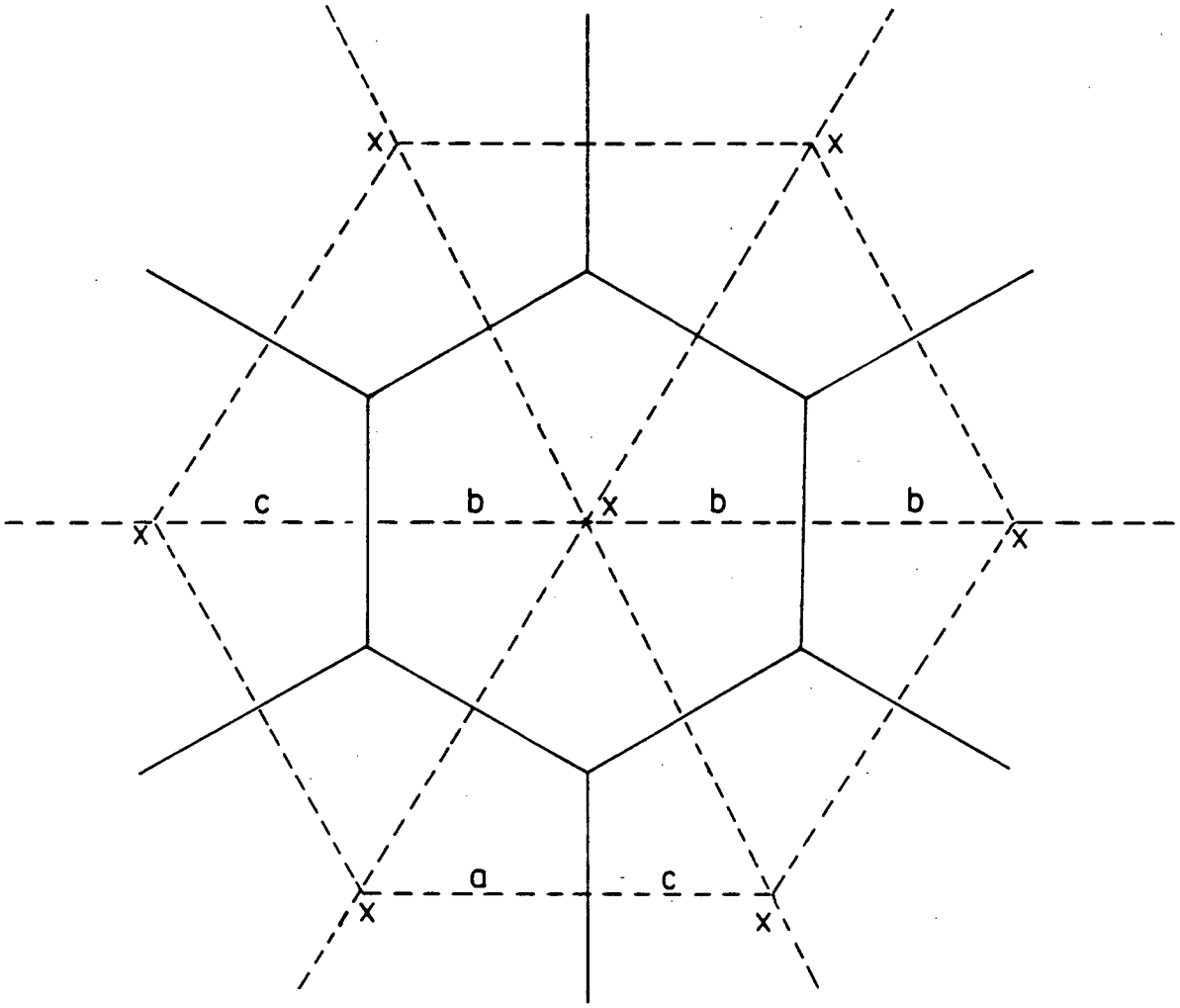

XBL839-6348

Fig.2.4

3. Spontaneous Microfracture in Microstructural Residual Stresses

3.1. Introduction

Brittle materials with microstructural residual stresses are often susceptible to microcracking, which can either occur spontaneously [1-5], upon cooling, or be induced by an external stress [6,7]. Microcracks are characteristically stable and isolated, because of the alternating tensile and compressive nature of the microstructural stress. Furthermore, the microcracks often form on interfaces where the fracture resistance is low and stress concentrations are present.

Spontaneous microcracking is generally observed to initiate at a threshold [3,5,8], such as a critical temperature change, ΔT_c, or a critical grain size, R_c^s. At ΔT_c or R_c^s, spontaneous microcracking initiates at grain boundary facets subject to the maximum residual tension [1,9,10].

A fracture mechanics analysis of micracracking reveals an essential dependence on microstructural dimensions [1,10] (even though the magnitude of the residual stresses is generally independent of these dimensions*). In particular, dimensional considerations dictate that microcracks initiate when the grain facets exceed a critical size l_c^s. Many experimental observations confirm the existence of a critical grain size [1,8,11,12,16]. Hence, a generalized microcracking criterion may be established by incorporating l_c^s as a parameter which is generally known or easily measurable.

Above the threshold, the microcrack propensity is expected to increase [10] as more grain boundary facets satisfy the microcracking criterion of microcracking. Many physical properties have been observed to be modified by microcracks under such situations. These include the thermal diffusivity [5],

*see section 2

dielectric constant, and acoustic transparency. Additionally, there is significant reduction in the elastic moduli (e.g. E,ν,μ) [3,4,8]. The intent of this section is to use the generalized microcracking criterion of microcracking to deduce both the microcracks density N and the elastic moduli. Correlations with experimental data are also presented.

3.2. Initiation of Spontaneous Microfracture

In single phase anisotropic polycrystalline materials, microcracks generally form at grain boundary facets, where the fracture resistance is lower than the grain interior. Moreover, stress concentration effects or nonuniformities near facet junctions assist the nucleation and formation of a facet microcrack. The stress concentration effect near a facet junction (Fig. 3.1) is characterized by a logarithmic singularity [1,13]

$$\sigma_{yy}(x)=[1+F_1(\vartheta_1,\vartheta_2,\vartheta_3,\varphi,....)ln(l/x)](\sigma_{yy})_M \tag{3.1a}$$

$$\sigma_{xy}(x)=[1+F_2(\vartheta_1,\vartheta_2,\vartheta_3,\varphi,....)ln(l/x)](\sigma_{xy})_M \tag{3.1b}$$

where $(\sigma_{ij})_M$ is the magnitude of the residual stress given in equation (2.12),

$$(\sigma_{yy})_M=-\sigma_R(\cos 2\vartheta_1+\cos 2\vartheta_2)/2 \tag{3.2a}$$

$$(\sigma_{xy})_M=\sigma_R(\sin 2\vartheta_1+\sin 2\vartheta_2)/2 \tag{3.2b}$$

where

$$\sigma_R\equiv E\Delta\alpha\Delta T/(1+\nu)$$

l is the grain facet size and F_1, F_2 are shape functions of the configuration parameters, ϑ_1, ϑ_2, ϑ_3, φ,....., of the grain facet (e.g. crystallographic orientations of adjacent grains, angles between facets, etc.). Due to the logarithmic term, $ln(l/x)$, the stresses are singular ($\sigma\to\infty$), near the junction ($x\to 0$). Therefore, facet microcracks are most likely nucleated at the junction and then propagate along the facet*. This argument may be substantiated by the experimental observation that the initiation of spontaneous microfracture is dependent upon

*In many ceramics, the crack blunting mode is suppressed because of limited plastic deformation.

the grain boundary facet size l. Such a behavior does not derive from the magnitude of the residual stress (σ_R), which does not depend on the grain facet size. However, the scale effect contained in the logarithmic singularity $ln(l/x)$ allows the stress to be sustained over a larger area of grain facet as l increases, thereby enhancing the tendency for microcrack nucleation. Consequently, larger grain facets subject to the same residual stress amplitude are more susceptible to microfracture.

The details of the nucleation subject to the logarithmic singularity are not well known. One postulate [1] is that the stress singularity acts in conjunction with an extrinsic inhomogeneity (e.g. voids, second phase inclusions) at the junction, forming a fracture system with the inhomogeneity as a microcrack precursor. Then, when l is large enough, the precursor becomes unstable and nucleates into a microcrack. After nucleation, the microcrack propagates along the grain facet, motivated by the net residual stresses, $(\sigma_{yy})_M$ and $(\sigma_{xy})_M$. Finally, the microcrack is arrested at the neighboring junctions, because the adjacent boundary facets are generally subject to residual compression and are inclined to the microcrack plane, causing the crack driving force to be greatly reduced (Fig. 3.2.).

Several analyses [1,9,13,14], based on different specific approaches, yield essentially the same relation for the critical facet size l_c^s for the initiation of spontaneous microfracture, on facets under maximum tension σ_R,

$$l_c^s=\beta(K_c^{g.b}/\sigma_R)^2 \tag{3.3}$$

where $K_c^{g.b}$ is the grain boundary facet toughness. Only the value of the coefficient β varies in different analysis. For example, the analysis by Evans [1] invoked the superposition method in fracture mechanics to calculate the stress intensity factors K of precursors of varying sizes c contained in the stress singularity (equation (3.1) with $\vartheta_1=\vartheta_2=\pi/2$). As seen from the result [13] in

Fig. 3.3, where K is normalized by $\sqrt{l}$, precursors on larger boundary facet are subject to higher K and hence, are more susceptible to microcrack nucleation. Furthermore, there is a maximum of K at $c/l \sim 0.2$. If l is small enough such that K_{max} is smaller than the grain boundary toughness $K_c^{g.b.}$, the microcrack nucleation should be fully suppressed. Following this criterion, the critical facet size l_c^s coincides with $\beta \sim 3.1$.

Alternatively, if it is assumed that $c/l = 0.1$ [14] is the most prevalent size of the precursor, a similar result is obtained with $\beta \sim 3.7$.

3.3. Microcrack Density versus Grain Size

In a material with uniform grains of facet size $l > l_c^s$, a proportion of grain facets subject to residual stresses lower than the maximum (due to misorientations of adjacent grains) may satisty the microcracking criterion. Generally, both normal σ and shear stress τ are present on the grain boundary facet, such that the microcrack is simultaneously under opening K_I and shearing K_{II} stress intensities.

In a uniform biaxial stress field with σ and τ resolved on the crack plane, K_I and K_{II} for a crack of diameter 2a are [18]

$$K_I = (2/\sqrt{\pi})\sigma\sqrt{a} \tag{3.4a}$$

$$K_{II} = (2/\sqrt{\pi})\tau\sqrt{a} \tag{3.4b}$$

and the generalized fracture criterion [15] is

$$K_{eff} \equiv (K_I^2 + K_{II}^2)^{1/2} \geq K_c \tag{3.5a}$$

$$K_I \geq 0 \tag{3.5b}$$

where K_c is the fracture toughness. It follows that an effective fracture stress σ_{eff} may be defined as

$$\sigma_{eff} = (\sigma^2 + \tau^2)^{1/2} \tag{3.6}$$

The effective residual stress σ_{eff} on a grain facet under biaxial stresses can be calculated from equation (3.2) as

$$\sigma_{eff} = \frac{1}{\sqrt{2}}[1+\cos(2\vartheta_1 - 2\vartheta_2)]^{1/2}\sigma_R \tag{3.7}$$

Generalizing the microcracking criterion, equation (3.3), by replacing σ_R with σ_{eff}, the condition for microcracking becomes,

$$l \geq \beta(K_c^{g.b} / \sigma_{eff})^2 \tag{3.8a}$$

and

$$(\sigma_{yy})_M \geq 0 \tag{3.8b}$$

The ambiguity regarding β and the difficulty of measuring $K_c^{g.b}$ may be removed by combining equations (3.3) and (3.8) to yield the generalized criterion for microcracking,

$$(l / l_c^s) \geq (\sigma_R / \sigma_{eff})^2 \tag{3.9a}$$

and

$$(\sigma_{yy})_M \geq 0 \tag{3.9b}$$

Inserting σ_{eff} in equation (3.7) and $(\sigma_{yy})_M$ from equation (3.2) into equation (3.9), it follows that a grain facet of size l would microcrack if the configuration parameters ϑ_1, ϑ_2 satisfy the relation

$$\frac{2}{1+\cos(2\vartheta_1 - 2\vartheta_2)} \leq \frac{l}{l_c^s} \tag{3.10a}$$

and

$$\cos 2\vartheta_1 + \cos 2\vartheta_2 \leq 0 \tag{3.10b}$$

In a material with a large number of randomly oriented grains of uniform facet size l, all possible facet configurations $(\vartheta_1, \vartheta_2)$ would occupy a square domain (Fig. 3.4), and each area element in the domain is equally populated. Points in the domain satisfying equation (3.10) correspond to microcracked grain boundary facets. Hence, the fraction f of spontaneously microcracked facets in the material is given by,

$$f = A_1 / A \tag{3.11}$$

where A_1 is the area encircled by equation (3.10) and A is the total area (π^2). Integrating the area encircled by equation (3.10), f is obtained as

$$f = \frac{1}{\pi}\cos^{-1}\sqrt{l_c^s / l} \tag{3.12}$$

The numerical result for f versus l/l_c^s is shown in Fig. 3.5. If there are g grain facets per unit volume in the medium, the microcrack density N is

$$N = gf = \frac{g}{\pi}\cos^{-1}\sqrt{l_c^s / l} \tag{3.13}$$

Furthermore, it is noted that in a uniform grained material, l is proportional to the grain size, R, hence

$$N = \frac{g}{\pi}\cos^{-1}\sqrt{R_c^s / R} \tag{3.14}$$

Additionally, since the residual stresses accumulated as $\sigma_R = E\Delta\alpha\Delta T/(1+\nu)$, a decrease in temperature below the critical temperature range ΔT_c, would result in a microcrack density

$$N = \frac{g}{\pi}\cos^{-1}(\Delta T_c / \Delta T) \tag{3.15}$$

3.4. Elastic Moduli of a Microcracked Body

Many physical properties of anisotropic materials have been reported to be modified by spontaneous microcracking. Most significant are the reduction of the elastic properties, Young's modulus E, Poisson ratio ν, and shear modulus μ. In particular, the Young's moduli of several noncubic ceramics have been observed [3,4,8] to decrease monotonically as the average grain size R became larger than the critical grain size R_c^s for spontaneous microcracking.

A theoretical analysis of the elastic properties of a microcracked body has been performed by Budiansky and O'Connell [17]. The elastic constants $\bar{E}$, $\bar{\nu}$ and $\bar{\mu}$ of a solid medium with a random distribution of circular microcracks of size 2a were calculated as,

$$\begin{aligned} \frac{\bar{E}}{E} &= 1 - \frac{16}{45}\frac{(1-\bar{\nu}^2)(10-3\bar{\nu})}{(2-\bar{\nu})}\varepsilon \\ \frac{\bar{\mu}}{\mu} &= 1 - \frac{32}{5}\frac{(1-\bar{\nu})(5-\bar{\nu})}{(2-\bar{\nu})}\varepsilon \\ \varepsilon \equiv N a^3 &= \frac{45}{16}\frac{(\nu-\bar{\nu})(2-\bar{\nu})}{(1-\bar{\nu}^2)[10\nu-\bar{\nu}(1+3\nu)]} \end{aligned} \tag{3.16}$$

It is noted that the microcrack density would saturate at $N=9/16a^3$ where the elastic constants →0.

From the trends in elastic constants plotted in Fig. 3.6, it is apparent that the variation in $\bar{E}/E$ or $\bar{\nu}/\nu$ with Na^3 may be approximated as

$$\frac{\bar{E}}{E}=\frac{\bar{\nu}}{\nu}=1-\frac{16}{9}Na^3 \tag{3.17}$$

As grain facet microcracks resemble circular cracks, equation (3.17) is expected to be valid for a microcracked material with $l=2a$. Hence, since the microcrack density N increases as the grain facet size l becomes larger (equation (3.14)), the elastic constants $\bar{E}$ and $\bar{\nu}$ would decrease accordingly as

$$\frac{\bar{E}}{E}=\frac{\bar{\nu}}{\nu}=1-\frac{2gl^3}{9\pi}\cos^{-1}\sqrt{R_c^s/R} \tag{3.18}$$

In the next section, comparison of this result with experimental data is presented and discussed.

3.5. Discussion

The primary contribution of the present section to the main topic, i.e. the mechanics of microcrack toughening, is the establishment of the generalized microcacking criterion. In later sections, it is incoporated into the analysis of induced microcracking subject to applied stress, which is an essential feature in the microcrack toughening process. The unique feature of the criterion is that it yields conditions of microcracking of facets subject to general stresses characterized by amplitudes σ_{eff}. In particular, it has been demonstrated that, based on the criterion, the microcrack density N above the spontaneous microcracking threshold ($R>R_c^s$) can be derived. Furthermore, the associated effect of moduli decrease has been quantified.

The prediction capability of the criterion can be justified from the comparison of the predicted Young's modulus (equation (3.18)) with experimental

observations such as the data for $MgTi_2O_5$ (R_c^s~1.5μm,E~36·10^{-6}psi), and Fe_2TiO_5 (R_c^s~1.5μm,E~25·10^{-6}psi) reported by Cleveland and Bradt [8], as shown in Fig. 3.7. It is seen that, the predicton fits the data points fairly well, if the grain facet density is taken to be $g^*=10/l^3$. This value is slightly higher than the facet density g expected in a microstructure of uniform equiaxed grains where each grain with 12 facets occupies volume ~$2l^3$, each facet is shared by two grains and

$$g \approx \frac{12}{2 \cdot 2l^3} = 3/l^3 \tag{3.19}$$

The deviation is believed to originate from the following simplifications. The analysis of the facet stress is based on a two-dimensional model. Additionally, the interactions among microcracks (e.g. modification of residual stresses, coalescence of adjacent microcracks, etc.) are excluded both in the calculation of microcrack density and in the the Budiansky and O'Connell's analysis where the relations for the elastic moduli of a microcracked medium are adopted. The good correlation between the prediction and experiments reflects that the qualitative results obtained conform to real systems. Quantitatively, in a practical three-dimensional system where interaction effects are present, the "effective" microcrack density $N^*=g^*f$ causing the elastic moduli decrease may be 2-3 times as large as N obtained in the present section. This conclusion will be further substantiated in later sections.

In many situations, spontaneous microcracking deteriorates special properties desired for certain applications. Sometimes, severe spontaneous microcracking causes disintegration of a sintered material [2]. In these cases, suppression of microcracking may be achieved by either reducing the magnitude of the residual stresses as proposed in section 2.3, or to control the microstructural dimension (e.g. grain size) below the threshold for spontaneous microcracking. In a few situations where controlled microcracking is desired,

such as to enhance thermal insulation, the relation for the microcrack density in equation (3.14) or (3.15), as dependent on various parameters, may be adopted for microstructural design purposes.

REFERENCES

1. A. G. Evans, Acta Met., 26, 1845 (1978).
2. Y. Matsuo and H. Sasaki, J. Am. Ceram. Soc., 49, 229 (1966).
3. J. A. Kuszyk and R. C. Bradt, J. Am. Ceram. Soc., 56, 420 (1973).
4. S. L. Dole, O. Hunter, Jr., F. W. Calderwood and D. J. Bray, J. Am. Ceram. Soc., 61, 486 (1978).
5. H. J. Siebeneck, D. P. H. Hasselman, J. J. Clevelend and R. C. Bradt, J. Am. Ceram. Soc., 59, 241 (1976).
6. F. A. McClintock and H. J. Mayson, ASME Applied Mechanics Conf. (June 1976).
7. R. C. Pohanka, R. W. Rice and B. E. Walker, Jr., J. Am. Ceram. Soc., 59, 71 (1976).
8. J. J. Clevelend and R. C. Bradt, J. Am. Ceram. Soc., 61, 478 (1978).
9. R. W. Davidge and G. Tappin, J. Mater. Sci., 3, 297 (1968).
10. R. W. Davidge, Acta Met., 29, 1696 (1981).
11. Y. M. Ito, M. Rosenblatt, L. Y. Cheng, F. F. Lange and A. G. Evans, Int. J. Fract., 17, 5, 483 (1981).
12. R. W. Rice and R. C. Pohanka, J. Am. Ceram. Soc., 62, 559 (1979).
13. Y. Fu, "Microfracture in Brittle Solids", M. S. Thesis, University of California, Berkeley (1980).
14. F. J. P. Clarke, Acta Met., 12, 139 (1964).
15. K. T. Faber, "Toughening of Ceramic Materials by Crack Deflection Process", Ph.D. Thesis, Univ. of Calif., Berkeley (1982).

16. E. D. Case, J. R. Smith and O. Hunter, J. Mater. Sci., 15, 149 (1980).

17. B. Budiansky and R. J. O'Connell, Int. J. Solid Struct., 12, 81 (1976).

18. G. C. Sih, "Handbook of Stress Intensity Factors", Lehigh Univ. Press (1973).

FIGURE CAPTIONS

3.1. Schematic of residual stresses on grain boundary facet arising from thermal contraction anisotropy of adjacent grains.

3.2. Schematic illustrating the alternating tension/compression nature of the grain facet residual stresses.

3.3. Plot of normalized stress intensity factor vs crack size for a grain facet microcrack precursor.

3.4. Schematic of grain facet configuration domain and configuration points corresponding to spontaneously microcracked facets.

3.5. Fraction of spontaneously microcracked facets vs normalized grain facet size in single phase anisotropic polycrystals above microcracking threshold.

3.6. Effective moduli of randomly distributed circular cracks (after Ref. 17).

3.7. Comparison of calculated Young's modulus decrease above microcracking threshold with experimental data of $MgTi_2O_5$, and Fe_2TiO_5 (after Ref.8).

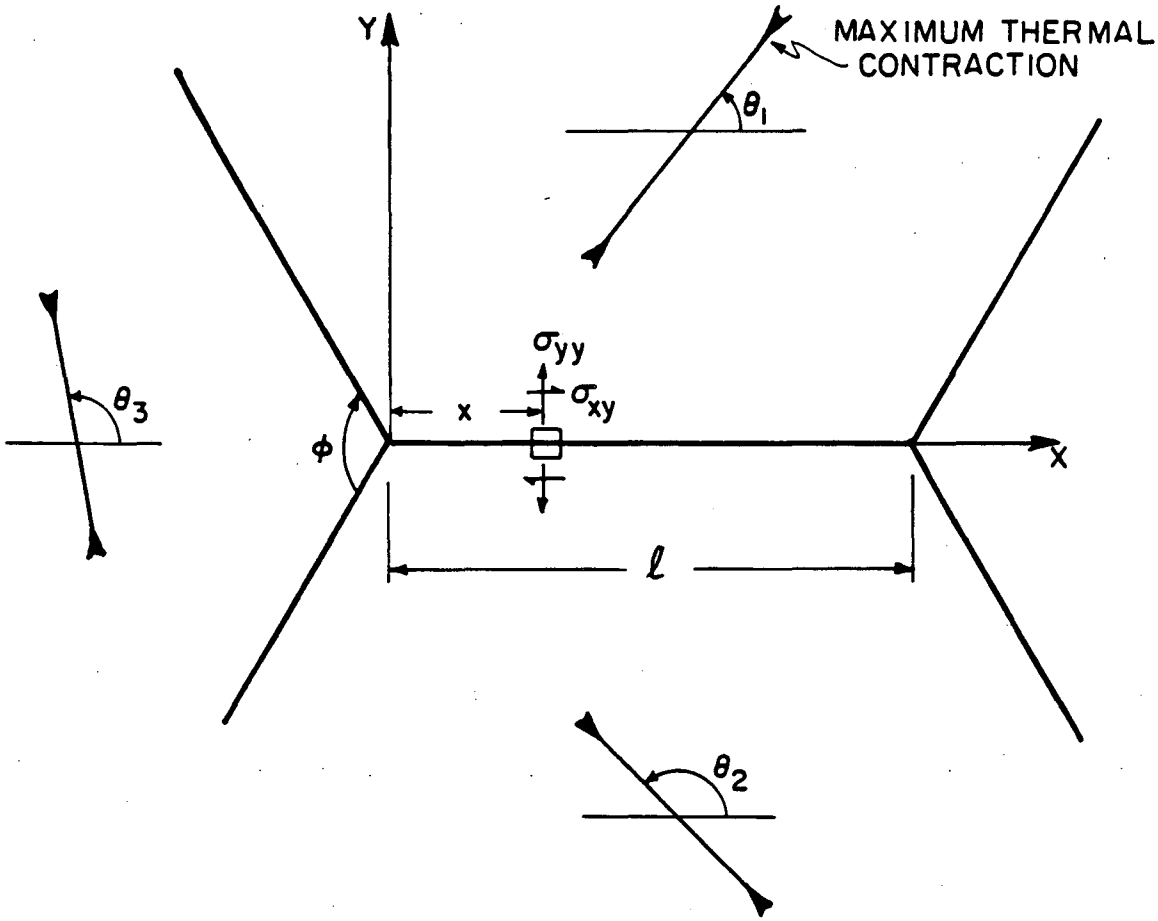
Y
MAXIMUM THERMAL
CONTRACTION
θ_1
θ_3
σ_{yy}
σ_{xy}
x
ϕ
X
ℓ
θ_2
XBL 839-6351

Fig.3.1

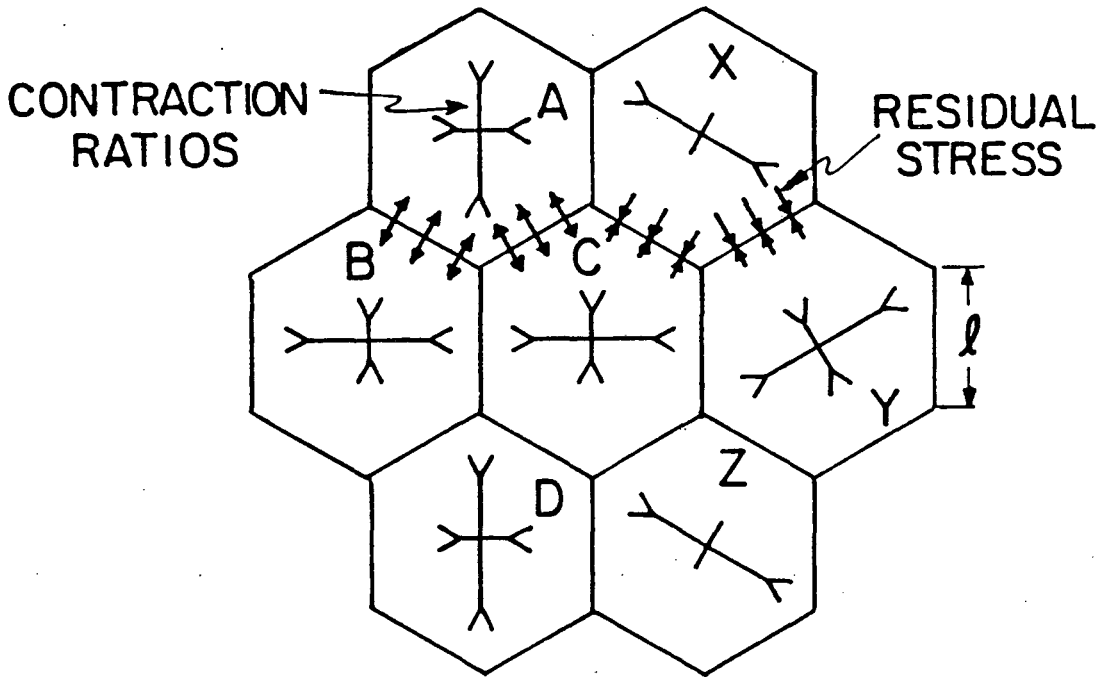

XBL 839-11653

Fig.3.2

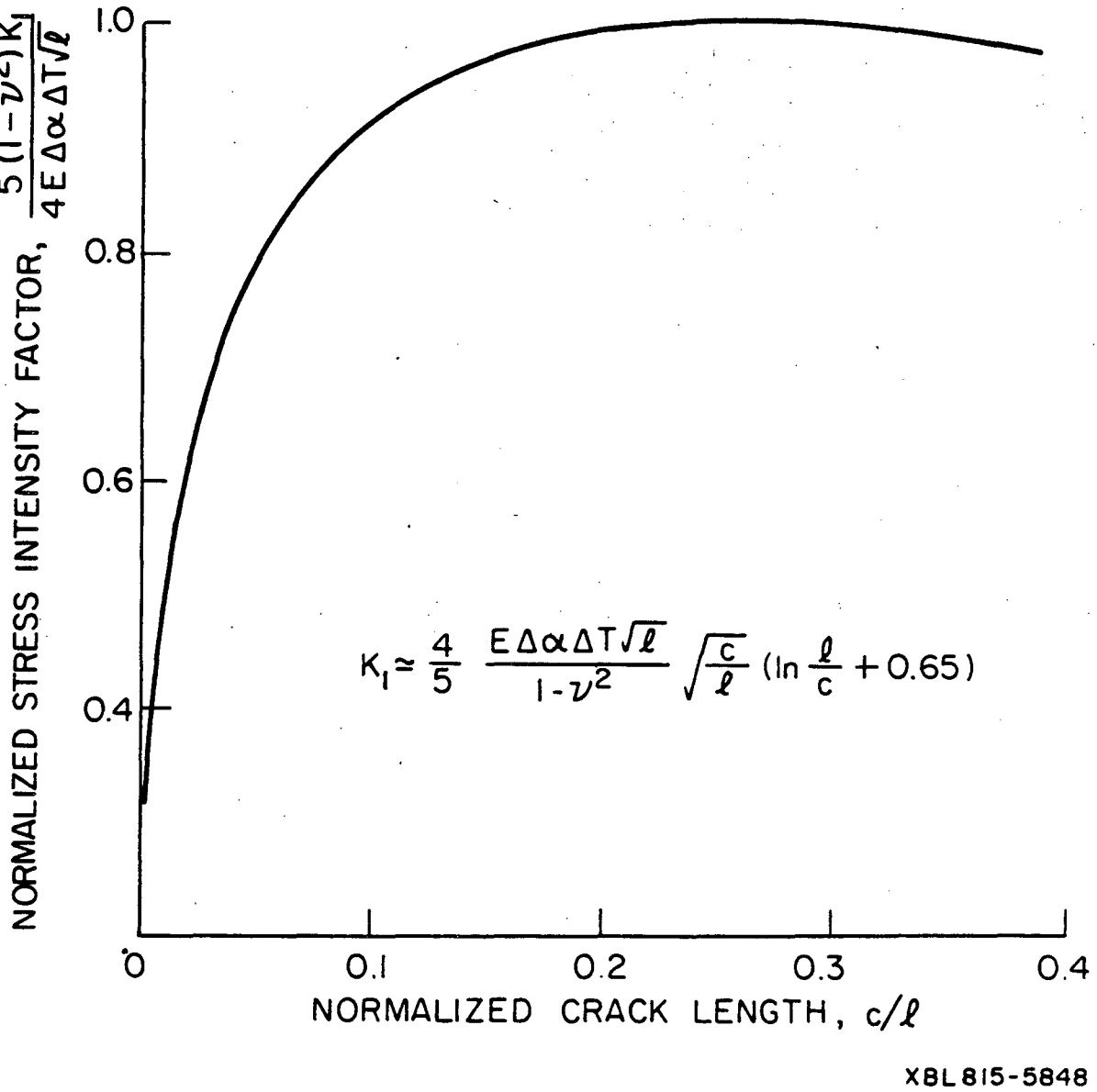
NORMALIZED STRESS INTENSITY FACTOR, $\frac{5(1-\nu^2)K_I}{4E\Delta\alpha\Delta T\sqrt{\ell}}$
1.0
0.8
0.6
0.4
0
0.1
0.2
0.3
0.4
NORMALIZED CRACK LENGTH, c/ℓ
$K_I \simeq \frac{4}{5} \frac{E\Delta\alpha\Delta T\sqrt{\ell}}{1-\nu^2} \sqrt{\frac{c}{\ell}} \left(\ln \frac{\ell}{c} + 0.65\right)$
XBL815-5848

Fig. 3.3

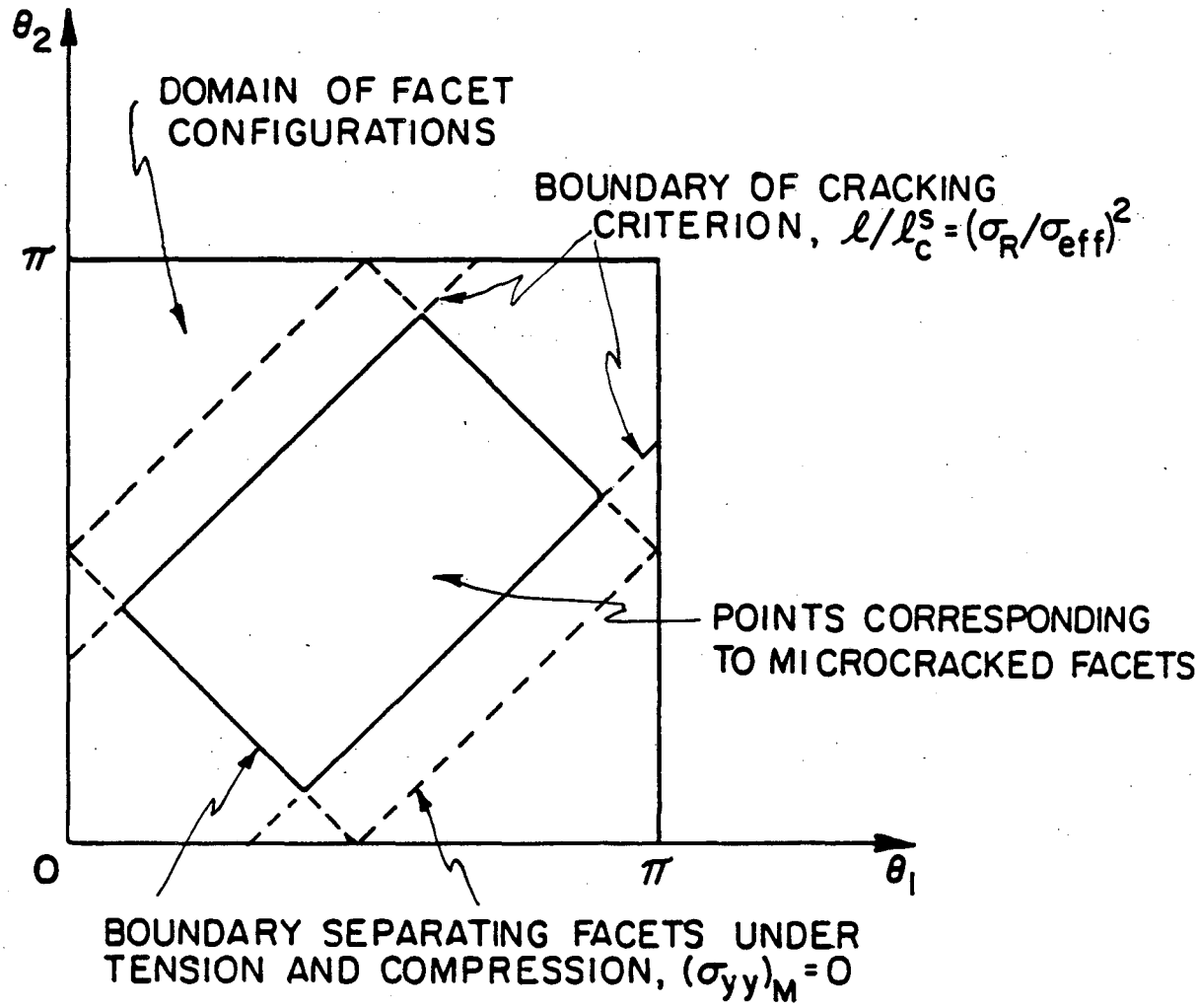

XBL 839-6352

Fig. 3.4

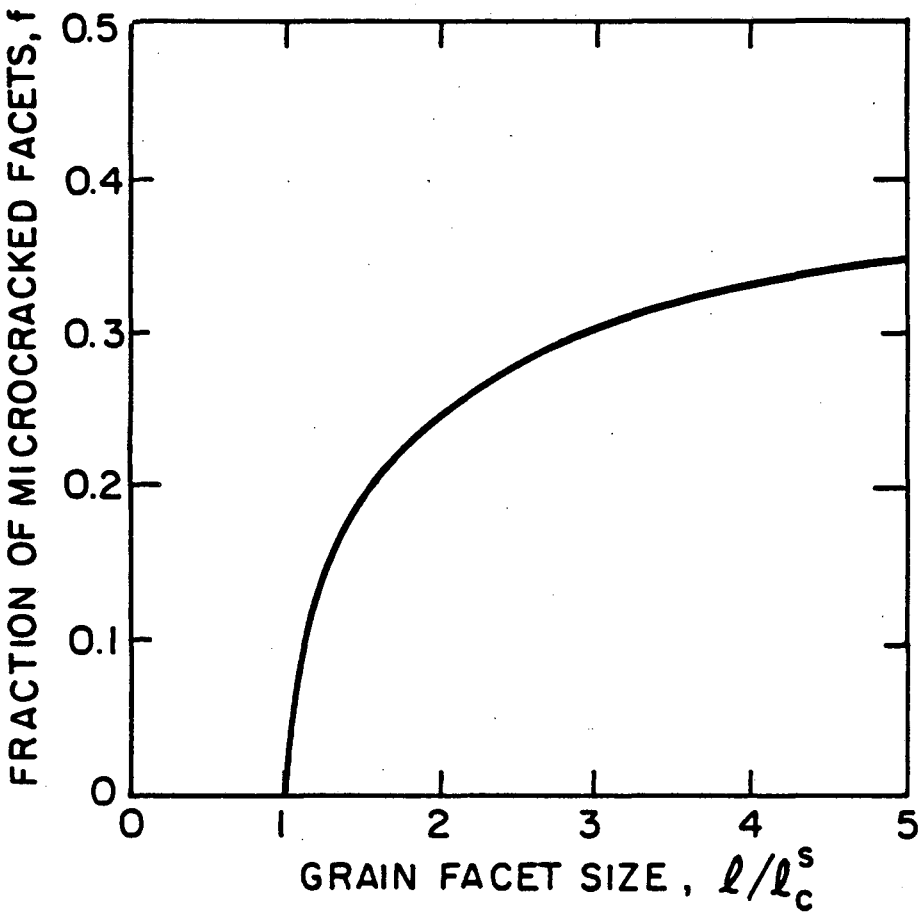

XBL 839-6353

Fig.3.5

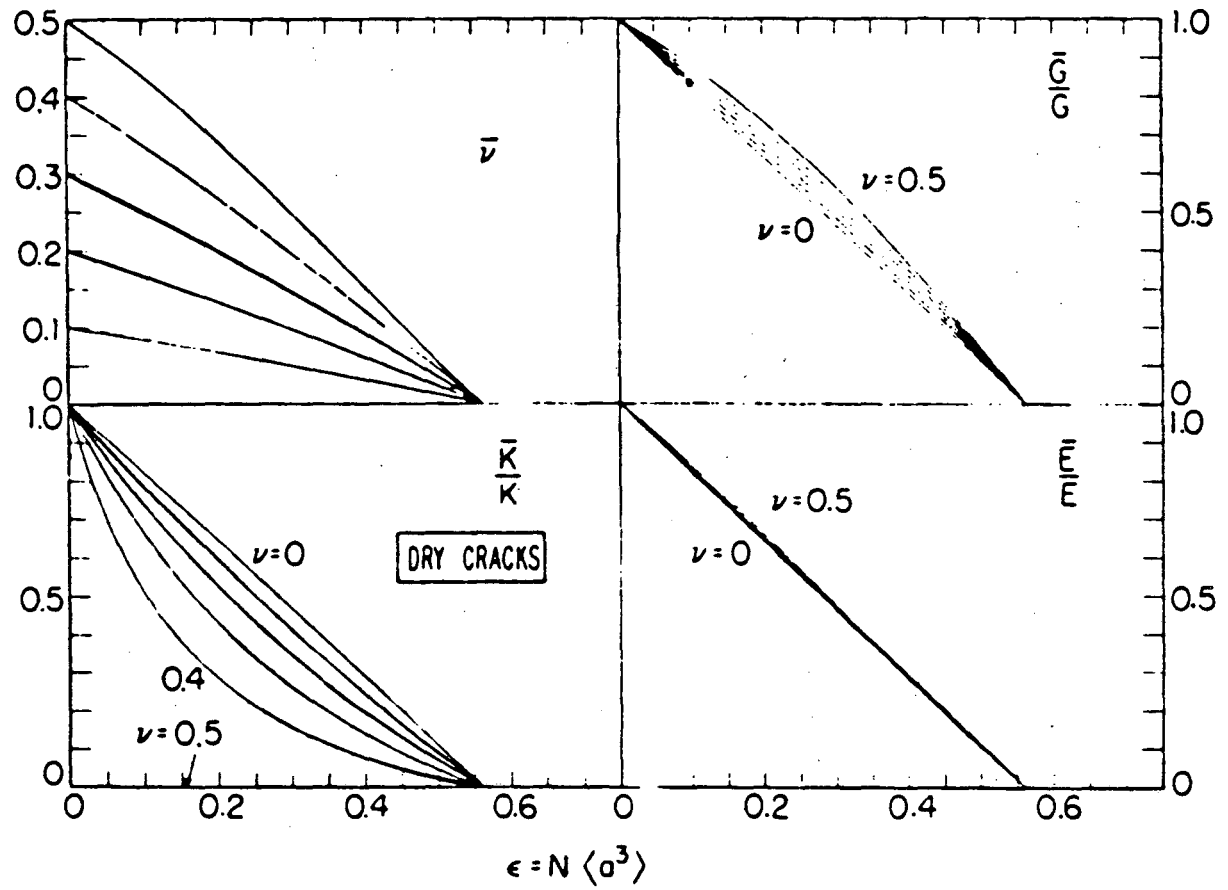

XBL 839-11652

Fig. 3.6

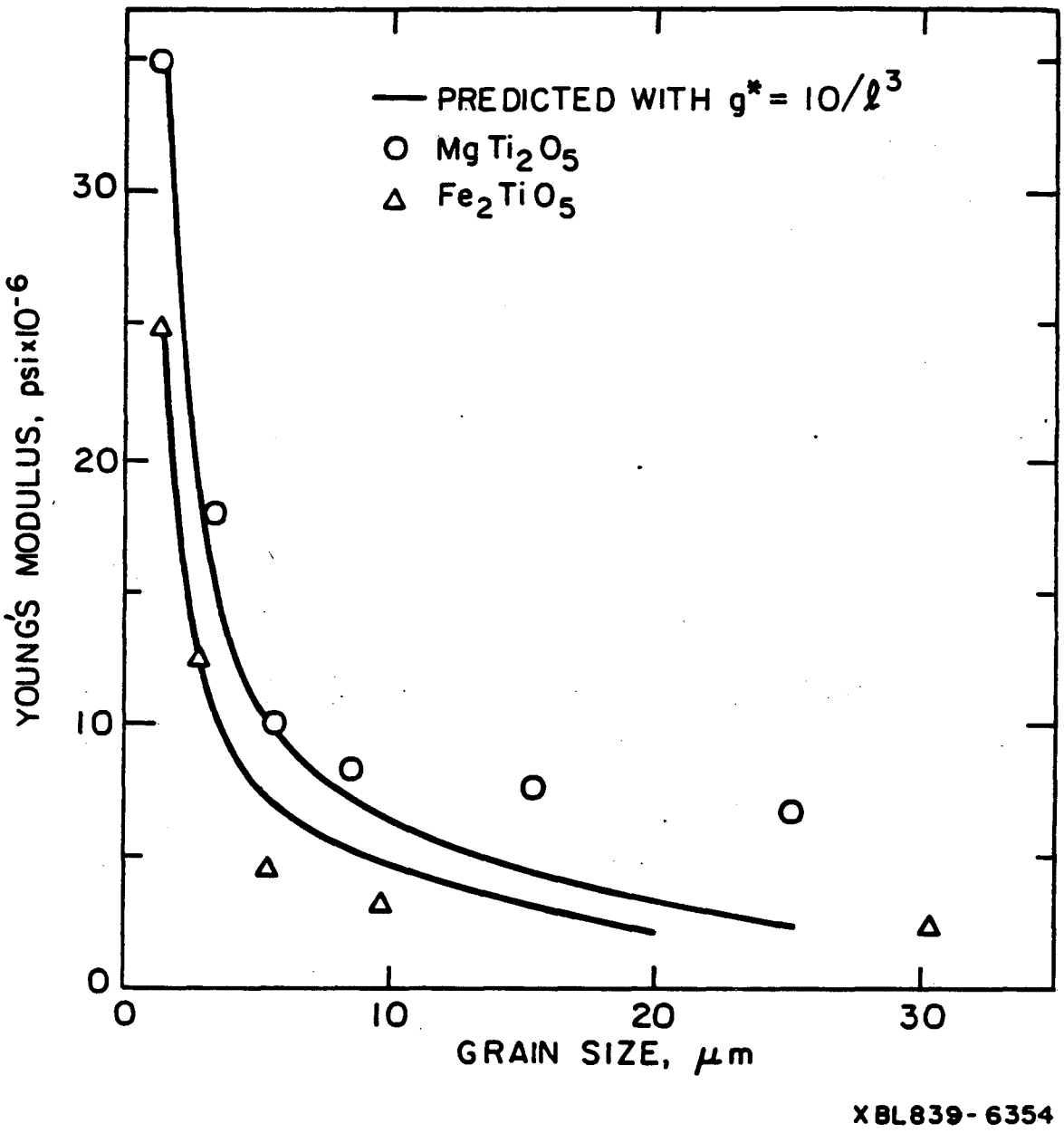
PREDICTED WITH $g^* = 10/\ell^3$
O $MgTi_2O_5$
Δ Fe_2TiO_5
YOUNG'S MODULUS, psi×10⁻⁶
0
10
20
30
GRAIN SIZE, μm
XBL839-6354

Fig.3.7

4. Induced Microcracking : Effects of Applied Stress

4.1. Introduction

Microfracture of grain boundary facets under residual stresses, which did not occur spontaneously, may be induced by applied stresses [1,2,3,4]. The applied stresses are linearly superposed on the residual stresses. Thus, the effective stress may be large enough to satisfy the generalized microcracking criterion.

Initiation of induced microcracking is expected to occur at a certain threshold load on grain facets under maximum effective stress. As load is increased further, microcrack propensity increases and the effective elastic moduli decrease accordingly, similar to the elastic behavior in spontaneous microcracking. By virtue of the moduli decrease [5], the strain increases, resulting in a nonlinear stress/strain behavior. During unloading, the microcrack density remains unchanged, the stress/strain trajectory deviates from the original in the loading stage and a hysteresis in the loading cycle is present (corresponding to dissipation of strain energy from the loading system). Such nonlinearity resembles that observed in work-hardening materials and martensitic composites [6,7].

The purpose of the present section is to study how microcracks are induced by applied stresses and the accompanying effects, namely, the nonlinear stress/strain laws, the energy dissipation, etc. The information obtained may then be incorporated into the analysis of the main topic of this study, mechanics of microcrack toughening, as will be done in section 6.

4.2. Microcracking under Applied Stress

4.2.1. Effective Stress on Grain Boundary Facet

Suppose that a uniform biaxial stress field (with principal stresses $\sigma_1 > \sigma_2$, $k=\sigma_2/\sigma_1$ and $\sigma_1>0$) is incrementally applied on a single phase anisotropic polycrystalline material with uniform microstructure (equiaxed grains with uniform grain size R and uniform facet size l). If R is smaller than R_c^s, spontaneous microcracking is fully suppressed. As the external stress field is applied, microcracking is expected to be induced when the resultant stresses on the grain facet are large enough.

Pertaining to the two-dimensional model of the grain boundary facet residual stresses established in section 2, an extended model incorporating the applied stresses may be constructed as shown in Fig. 4.1. The configuration of the grain facet is now characterized by three parameters, i.e. crystallographic orientations of the adjacent grains ϑ_1, ϑ_2 and the angle α between the facet and σ_1. With $0\le\vartheta_1, \vartheta_2, \alpha\le\pi$, all possible combinations of ϑ_1, ϑ_2 and α would occupy a cubic domain in a three-dimensional space (Fig. 4.2). Each volume element in the cubic domain is equally populated with facets of the corresponding configuration ϑ_1, ϑ_2 and α.

The applied stresses resolved on the grain facet would be

$$\sigma_a = \sigma_1 \sin^2\alpha + \sigma_2 \cos^2\alpha \tag{4.1a}$$

$$\tau_a = (\sigma_1 - \sigma_2) \sin\alpha \cos\alpha \tag{4.1b}$$

By superposition theory, these stresses are linearly superimposed upon the residual stresses (equation (2.12)) to obtain the total stresses on the grain facet as

$$\sigma_t = -\sigma_R \frac{\cos 2\vartheta_1 + \cos 2\vartheta_2}{2} + \sigma_1 \sin^2\alpha + \sigma_2 \cos^2\alpha \tag{4.2a}$$

$$\tau_t = \sigma_R \frac{\sin 2\vartheta_1 + \sin 2\vartheta_2}{2} + (\sigma_1 - \sigma_2) \sin\alpha \cos\alpha \tag{4.2b}$$

and the effective stress σ_{eff} defined in equation (3.6) would be

$$\sigma_{eff}=[H(\vartheta_1,\vartheta_2,\alpha,s_1,s_2)]^{\frac{1}{2}}\sigma_R \tag{4.3}$$

where

$$\begin{aligned}H(\vartheta_1,\vartheta_2,\alpha,s_1,s_2)\equiv 1/2+1/2\cos(2\vartheta_1-2\vartheta_2)+s_1^2\sin^2\alpha+s_2^2\cos^2\alpha\\ -\cos 2\vartheta_1\cos 2\vartheta_2(s_1\sin^2\alpha+s_2\cos^2\alpha)\\ +(\sin 2\vartheta_1+\sin 2\vartheta_2)(s_1-s_2)\sin\alpha\cos\alpha\end{aligned}$$

4.2.2. Threshold Load for Initiation of Induced Microfracture

As the external load is gradually applied, initiation of microcracking is expected to occur at grain boundary facets under maximum effective stress σ_{eff}, i.e. $\vartheta_1=\vartheta_2=\alpha=\pi/2$, as,

$$\sigma_{eff}=\sigma_R+\sigma_1 \tag{4.4}$$

Thus, invoking the generalized microcracking criterion established in section 3.3, induced microcracking would initiate when σ_1 reaches the critical value σ_a^c which satisfies the criterion,

$$l/l_c^s=(\frac{\sigma_R}{\sigma_{eff}})^2=(\frac{\sigma_R}{\sigma_a^c+\sigma_R})^2 \tag{4.5}$$

or equivalently,

$$\sigma_a^c=(\sqrt{l_c^s/l}-1)\sigma_R \tag{4.6}$$

4.2.3. Microcrack Density versus Applied Stress

As the applied stress σ_1 exceeds σ_a^c, more grain facets would satisfy the microcracking criterion and the microcrack density N is expected to increase. Following the general relation of the effective stress, eqation (4.3), microcracking would occur at facets where the configuration parameters ϑ_1, ϑ_2 and α satify the relations,

$$H(\vartheta_1,\vartheta_2,\alpha,s_1,s_2)\geq l_c^s/l \tag{4.7a}$$

and

$$\frac{\sigma_1}{\sigma_R}=-\frac{\cos 2\vartheta_1+\cos 2\vartheta_2}{2}+s_1\sin^2\alpha+s_2\cos^2\alpha>0 \tag{4.7b}$$

and the corresponding points in the configuration domain (Fig. 4.2) would

occupy a certain volume V which is a function of s_1, s_2 and l/l_c^s. The fraction f of facets microcracked is then

$$f = V/\pi^3 \tag{4.8}$$

and, from equation (3.13), the microcrack density N is

$$N = gf = gV/\pi^3 \tag{4.9}$$

Numerical integration methods* are used to calculate f and results are shown in Fig. 4.3. Several unique features are observed. The fraction f of microcracked facets is approximately proportional to $(\sigma_1 - \sigma_a^c)$ as

$$f = m(\sigma_1 - \sigma_a^c)/\sigma_R \tag{4.10}$$

The coefficient m is dependent upon the ratio $k = \sigma_2/\sigma_1$, varying from m= 1/2 at k=1 to m=1/4 at k=0, and insensitive to the normalized grain facet size l/l_c^s. Meanwhile, the microcrack density N may be obtained as

$$N = gm(\sigma_1 - \sigma_a^c)/\sigma_R \tag{4.11}$$

4.3. Stress/Strain Laws for Microcracking Material

4.3.1. Nonlinear Strain Response

Microcracks induced by an external load will interact with the external load, as reflected in the nonlinear strain response of the microcracked medium. One significant effect deriving from such interactions is the microcrack toughening mechanism.

As shown in section 3.3, microcracking reduces the elastic moduli, E and ν, (equation (3.17)). Microcracks induced by the applied stresses σ_1 and σ_2 are expected to react similarly, such that the elastic moduli can be obtained by combining equations (4.11) and (3.17) as

$$\bar{E}/E = \nu/\nu = 1 + \gamma - B\sigma_1/\sigma_R \tag{4.12}$$

*Both Gaussian method and Monte Carlo method were invoked, and similar results were obtained.

where

$$B=2gl^3m/9 \tag{4.13}$$

$$\gamma=B\sigma_a^c/\sigma_R=B(\sqrt{l_c^s/l}-1) \tag{4.14}$$

The second equality in equation (4.14) derives from equation (4.6). Moreover, it is noticed that the elastic moduli pertinent to the overall strain response of the medium, are controlled by the applied stresses.

Thus, the overall principal strains ε_1 and ε_2 are

$$\varepsilon_1=(\sigma_1-\bar{\nu}\sigma_2)/\bar{E} \tag{4.15a}$$

$$\varepsilon_2=(\sigma_2-\bar{\nu}\sigma_1)/\bar{E} \tag{4.15b}$$

With $\bar{E}$ and $\bar{\nu}$ given in equation (4.12), the stress/strain laws of a microcracking medium (if $\sigma_1>\sigma_a^c$) would be

$$e_1=s_1[1-k\nu(1+\gamma-Bs_1)]/(1+\gamma-Bs_1) \tag{4.16a}$$

$$e_2=s_2[1-\nu(1+\gamma-Bs_2/k)/k]/(1+\gamma-Bs_2/k) \tag{4.16b}$$

where $e=(1+\nu)/\Delta\alpha\Delta T$. Notice that, the principal strain is dictated only by the pricipal stress along the same axis. Other unique features are observed in the numerical results of equation (4.16) as shown in Fig. 4.4. If the ratio k is kept constant during loading ($d\sigma/dt>0$), the stress/strain response would be linear below the microcracking threshold ($\sigma_1<\sigma_a^c$). Above it, the stress/strain response becomes nonlinear since the microcrack propensity increases and the stiffness of the medium decreases. The nonlinear response resembles that of a work-hardening material. Furthermore, the trajectory of the stress/strain curve may depend upon the history of loading (if k varies). Yet, the total strain ε at a certain stress σ is only dictated by the current stress state (σ_1 and σ_2), as shown schematically on Fig. 4.5.

4.3.2. Stress/Strain Hysteresis

Another important characteristic of a microcracking material is the stress/strain hysteresis. Following the previous system, if the applied stress is

removed after reaching a peak value σ_P, the microcrack density is retained since microcracking is an irreversible process. Accordingly, the elastic moduli $\bar{E}_p$ and $\bar{\nu}_p$ remain constant as,

$$\bar{E}/E=\bar{\nu}/\nu=1+\gamma-B\sigma_p/\sigma_R \tag{4.17}$$

Therefore, the unloading stress/strain trajectory is linear (Fig. 4.6), resulting in a clock-wise hysteresis. From a thermodynamics viewpoint, a part of the strain energy dissipates (through microcracking) during loading and cannot be retrieved during unloading. The amount of strain energy dissipation, equivalent to the area enclosed by the hysteresis, corresponds to the work done by the external load through a complete cycle of loading. The stress/strain trajectory during further loading follows the straight line characterized by $\bar{E}_p$ and $\bar{\nu}_p$ until $sigms_p$ is reached. At this point, new microcracks are induced and the non-linear behavior resumes. Such hystereses are also observed in work-hardening materials and martensitic composites [7].

4.4. Discussion

The stress applied on a grain facet to induce microcracking is refered to as the grain facet strength S. In some studies [1,2], this parameter has been treated as a constant. More generally, a Weibull distribution has been assumed [8]

$$P=1-exp[-(S/S)^q A] \tag{4.18}$$

where P is the probability that a grain facet will fracture at S, and A,S^1,q are constants. From the present study, it is seen that the statistical nature of S derives from the variation of the effective stress on the grain facet configuration parameters inherent in orientation randomness. Therefore, f given in equation (4.8) may readily be viewed as the distribution function equivalent to P. It is seen that the distribution depends upon the facet size l as well as the magnitude of the residual stress σ_P.

Evans [9] et al observed that, acoustic emission can be monitored in polycrystalline Al_2O_3 as grain facet microcracking is induced by the applied stress. In modeling the process, they assumed a simplified Weibull distribution for the grain facet strength S as

$$f = A(S/S)^q \tag{4.19}$$

By comparing the model with the observed data, q=10 was obtained. This result can be correlated to the distribution function f obtained in equation (4.8). As shown in Fig. 4.7, the numerical results of f versus σ_1 (equivalent to S) calculated from equation (4.8) have been plotted on logarithmic axes. In the proper range of microcrack density (f~0.1-0.5) relevent to the slow crack growth system, the f versus σ_1 relation may be approximated as the simplified Weibull function and the corresponding exponent q may be obtained from the slope of the curve as q~3-10, conforming also to the experimental observations. Furthermore, in a material with a statistical distribution of grain facet size, the strength will be modified as

$$P(S) = \int_0^\infty f(S,l)p(l)dl \tag{4.20}$$

where $p(l)dl$ is the fraction of facets with sizes between l and $l+dl$.

Induced microcracking influences the mechanical strength of a material in the following aspects. Two failure modes in a material loaded without precracking have been observed in different grain size regimes. In small grain samples, failure generally originates from pre-existing flaws appreciably larger than the average grain size, and no induced microcracking is observed [10]. In large grain samples, however, a prominant grain size dependence of strength is observed [11], which has been attributed [12] to a failure mode of coalescence of stress induced microcracks. More significantly, during fracture of a precracked material, formation of a process zone around the macrocrack, consisting of stress induced microcracks has been observed to modify the fracture

resistance of the material. The compliant microcrack zone shields the macrocrack, relaxes the stress singularity at the crack tip, and hinders the crack propagation. Such interactions among the induced microcracks and the stress field are contained in the stress/strain chacteristic of the microcrack zone. Hence, the mechanics of toughening may readily be analysed based upon such characterictics. Analyses following this approach are presented in section 6.

Although nonlinear behavior of a microcracking material is predicted, no direct experimental observation has been reported. The primary reason is that, in the majority of tests where the bulk sample is stressed, the coalescence of microcracks leads to catastrophic failure before appreciable nonlinearity is established. Hence, nonlinearity may only obtain in the microcrack process zone, restrained by the unmicrocracked surrounding.

Analagous to the analysis in section 3 on spontaneous microcracking, the analysis in the present section is based on a simplified two dimensional stress field and the interactions among the microcracks are excluded. Due to these simplifications, it has been suggested in section 3 that the "effective" microcrack density causing the moduli decrease might be higher than the calculated one. A similar situation is expected here, namely, the coefficient B in equation (4.13) characterizing the extent of moduli decrease ($dE/d\sigma$), is larger than predicted (i.e. m~1/4–1/2, g~$3/l^3$ and B~1/3–2/3). This statement will be further substantiated in section 6 where the nonlinear characteristics are incorporated into the analysis of microcrack toughening at steady-state cracking stage and predictions are compared with experimental data.

Finally, another simplification is the exclusion of permanent strains associated with spontaneous microcracking, which are expected to be present in actual situations since residual strains are relaxed during microcracking. Consequently, in a real system, strains should be higher, permanent strains should

exist after unloading, and more strain energy should be dissipated (Fig. 4.8). Incorporation of such effects is encouraged in future studies.

REFERENCES

1. R. G. Hoagland, J. D. Embury and D. J. Green, Scr. Metall., 9, 9, 907 (1975).
2. A. G. Evans, Scr. Metall., 10, 1, 93 (1976).
3. R. C. Pohanka, R. W. Rice and B. E. Walker, Jr., J. Am. ceram. Soc., 59, 71, (1976).
4. F. A. McClintock, Fracture Mechanics of Ceramics, (Ed. R. C. Bradt, D. P. H. Hasselman and F. F. Lange) Plenum, N.Y., vol.1, 93 (1974).
5. B. Budiansky and J. O'Connell, Int. J. Solids and Structure, 12, 81 (1976).
6. F. F. Lange, J. Mater. Sci., 17, 225 (1982).
7. B. Budiansky, J. Hutchinson and J. Lambropolous, Int. J. Solids and Structure, 19, 337 (1983).
8. A. G. Evans, J. Am. ceram. Soc., 58, 239 (1974).
9. A. G. Evans and M. Linzer, J. Am. ceram. Soc., 56, 575 (1973).
10. A. G. Evans, J. Am. ceram. Soc., 65, 127 (1982).
11. R. W. Rice, Treatise on Materials Science and Technology, 11, 199 (1977).
12. A. G. Evans and Y. Fu, to be published in Advances in Ceramics.

FIGURE CAPTIONS

4.1. Schematic of resultant stresses on boundary facets of anisotropic grains subject to applied stress.

4.2. Schematic of facet configuration domain with points corresponding to microcracked facets subject to loading.

4.3. Fraction of microcracked facets vs normalized applied stress in anisotropic polycrystalline materials a) with varying facet size subject to uniaxial loading b) with fixed facet size subject to biaxial loading.

4.4 Nonlinear stress/strain curve of a microcracking material in loading stage ($d\sigma/d\varepsilon>0$).

4.5. Schematic illustrating non-linear stress/strain characteristic of a microcracking medium.

4.6. Schematic illustrating hysteresis in stress/strain cycle.

4.7. Plot of fraction of microcracked facets vs normalized applied stress on logarithmic axes.

4.8. Schematic illustrating effects of permanent strain associated with microcracking.

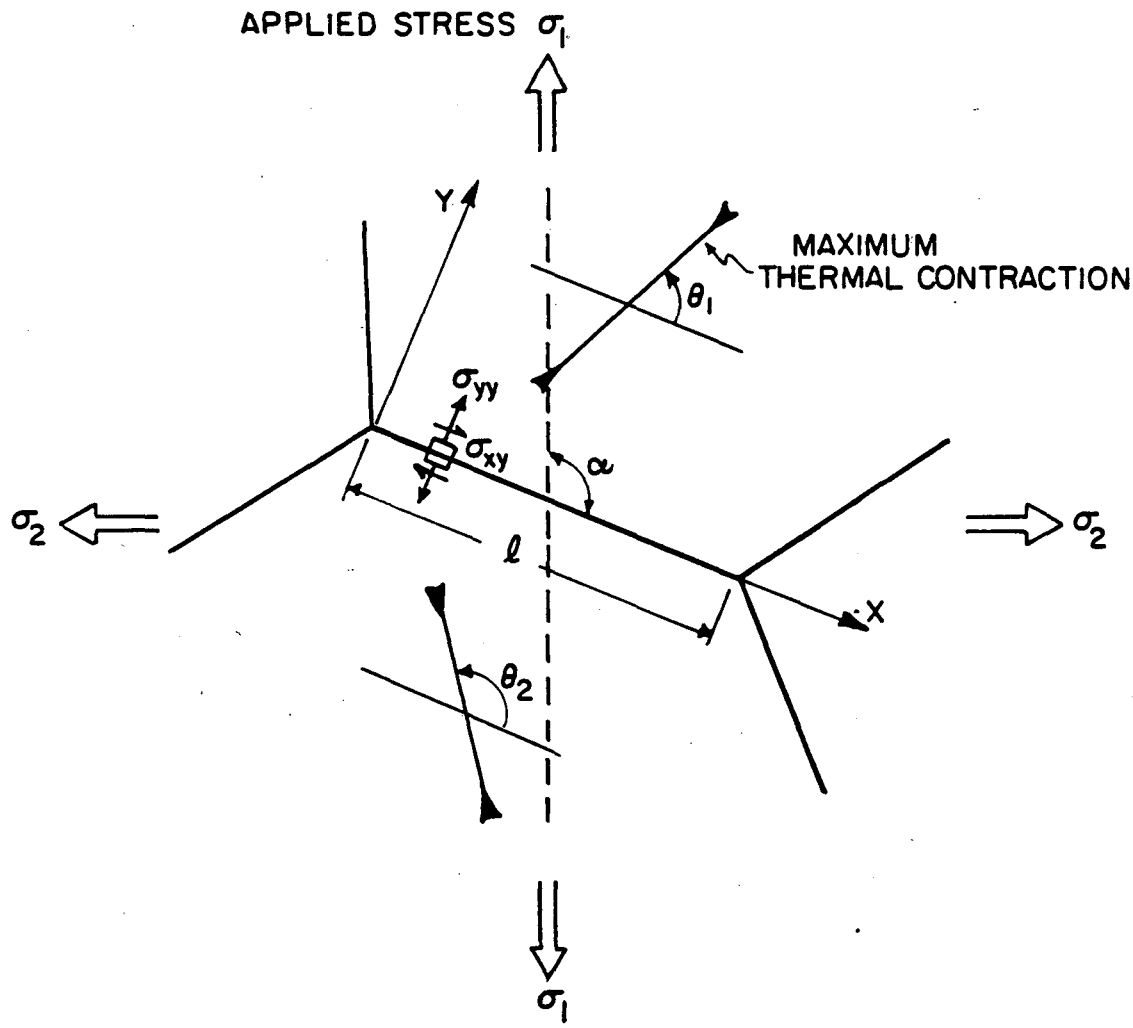
APPLIED STRESS σ_1
Y
MAXIMUM
THERMAL CONTRACTION
θ_1
σ_{yy}
σ_{xy}
α
σ_2
σ_2
ℓ
X
θ_2
σ_1
XBL839-6355

Fig.4.1

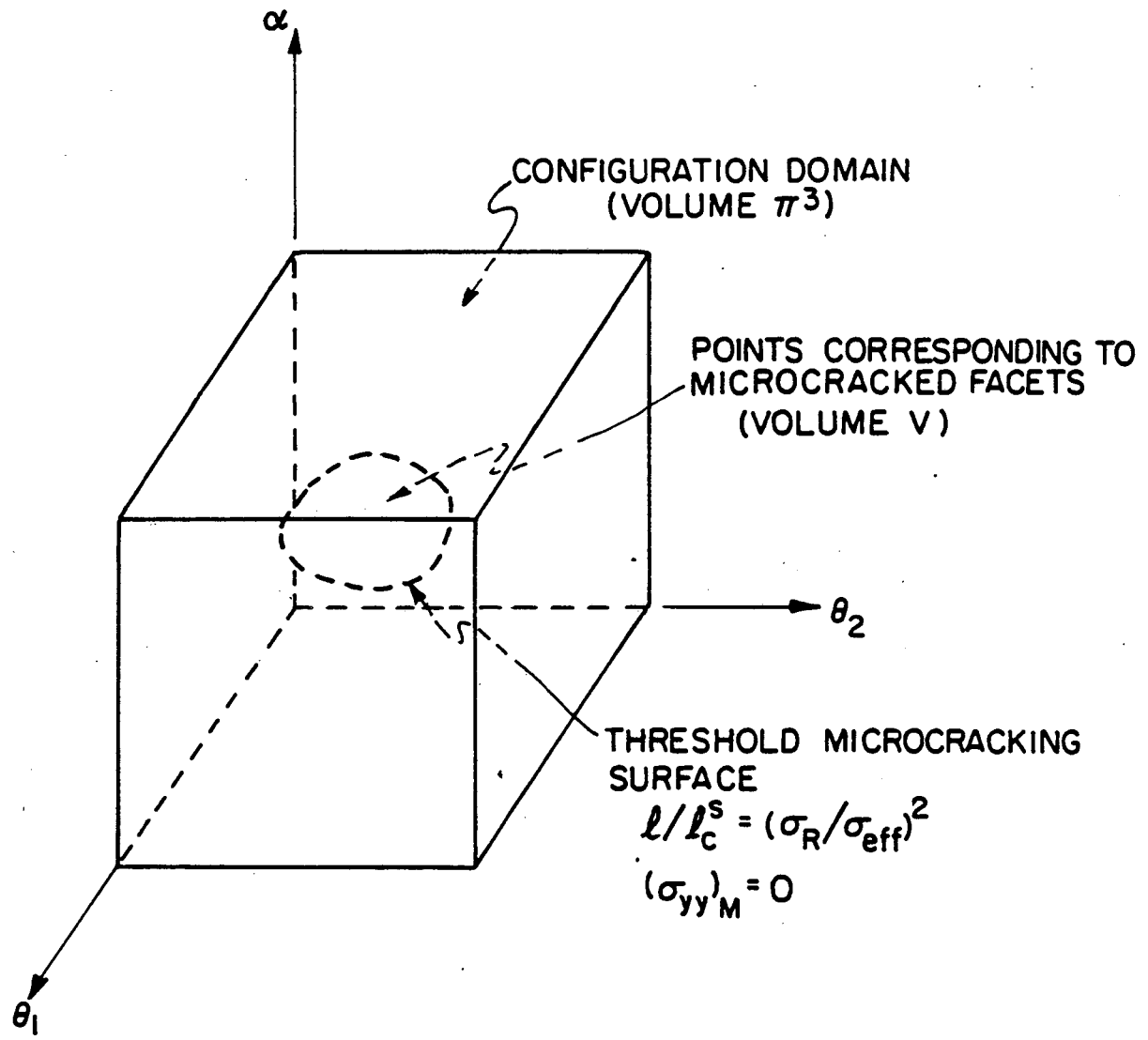
α
CONFIGURATION DOMAIN
(VOLUME π³)
POINTS CORRESPONDING TO
MICROCRACKED FACETS
(VOLUME V)
θ2
THRESHOLD MICROCRACKING
SURFACE
ℓ/ℓc^s = (σR/σeff)²
(σyy)M = 0
θ1
XBL839-6356

Fig.4.2

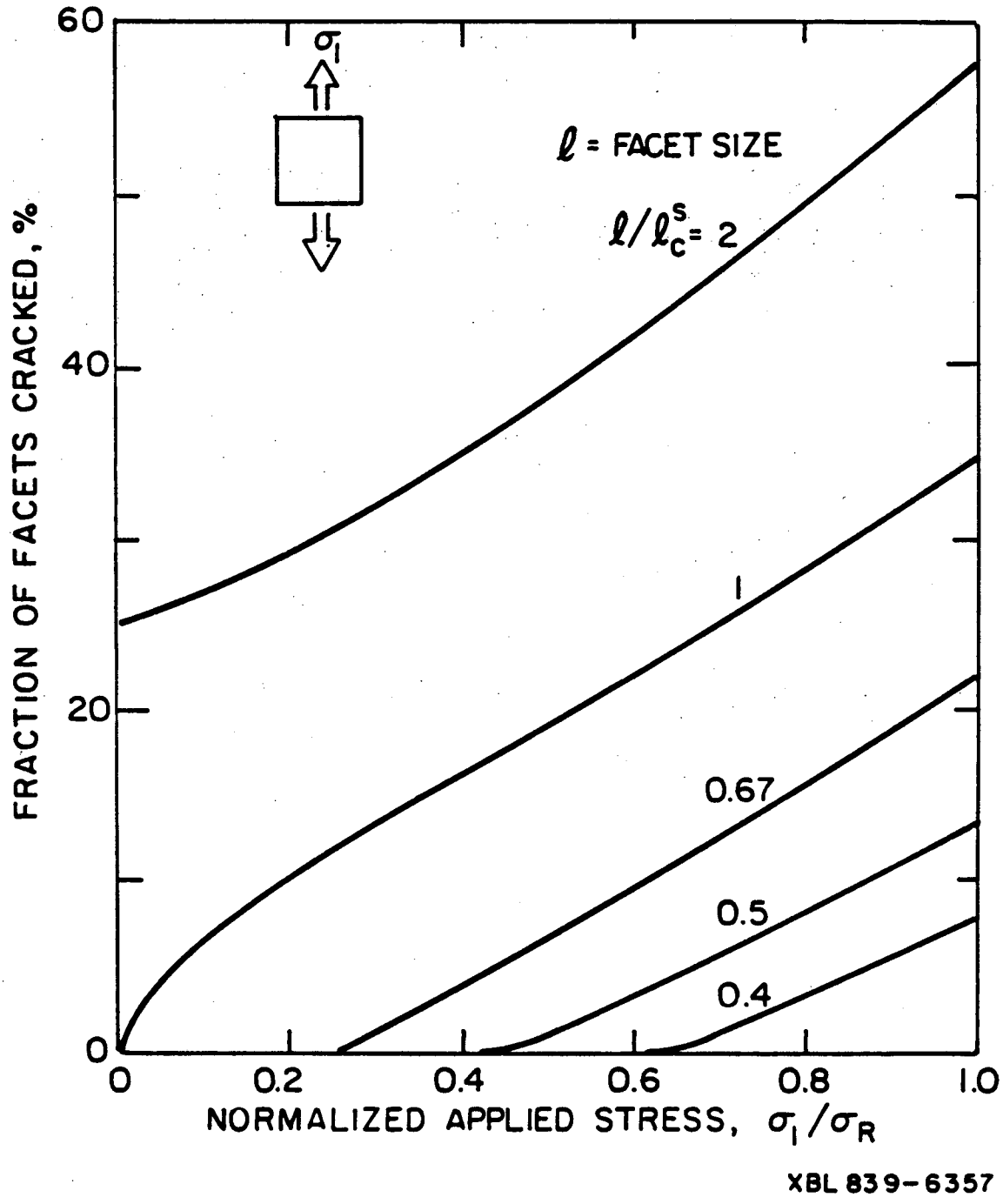
60
40
20
0
σ_1
ℓ = FACET SIZE
ℓ/ℓ_c^s = 2
1
0.67
0.5
0.4
FRACTION OF FACETS CRACKED, %
0
0.2
0.4
0.6
0.8
1.0
NORMALIZED APPLIED STRESS, σ_1/σ_R
XBL 839-6357

Fig.4.3a

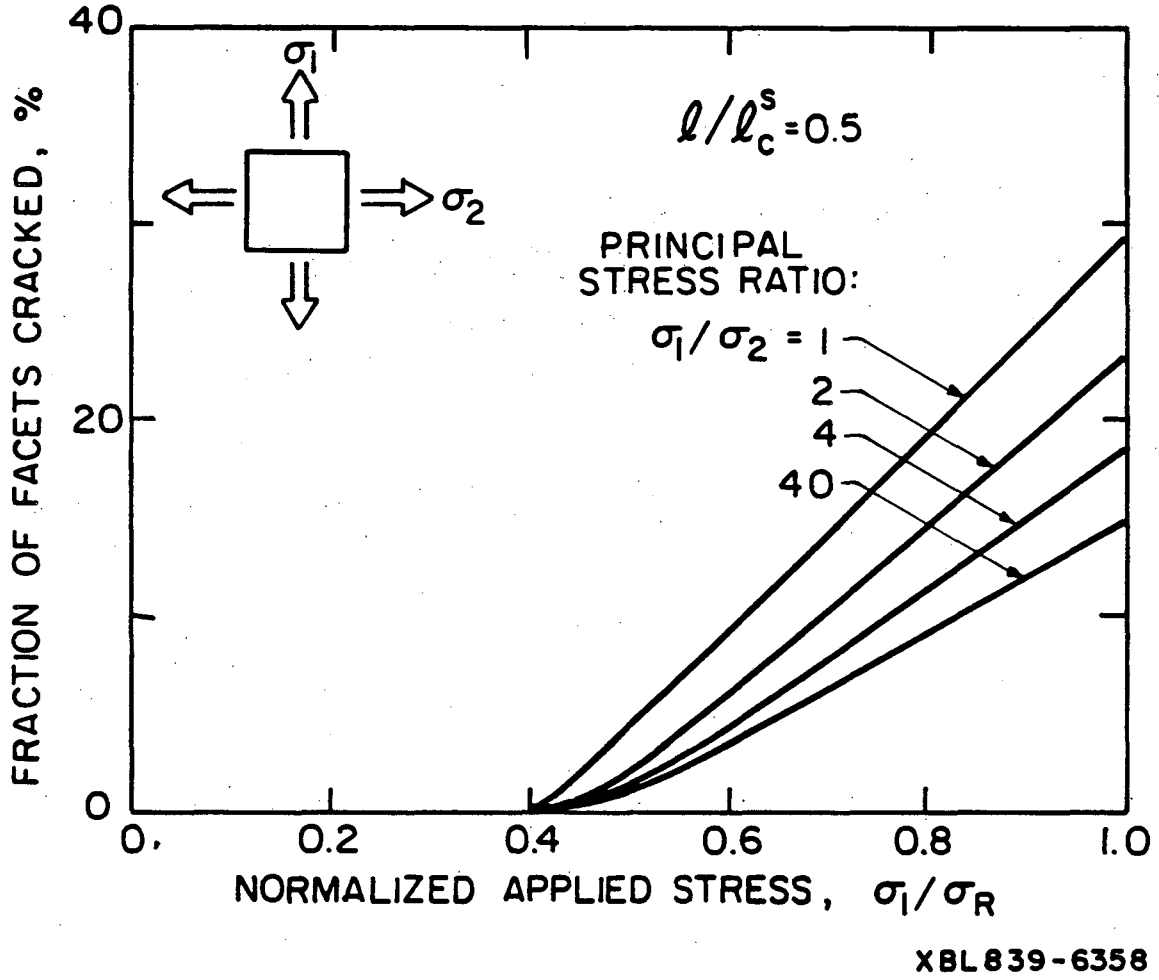
40
20
0
0.
0.2
0.4
0.6
0.8
1.0
FRACTION OF FACETS CRACKED, %
NORMALIZED APPLIED STRESS, σ_1/σ_R
σ_1
σ_2
ℓ/ℓ_c^s=0.5
PRINCIPAL
STRESS RATIO:
σ_1/σ_2 = 1
2
4
40
XBL839-6358

Fig.4.3b

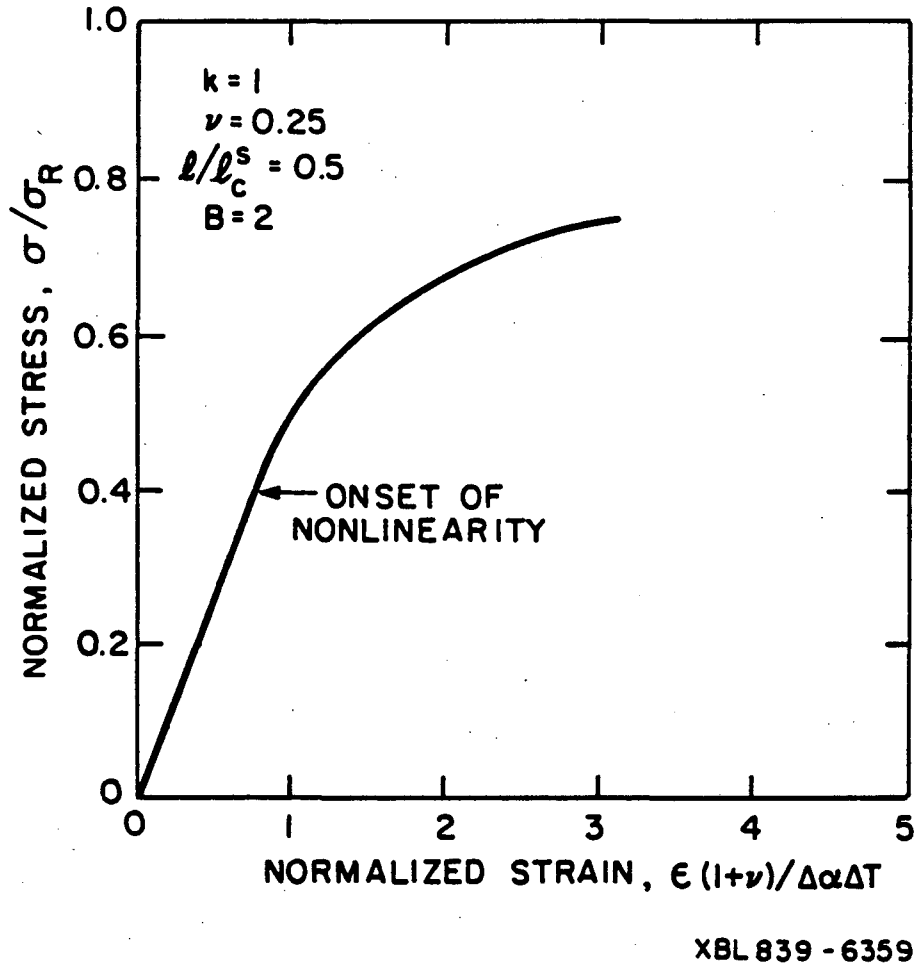
1.0
0.8
0.6
0.4
0.2
0
k = 1
ν = 0.25
ℓ/ℓ_c^s = 0.5
B = 2
NORMALIZED STRESS, σ/σ_R
ONSET OF
NONLINEARITY
0
1
2
3
4
5
NORMALIZED STRAIN, ε(1+ν)/ΔαΔT
XBL 839-6359

Fig.4.4

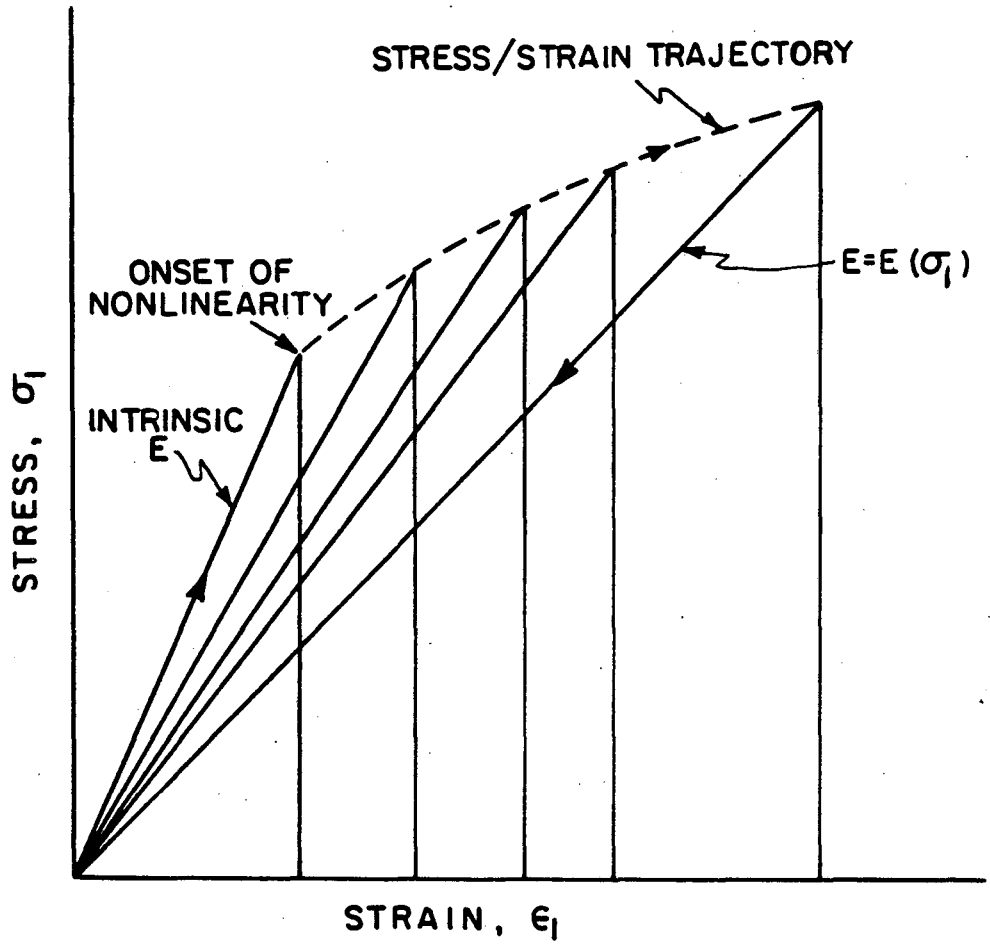
STRESS/STRAIN TRAJECTORY
ONSET OF NONLINEARITY
INTRINSIC E
E=E (σ1)
STRESS, σ1
STRAIN, ε1
XBL839-6360

Fig.4.5

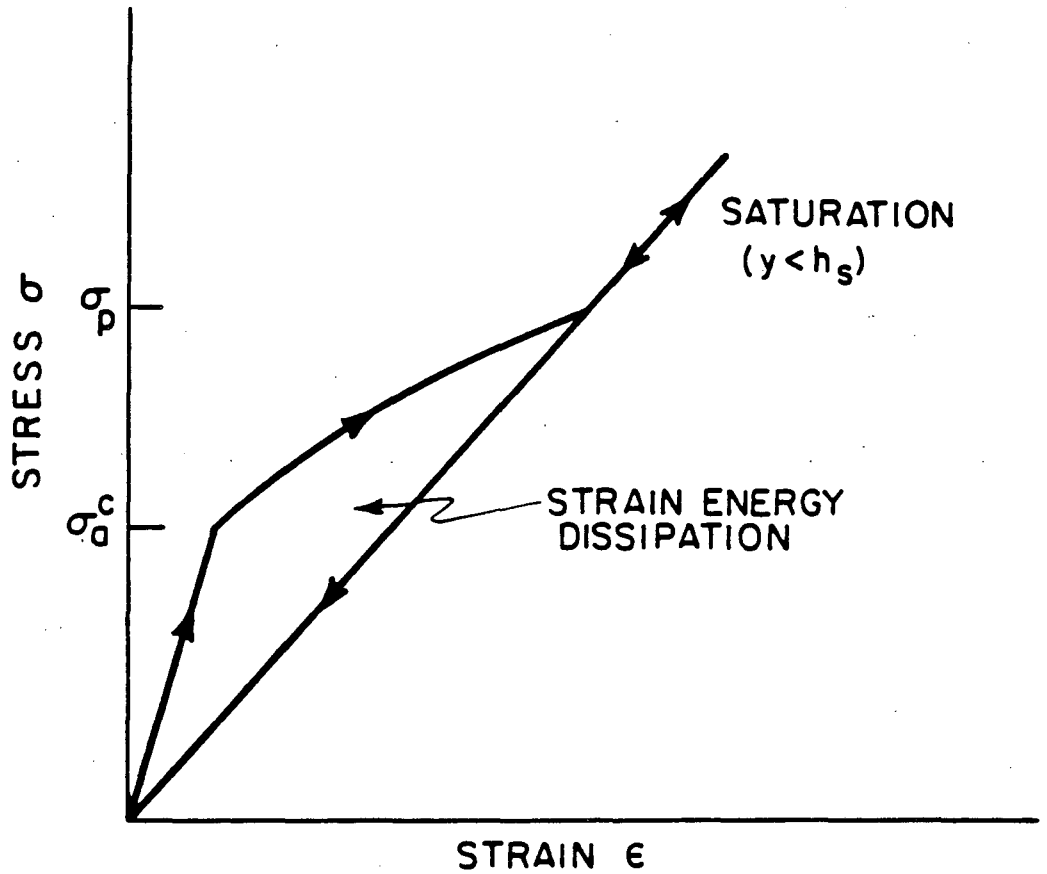
STRESS σ
q_p
q_c
SATURATION
(y<h_s)
STRAIN ENERGY
DISSIPATION
STRAIN ε
XBL839-6341

Fig.4.6

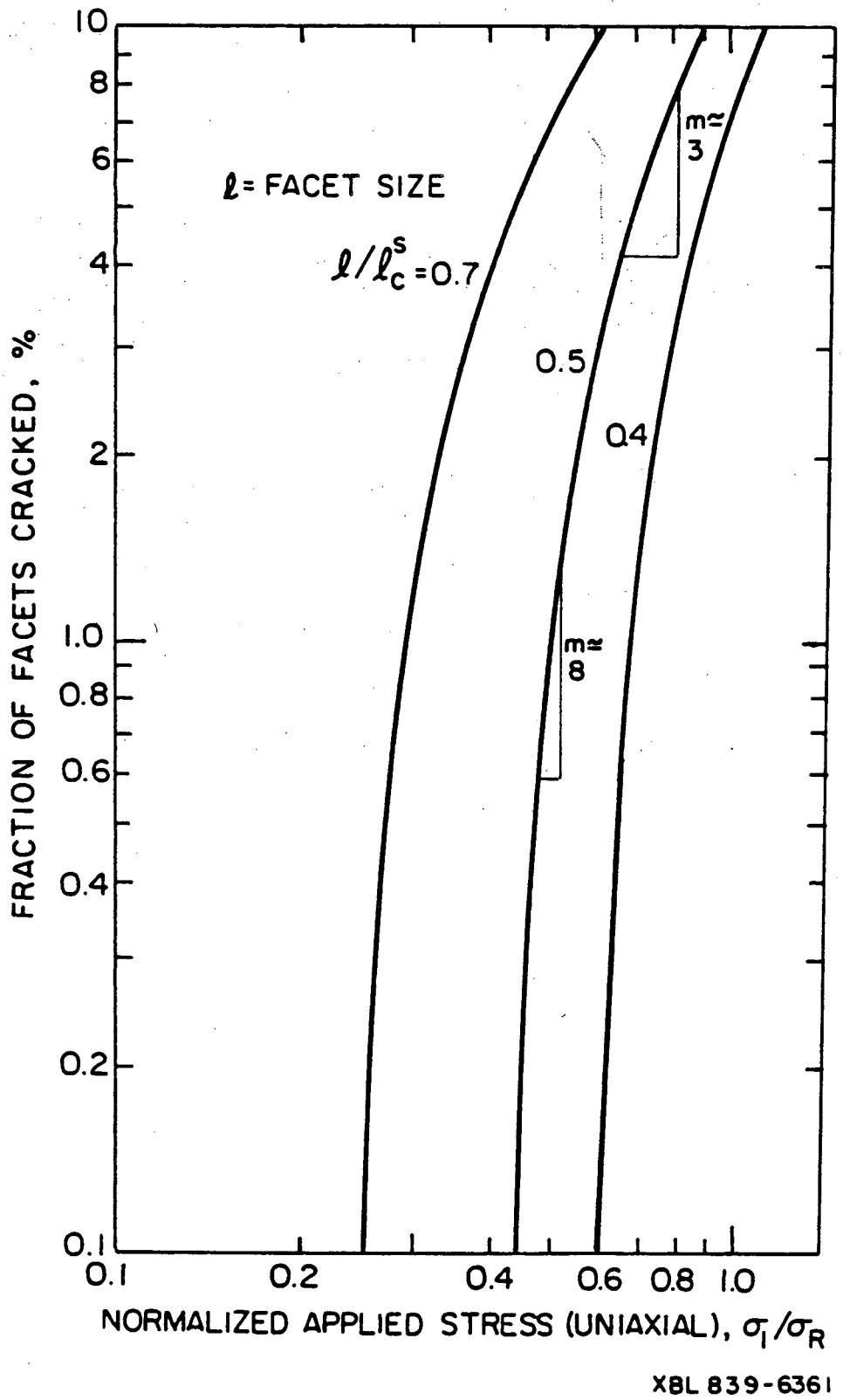
FRACTION OF FACETS CRACKED, %
NORMALIZED APPLIED STRESS (UNIAXIAL), σ_1/σ_R
ℓ = FACET SIZE
ℓ/ℓ_c^s = 0.7
0.5
0.4
m≈3
m≈8
10
8
6
4
2
1.0
0.8
0.6
0.4
0.2
0.1
0.1
0.2
0.4
0.6
0.8
1.0
XBL 839-6361

Fig.4.7

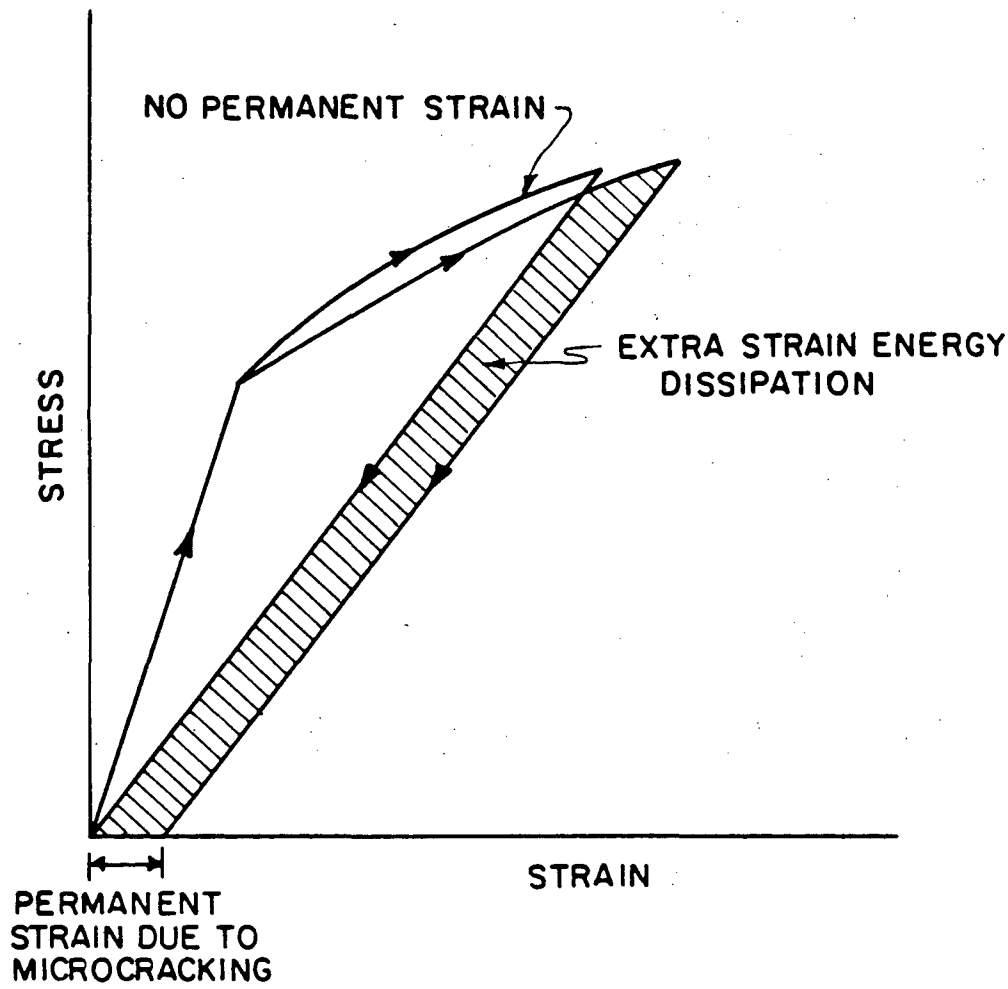
NO PERMANENT STRAIN
EXTRA STRAIN ENERGY DISSIPATION
STRESS
STRAIN
PERMANENT STRAIN DUE TO MICROCRACKING
XBL 839-6362

Fig.4.8

5. Onset of Microcrack Toughening

5.1. Introduction

When a macrocrack is present in a single phase anisotropic polycrystalline material, the crack tip stress field may induce microcracking at nearby grain boundary facets to form a microcrack zone around the macrocrack (Fig. 5.1). The microcrack zone is capable of modifying the toughness of the medium, thus yielding a toughening effect [1-4]. Experimental observations [5] showed that, in single phase anisotropic polycrystalline ceramics, the toughening mechanism is suppressed below a certain grain size threshold (Fig. 5.1). The physical origin of this threshold may be attributed to the condition of nucleating discrete microcracks ahead of the macrocrack tip. Evidently, this process is assisted by the presence of residual stresses; otherwise, the direct propagation of the macrocrack would dominate the nucleation of discrete microcracks.

In section 3, the process of microcracking at grain boundary facets subject to residual stresses has been studied. In the presence of a macrocrack, the residual stresses can both encourage the initiation of a discrete microcrack and suppress macrocrack extension. The specific intent of the present section is to analyze this dual influence of residual stress and hence, to establish the existence of a critical grain size for process zone initiation. Specifically, the Eshelby method is invoked to analyse the stress distribution, since the onset condition is dictated by the detailed structure of the stress field. Finally, the critical grain size for the onset of microcrack toughening may be predicted and correlated with experimental observations.

5.2. The Stress Analysis

The microcrack initiation problem is addressed by considering the simplified plane stress configuration depicted in Fig. 5.2, consisting of a hexago-

nal grain (subject to thermal contraction anisotropy) located at a crack tip in an, otherwise, isotropic body. This configuration is used to permit a direct comparision of primary crack extension along the grain boundary with microcrack initiation at one of the neighboring grain corners. This comparison is achieved by adopting the following procedure. The residual stress in the crack-free body is computed. The primary crack is then inserted into the system and the stress intensity factor K at the primary crack, associated with the residual and applied field, is calculated (as a function of crack advance along the contiguous grain boundary). Thereafter, the modified residual field induced by the relaxation of the stress along the crack surface is determined and used to calculate the stress intensity factor at a secondary crack located on the neighboring grain corner. Finally, the incidence of discrete microcracking is assessed by allowing K at the secondary crack to exceed K at the primary crack.

5.2.1. The Residual Stress

The residual stress in the crack-free body can be calculated using the Eshelby procedure as described in section 2. The stresses are computed for the grain configuration in which the maximum thermal contraction is perpendicular to the main crack, as required to optimize secondary crack nucleation prior to primary crack extension (by providing both a maximum tensile stress along the neighboring grain boundary and a maximum closure at the primary crack). The stresses at the location of present interest along the prospective crack plane, the contiguous grain boundary and adjacent to the neighboring grain corner, are plotted in Fig. 5.3. The stresses along the neighboring grain boundary are tensile; while compression develops along both the contiguous boundary and along the prospective crack plane.

5.2.2. Stress Intensity Factors

5.2.2.1. The Primary Crack.

The local stress intensity factor at the primary crack tip, when located at the grain corner, can be ascertained from the residual and applied field by applying the weight function [6]

$$K^{local} = K^{\infty} + \int_{S_T} Th\,dS \tag{5.1}$$

where K^{∞} is the applied stress intensity factor, T is the traction associated with the second step in the Eshelby procedure, applied through the line S_T in the plane, and h is a weight function,

$$h_x = \cos\frac{\vartheta}{2}(2\nu - 1 + \sin\frac{\vartheta}{2}\sin\frac{3\vartheta}{2}) / 2\sqrt{2}\pi(1-\nu)\sqrt{r}$$

For a mode I applied stress intensity factor, K_I^{∞}, the local stress intensity factor deduced from equation (5.1) becomes

$$K_I^{local} = K_I^{\infty} - 0.7E\Delta\alpha\Delta T\sqrt{l} / (1+\nu) \tag{5.2a}$$

$$K_{II}^{local} = 0 \tag{5.2b}$$

Propagation of the primary crack along the contiguous grain boundary modifies the stress intensity factor. The modification can be approximately determined by adopting the following procedure. The stress intensity associated with the residual field is ascertained by regarding the crack as a coplanar extension of the kink (Fig. 5.4): with closure tractions placed over the crack surface during the second step in the Eshelby procedure and opposing tractions imposed over the top surface of the crack and along the remainder of the grain boundary during the third step. The resultant traction distribution is depicted in Fig. 5.4. The tractions over the crack surface generate the stress intensity factors

$$k_I^k = \left(\frac{2}{\pi}\right)^{\frac{1}{2}} \cos\left(\frac{2\pi}{3}\right) E\Delta\alpha\Delta T\sqrt{\Delta a} / (1+\nu) \tag{5.3a}$$

$$k_{II}^{k}=\left(\frac{2}{\pi}\right)^{\frac{1}{2}}\sin\left(\frac{2\pi}{3}\right)E\Delta\alpha\Delta T\sqrt{\Delta a}/(1+\nu) \tag{5.3b}$$

where Δa is the kink crack length. The tractions over the grain boundary influence k in accord with the weight function described by equation (5.1), as expressed by

$$k_{I}^{k}=-[E\Delta\alpha\Delta T\sqrt{l}/(1+\nu)]\chi_1(\Delta a/l) \tag{5.4a}$$

$$k_{II}^{k}=[E\Delta\alpha\Delta T\sqrt{l}/(1+\nu)]\chi_2(\Delta a/l) \tag{5.4b}$$

where χ_1 and χ_2 are functions of $\Delta a/l$. The stress intensity at the kink induced by the applied field is expressed in terms of stress intensities k_I^{∞} and k_{II}^{∞} deduced from the angular dependence of the original, unkinked crack tip field as [7]

$$k_{I}^{k}=K_I^{\infty}[3\cos(\vartheta/2)+\cos(3\vartheta/2)]/4 \tag{5.5a}$$

$$k_{II}^{k}=K_I^{\infty}[\sin(\vartheta/2)+3\sin(3\vartheta/2)]/4 \tag{5.5b}$$

where $\vartheta=\pi/3$ is the kink angle.

Extension of the kinked crack along the contiguous grain boundary is assumed to occur in accord with a critical value of the strain energy release rate. Hence, a coplanar strain energy release rate, , is determined from the stress intensity factors using

$$E/(1-\nu^2)=(\sum k_I^{k})^2(\sum k_{II}^{k})^2\equiv(K^{*})^2 \tag{5.6}$$

where the summation is taken over the contributions to k from the surface tractions, the grain boundary tractions and the applied field. The final result can be expressed in the form

$$\frac{K^{*}(1+\nu)}{E\Delta\alpha\Delta T\sqrt{l}}=F_k\left[\frac{E\Delta\alpha\Delta T\sqrt{l}}{K_I^{\infty}(1+\nu)},\Delta a/l\right] \tag{5.7}$$

where F_k is the function plotted in Fig. 5.5. The effective stress intensity factor typically decreases as a function of kink advance, up to kink crack length ~0.1 l. The kink crack is thus capable of initial stable advance under increased external loading: a feature that must be accounted for in subsequent analysis.

5.2.2.2. The Secondary Crack

The analysis of secondary crack initiation requires that the residual stress along the neighboring boundary firstly be computed in the presence of the primary crack. This is achieved in accord with the method devised by Hirth et al. [8] involving the determination of the elastic interaction field between the Eshelby tractions and the crack. The analysis establishes that the incorporation of the primary crack reduces the residual tension along the boundary, as depicted in Fig. 5.6. The stresses associated with the applied loading are then superimposed, in order to obtain the total stress along the neighboring boundary.

The initiation of a secondary crack is presumed to occur from small defects located near the three grain interface, as in prior analyses of thermal expansion induced microcracking *. A stress intensity factor may then be deduced from the stresses by applying the superposition solutions [9].

$$k_I^s=(2/\pi c)^{1/2}\int_0^c \sigma(x)\sqrt{x/(c-x)}\,dx \tag{5.8a}$$

$$k_I^s=(2/\pi c)^{1/2}\int_0^c \tau(x)\sqrt{x/(c-x)}\,dx \tag{5.8b}$$

where c is the length of the secondary crack, and σ and τ are the normal and shear stresses along the crack-free grain boundary. Incorporating the stresses σ and τ into equation (5.8), and using the coplanar strain energy release rate criterion (equation (5.6)) to establish an effective K for secondary cracking, yields an expression of the form

$$\frac{K^s(1+\nu)}{E\Delta\alpha\Delta T\sqrt{l}}=F_s\left[\frac{E\Delta\alpha\Delta T\sqrt{l}}{K_I^m(1+\nu)},c/l\right] \tag{5.9}$$

where F_s is the function plotted in Fig. 5.7.

*Although the necessity for a small defect is an unsatisfactory feature of this type of analysis (an unidentified strong elastic singularity may exist at the grain junction), reasonable correlations with experiment can be achieved.

5.3. Microcrack Initiation

The initiation of a discrete microcrack ahead of the primary crack requires that the stress intensity factor associated with the defect at the neighboring three grain corner attain the critical value for grain boundary rupture, $K_c^{g.b.}$, before the stress intensity at the primary crack kink becomes critical. This is achieved when

$$K^s = K_c^b > K^*. \tag{5.10}$$

The appropriate choice of K^* coincides with the minimum K^*_{min} that obtains during kink advance, because this minimum presages the onset of unstable extension of the kink to the neighboring corner, when $K^*_{min} = K_c^{g.b.}$. The K^s pertinent to microcrack initiation is assumed to be the value that obtains when $c/l \approx 0.1$, as suggested by prior studies of spontaneous microcracking. Applying these selections for K^* and K^s to equation (5.10) allows the critical condition for microcrack initiation to be expressed as

$$K^*_{min} = K_{(c/l=0.1)} = K_c^b = \frac{0.36 E \Delta\alpha \Delta T \sqrt{l_c}}{(1+\nu)} \tag{5.11a}$$

when

$$K_I^\infty (1+\nu)/ E\Delta alphs\, \Delta T \sqrt{l} \approx 1.5. \tag{5.11b}$$

For

$$K_I^\infty (1+\nu)/ E\Delta\alpha\Delta T\sqrt{l} < 1.5 \ , \ K^*_{min} < K^s_{(c/l=0.1)} \tag{5.12}$$

and the secondary crack forms prior to extension of the primary crack along the contiguous boundary.

The result expressed by equation (5.11) can be reformulated in terms of a critical grain size, l_c, for discrete microcrack formation

$$l_c = 7.7 (K_c^b)^2 (1+\nu)^2 / (E\Delta\alpha\Delta T)^2$$

It is instructive to compare this critical grain size with that associated with spontaneous microfracture during cooling, l_c^s. For the grain configuration depicted in Fig. 5.2, the spontaneous microcrack condition is given by

$$l_c^s = 19.6(K_c^0)^2(1+\nu)^2/(E\Delta\alpha\Delta T)^2 \quad (5.13)$$

Comparison of equations (5.12) and (5.13) gives

$$l_c = 0.4 l_c^s. \quad (5.14)$$

Discrete microcrack initiation around a primary crack thus occurs when the grain size reaches ~40% of the grain size needed to induce spontaneous microfracture during cooling.

5.4. Discussion

The preceding analysis has indicated that discrete microcracks can initiate prior to primary crack extension whenever the material grain size exceeds a threshold value. This threshold grain size is appreciably smaller than the critical grain size for spontaneous microcracking. For the specific, simplified grain configuration employed in the present analysis, discrete microcracking occurs at grain sizes > 40% of the level required for spontaneous microcracking. Moreover, it is noticed that this ratio does not involve other microstructural parameters, so, the prediction is readily applicable to single phase systems.

The predictive capability of the analysis may be substantiated by the experimental data for Al_2O_3, $BaTiO_3$ and Nb_2O_5 as shown in Fig. 5.8. Although only the onset of toughening is analysed in this section, an analysis of the toughening effect within the operative regime will be presented in section 6 where it is shown that the toughness enhancement is fully suppressed at R=R_s^s. From data for Al_2O_3 in Fig. 5.8, R_c^s is observed to be ~150μm, thus the predicted onset condition is R_c~60μm, which is close to the observation, R_c~30μm. Similarly, for $BaTiO_3$, observed R_c^s is ~20μm, observed R_c is ~10μm and predicted R_c is ~8μm. For Nb_2O_5, observed R_c^s is ~10μm, observed R_c is ~3μm and predicted R_c is ~4μm. So, a satisfactory correlation between the prediction and experimental data is obtained.

Several implications may be derived from the present analysis. In studying the influence of grain size on toughness, the microcrack toughening mechanism can be excluded in small grain samples. If this mechanism is to be used for the purpose of toughness enhancement, the grain size of the material should exceed R_c , which can be predicted if R_c^s is known. More preferably, the grain size should be set between $0.4R_c^s$ and R_c^s where toughness enhancement is optimal. Finally, it is encouraged to study the microcrack toughing process in composite systems to see if similar threshold conditions exist.

REFERENCES

1. A. G. Evans, A. H. Heuer and D. L. Porter, "Fracture '77", vol.1, pp.529, edited by D. M. R. Taplin, Univ. of Waterloo Press, Waterloo, Ontario, Canada (1977).

2. R. G. Hoagland, C. W. Marschall, A. R. Rosenfield, G. Hollenberg and R. Ruh, Mater. Sci. Eng., 15, 1, 51 (1974).

3. C. C. Wu, S. W. Freiman, R. W. Rice and J. J. Mecholsky, J. Mater. Sci., 13, 12, 2659 (1978).

4. R. G. Hoagland, G. T. Hahn and A. R. Rosenfield, Rock Mech., 5, 2, 77 (1973).

5. R. W. Rice, S. W. Freiman and P. E. Becher, J. Am. Ceram. Soc., 64, 345 (1981).

6. P. C. Paris, R. M. McMeeking and H. Tada, "Cracks and Fracture", pp.471, ASTM STP 601, ASTM, Philadelphia (1976).

7. B. Cotterell and J. R. Rice, Int. J. Fract., 16, 155 (1980).

8. J. P. Hirth, R. G. Hoagland and P. C. Gehlen, Int. J. Solids & Structure, 10, 997 (1974).

9. G. C. Sih, "Handbook of Stress Intensity Factors", Lehigh Univ. Press (1973).

FIGURE CAPTIONS

5.1. The expected variation of fracture toughness with grain size.

5.2. Schematic illustrating the formation of kink and secondary cracks (discrete microcrack) during crack propagation in polycrystals.

5.3. Plot of normalized residual stress (a) along the prospective main crack plane, (b) along the contiguous grain boundary, (c) along the neighboring grain boundary, for the configuration shown in the picture.

5.4. Schematic of the kink crack system showing the boundary tractions and effective crack for stress intensity factor calculations.

5.5. Normalized stress intensity factor vs relative crack length for the kink crack (shown in Fig. 5.2).

5.6. Normalized tensile stresses on the neighboring grain boundary with and without crack.

5.7. Normalized stress intensity factor vs relative crack length for the secondary crack (shown in Fig. 5.2).

5.8. The grain size dependence of the fracture energy for Al_2O_3, Nb_2O_5 and TiO_2 (after Ref.5).

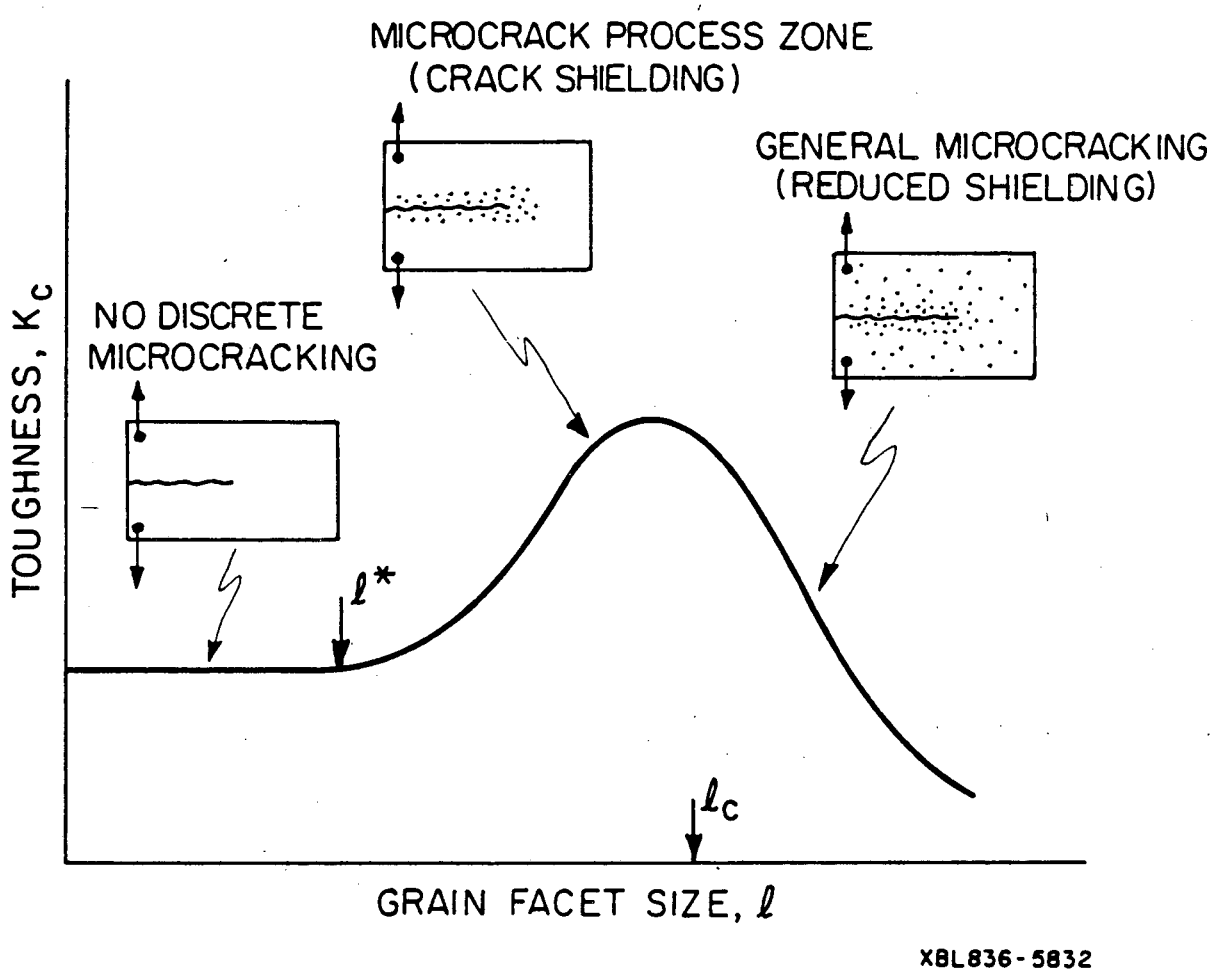
MICROCRACK PROCESS ZONE
(CRACK SHIELDING)
GENERAL MICROCRACKING
(REDUCED SHIELDING)
NO DISCRETE
MICROCRACKING
TOUGHNESS, K_c
ℓ^*
ℓ_c
GRAIN FACET SIZE, ℓ
XBL836-5832

Fig.5.1

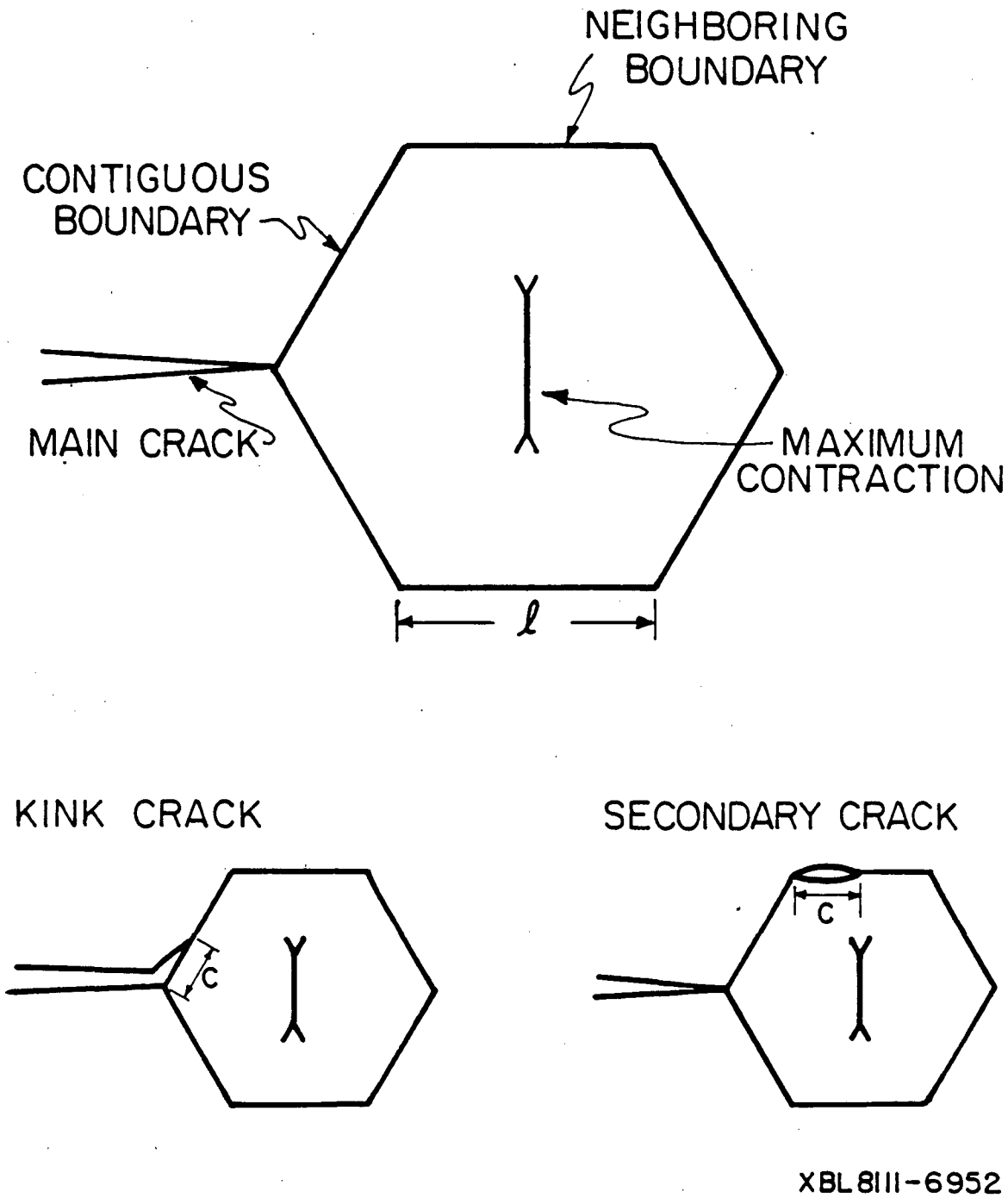
NEIGHBORING
BOUNDARY
CONTIGUOUS
BOUNDARY
MAIN CRACK
MAXIMUM
CONTRACTION
ℓ
KINK CRACK
c
SECONDARY CRACK
c
XBL8111-6952

Fig.5.2

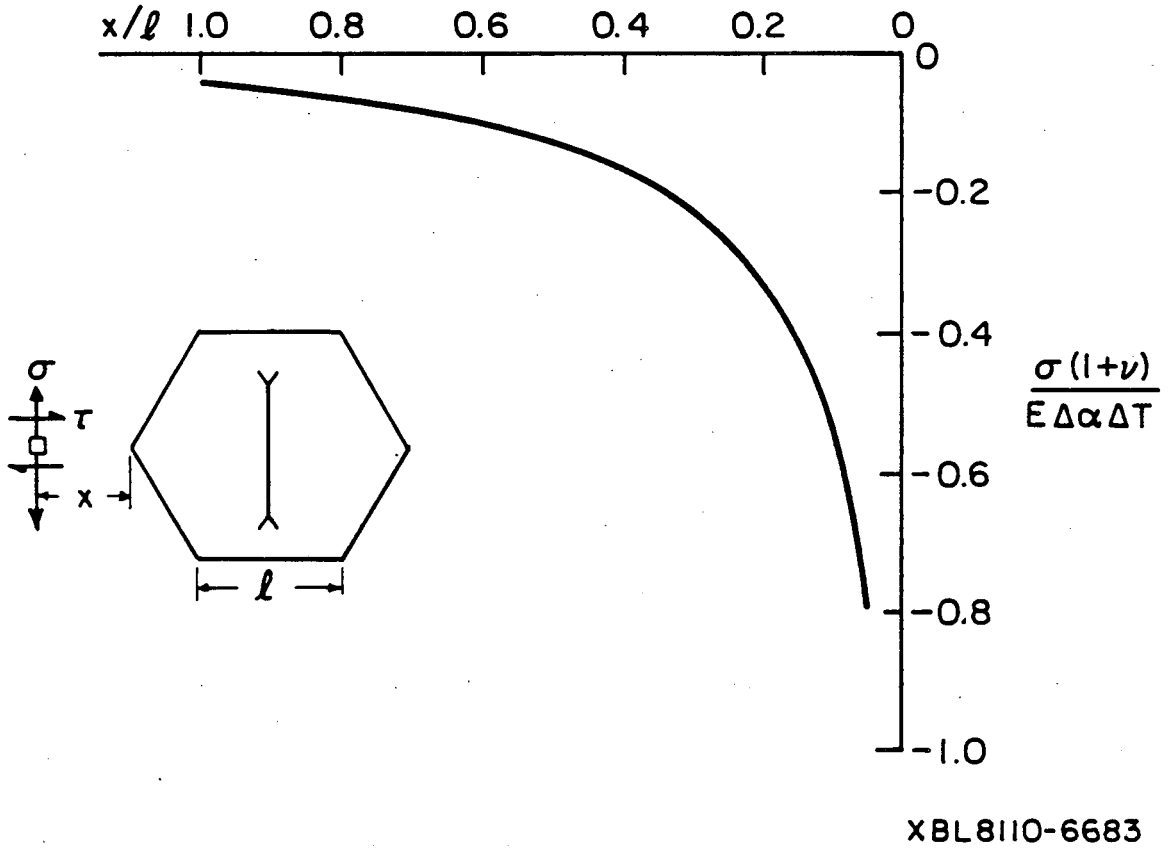

Fig.5.3a

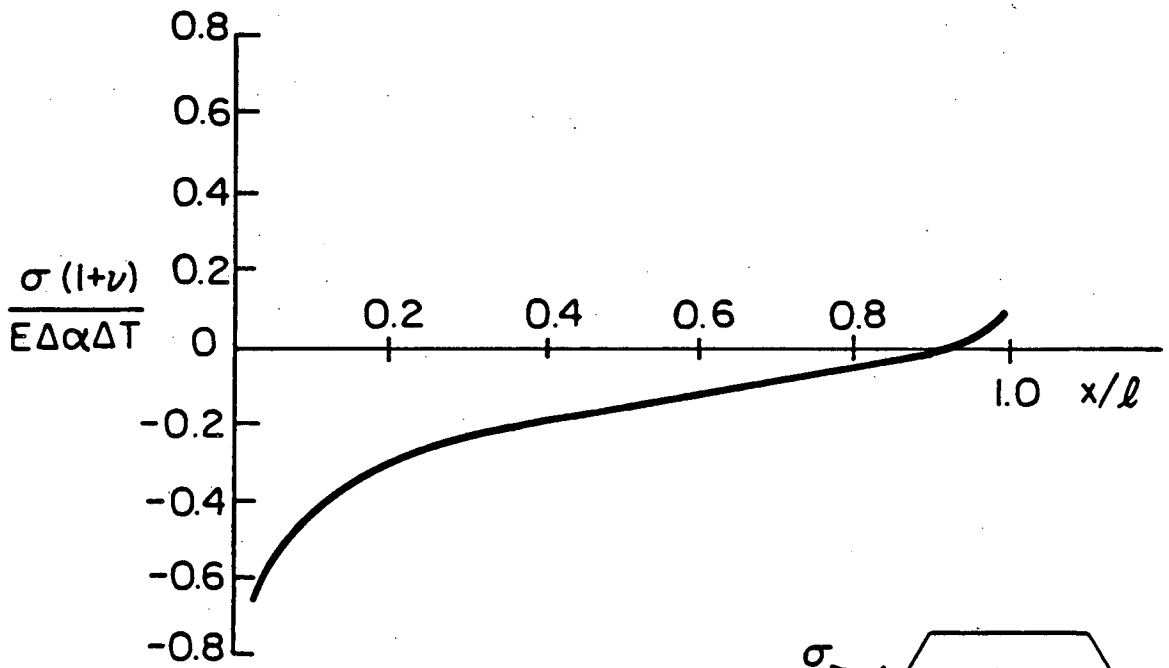

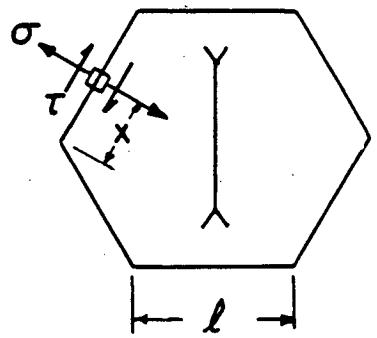

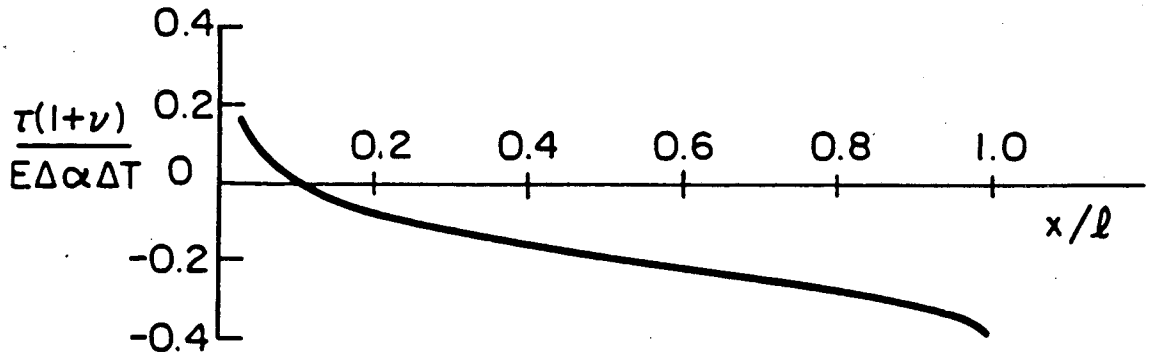

XBL8110-6681

Fig.5.3b

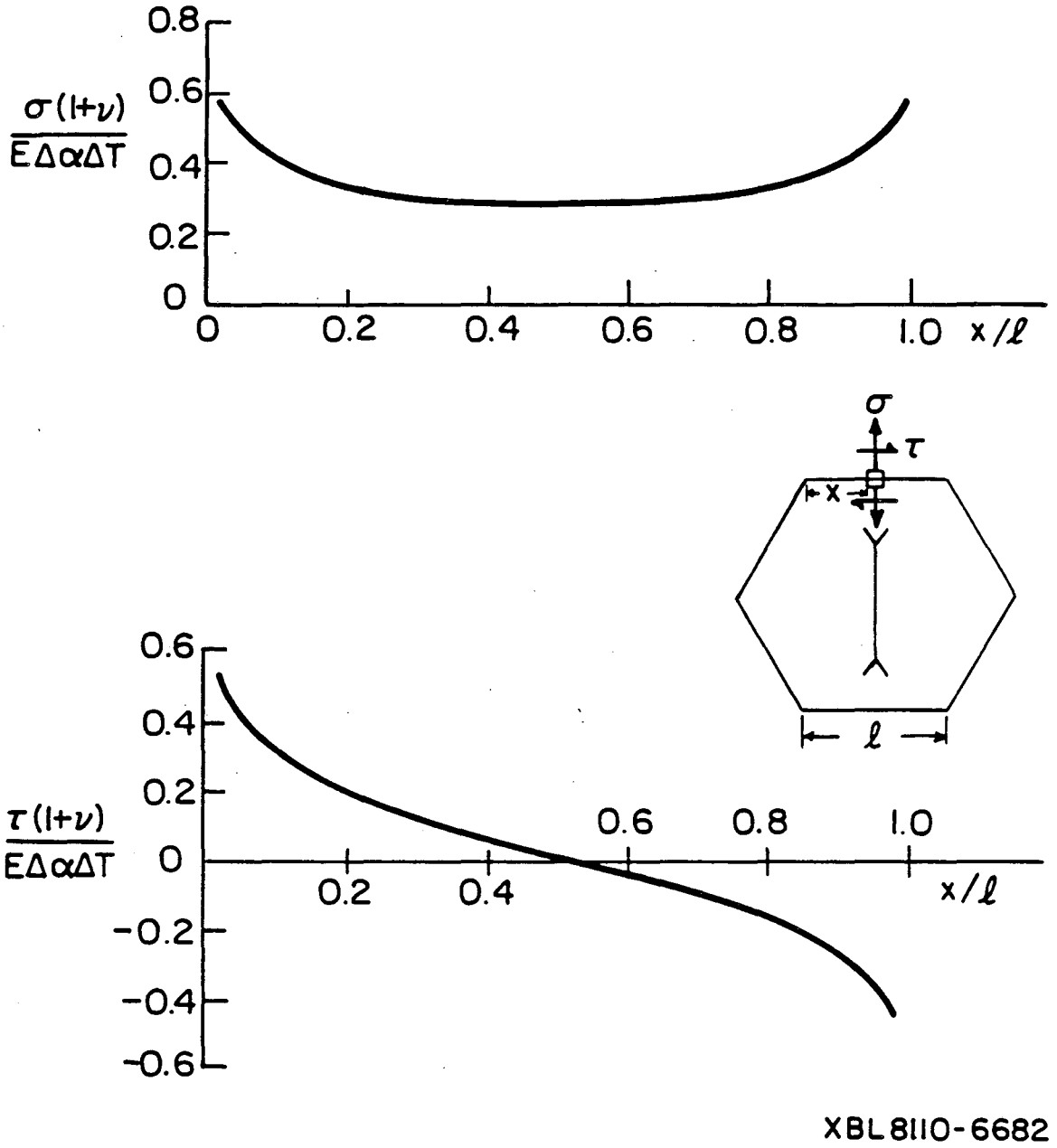
0.8
0.6
0.4
0.2
0
σ(1+ν)/EΔαΔT
0
0.2
0.4
0.6
0.8
1.0
x/ℓ
σ
τ
x
ℓ
0.6
0.4
0.2
0
-0.2
-0.4
-0.6
τ(1+ν)/EΔαΔT
0.2
0.4
0.6
0.8
1.0
x/ℓ
XBL8110-6682

Fig.5.3c

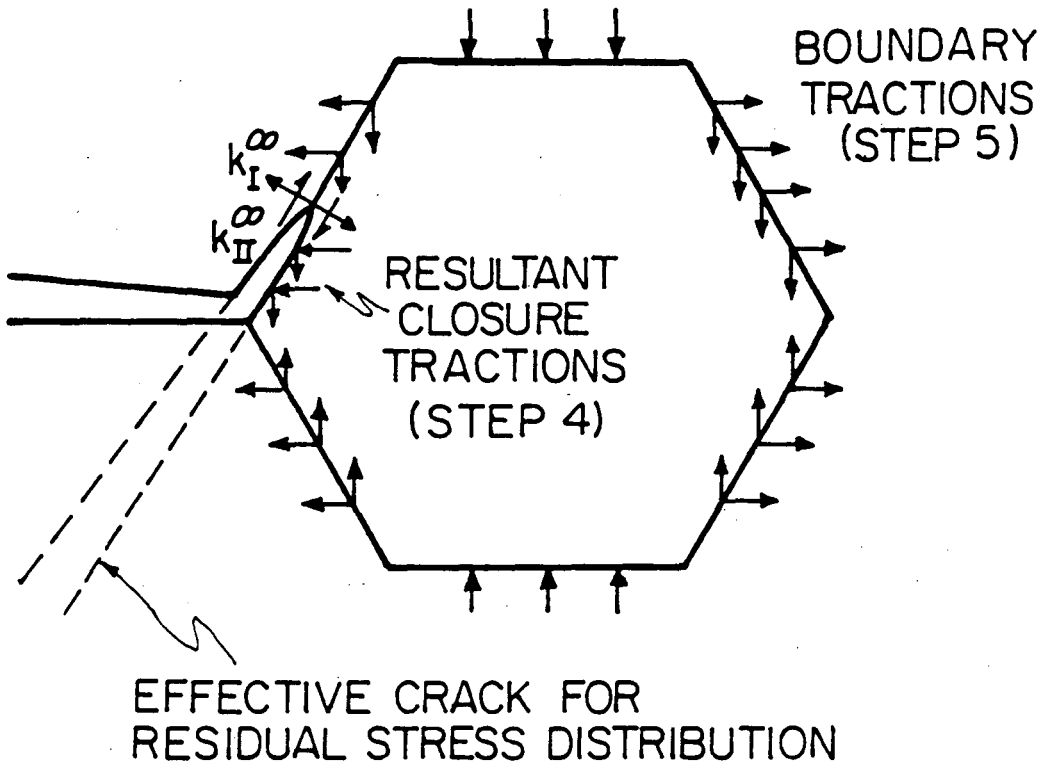
BOUNDARY
TRACTIONS
(STEP 5)
k_I^∞
k_{II}^∞
RESULTANT
CLOSURE
TRACTIONS
(STEP 4)
EFFECTIVE CRACK FOR
RESIDUAL STRESS DISTRIBUTION
XBL8111-6953

Fig.5.4

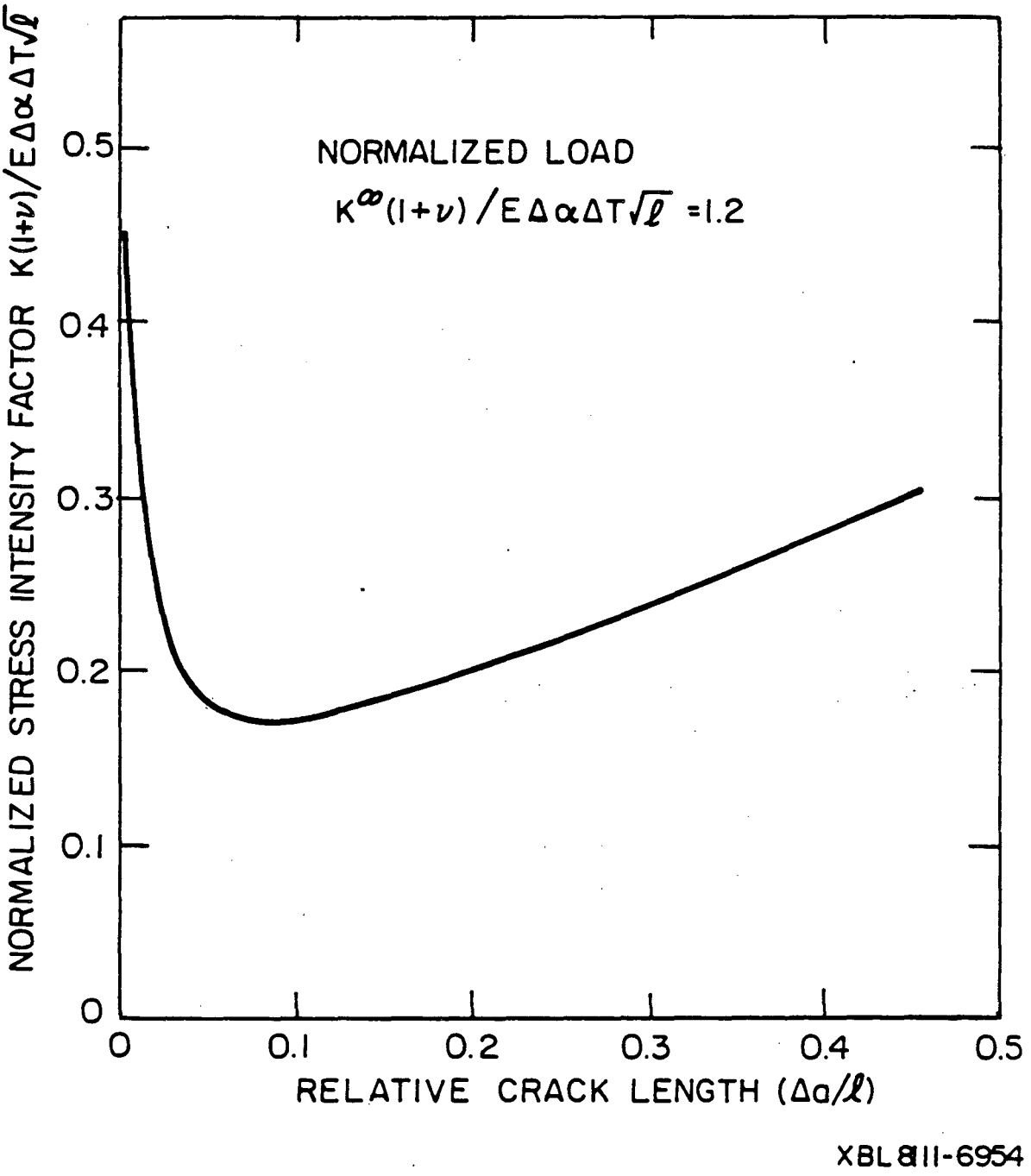
NORMALIZED LOAD
$K^{\infty}(1+\nu)/E\Delta\alpha\Delta T\sqrt{\ell}$ =1.2
NORMALIZED STRESS INTENSITY FACTOR $K(1+\nu)/E\Delta\alpha\Delta T\sqrt{\ell}$
RELATIVE CRACK LENGTH ($\Delta a/\ell$)
0
0.1
0.2
0.3
0.4
0.5
XBL 811-6954

Fig.5.5

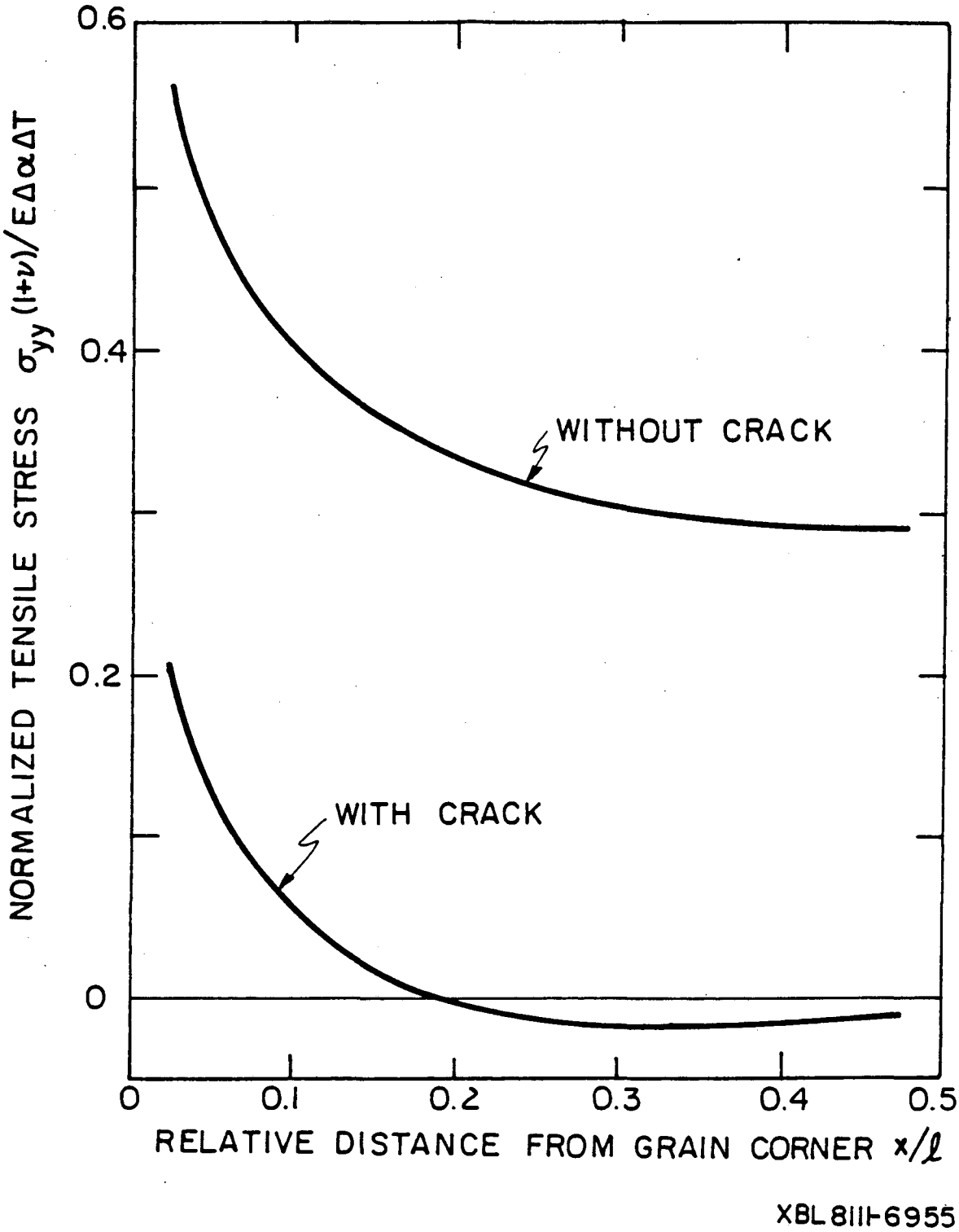
0.6
0.4
0.2
0
NORMALIZED TENSILE STRESS $\sigma_{yy}(1+\nu)/E\Delta\alpha\Delta T$
WITHOUT CRACK
WITH CRACK
0
0.1
0.2
0.3
0.4
0.5
RELATIVE DISTANCE FROM GRAIN CORNER x/ℓ
XBL 8111-6955

Fig.5.6

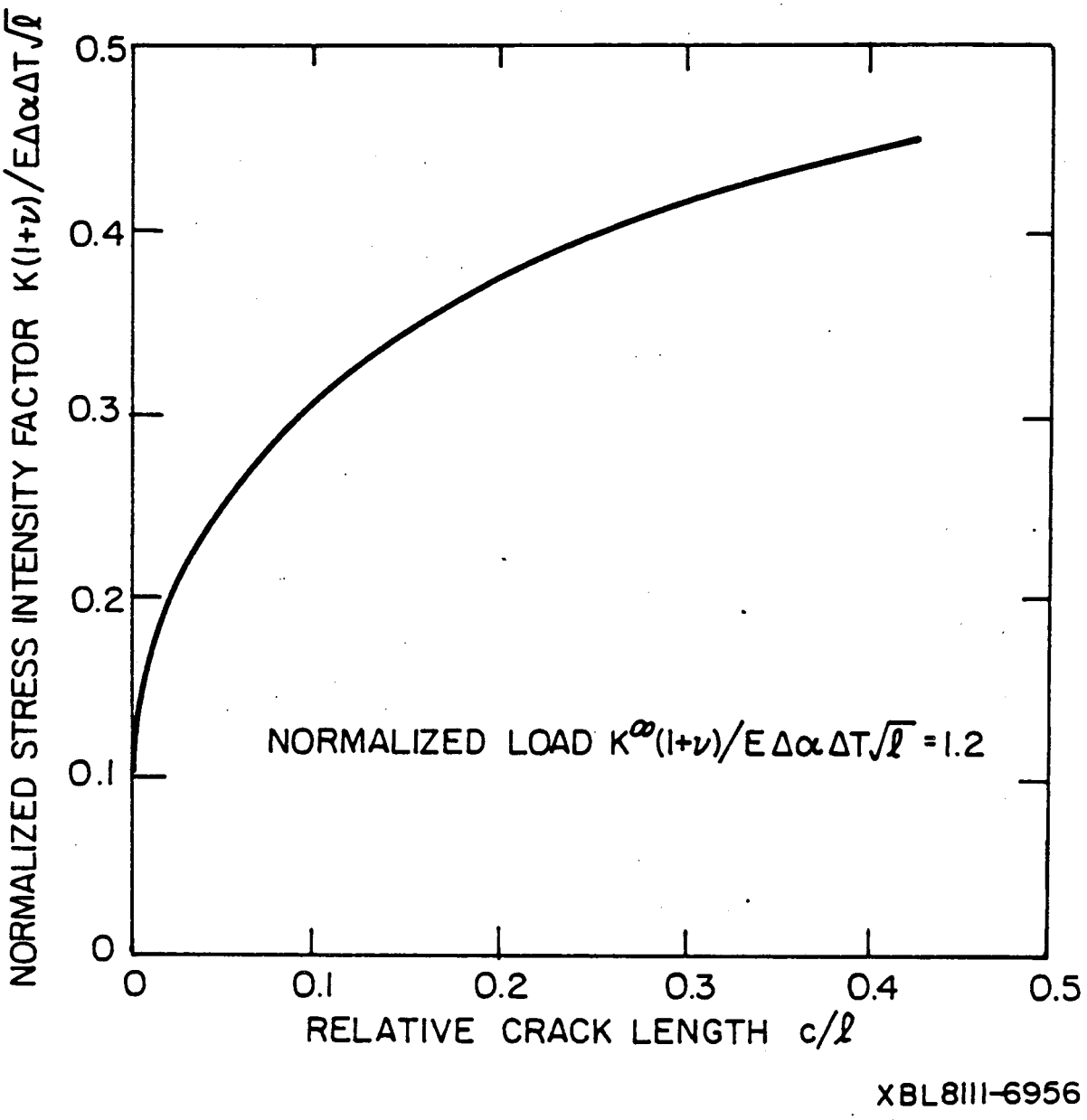
NORMALIZED STRESS INTENSITY FACTOR $K(1+\nu)/E\Delta\alpha\Delta T\sqrt{\ell}$
0.5
0.4
0.3
0.2
0.1
0
NORMALIZED LOAD $K^{\infty}(1+\nu)/E\Delta\alpha\Delta T\sqrt{\ell} = 1.2$
0
0.1
0.2
0.3
0.4
0.5
RELATIVE CRACK LENGTH c/ℓ
XBL8111-6956

Fig.5.7

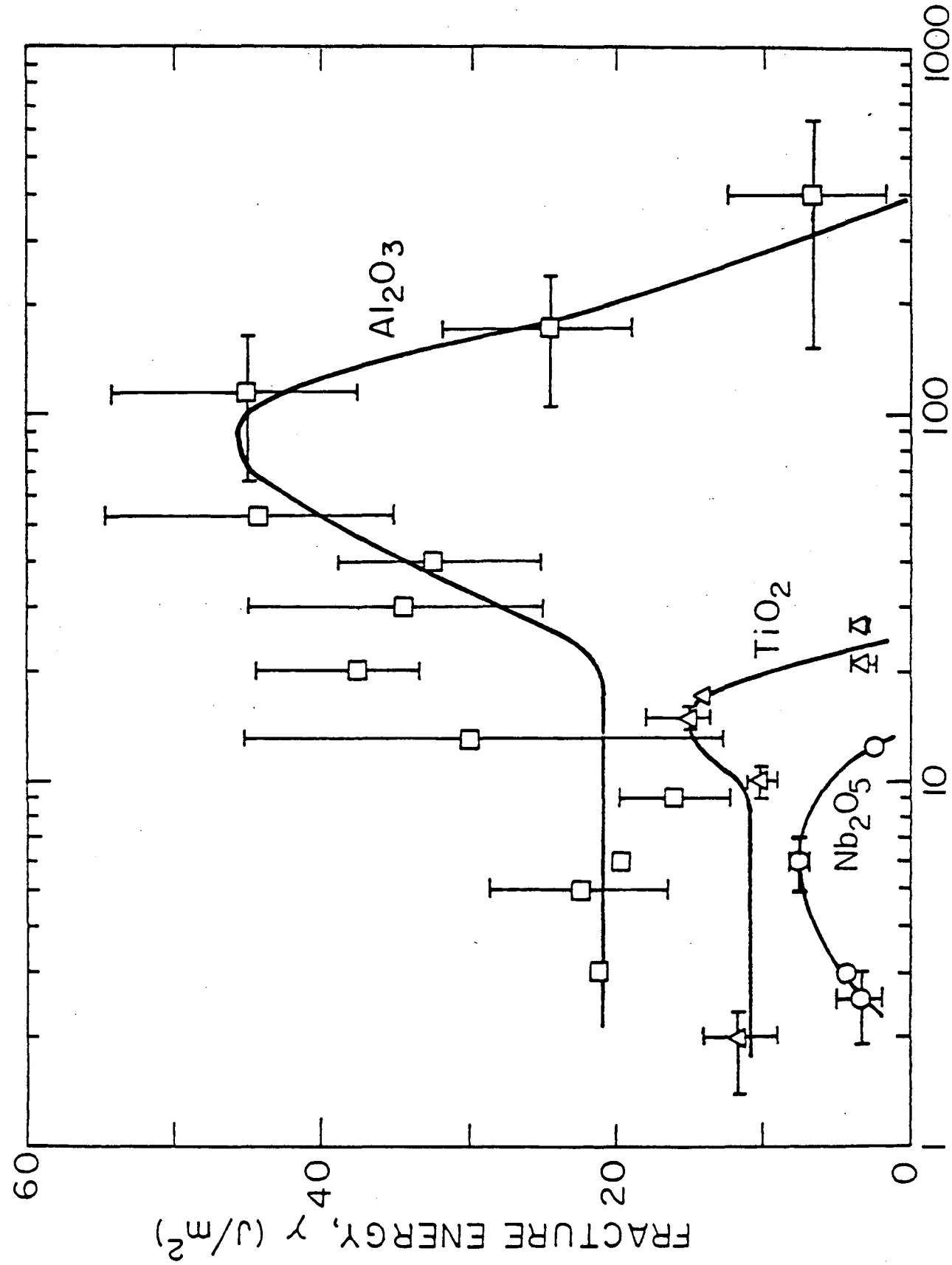

XBL8111-6951

Fig.5.8

6. Mechanics of Microcrack Toughening

6.1. Introduction

In single phase anisotropic polycrystalline materials, the occurrence of microcracking is associated with the microstructural residual stresses arising from thermal contraction mismatch among randomly oriented grains. In the presence of a macrocrack subject to load, the crack tip stress field induces discrete microcracks at the nearby boundary facets to form a microcrack process zone. This process zone is expected to modify the fracture toughness [1-16]. In particular, the microcracked process zone is more compliant than the un-microcracked region [1,16]. Hence, the crack tip stress singularity is relaxed, rendering an increase in toughness. However, the microcracks adjacent to the macrocrack tip deteriorate the local fracture resistance of the medium and thus, partially counteract the compliance toughening [16].

An important characteristic of the microcrack toughening process is the existence of resistance(R) curve behavior [9,12-15] (Fig. 6.1), i.e. the fracture resistance, G_c, is a monotonically increasing function of the crack tip advance distance Δa, i.e. $G_R(\Delta a)$, rather than a single-valued parameter. Several experimental observations [2,14,15] of prominent R-curve behavior have been reported. Yet the basis for its existence has not been well established and confusion often arises among experimental toughness measurements obtained with different tests [22-29] (e.g. notch beam and double cantilever beam tests) which monitor fracture instability at different stages of crack propagation. Furthermore, most of the theoretical analyses [7,8,10,12] attempting to simulate microcrack toughening have not incorporated the R-curve effect.

A recently established continuum mechanics description [17,18] of martensitic transformation toughening [19,20] has features similar to microcrack toughening: specifically, the existence of nonlinearity and hysteresis in the

stress/strain response of the process zone [18] (Fig. 3.2). Studies by McMeeking and Evans [17] and Budiansky et al [18] revealed that R-curve behavior is inherent in the martensitic transformation system, originating from the gradual unloading of the process zone wake which forms during crack propagation. The purpose of the present study is to establish a similar continuum mechanics description of microcrack toughening, as needed to quantify the toughening process, to identify the physical origin of the R-curve and to clarify the toughness measurements obtained with various tests. For this purpose, the nonlinear characteristic of a microcracking medium is analysed. The fracture energies may then be calculated both at the initiation of crack propagation and at the steady-state crack propagation stage, corresponding to the two extremities on the R-curve. Correlations between the results of the theoretical analysis and experimental data of several noncubic ceramics are also presented.

6.2. Nonlinear Characteristics of a Microcracking Medium

Pertinent to the macrocrack tip stress state, the nonlinear stress/strain characteristics of the microcrack zone are constructed on the overall strain response of a microcracking medium subject to a uniform plane-strain stress field (with principal stresses $\sigma_1 > \sigma_2$, $\sigma_1 > 0$ and $\sigma_3 = \nu(\sigma_1 + \sigma_2)$. While parallel analyses have been performed in section 4, based on a two-dimensional stress model, a few modifications are required for the present system.

From the discussion in section 4, it has been suggested that, in generalizing the analysis from two-dimensional to three-dimensional, the relations of the elastic moduli $\bar{E}$ and $\bar{\nu}$ above the microcracking threshold $\sigma_1 > \sigma_a^c$ given in equation (4.13) remains valid,

$$\bar{E}/E = \bar{\nu}/\nu = 1 + \gamma - B\sigma_1/\sigma_R \tag{6.1}$$

where

$$B=2gl^3m/9 \tag{6.2}$$

$$\gamma=B\sigma_a^c/\sigma_R=B(\sqrt{l_c^s/l}-1) \tag{6.3}$$

except that B will be larger than predicted from the two-dimensional analysis.

The constitutive equations for the principal strains ε_1, ε_2 and ε_3 can be expressed in terms of the elastic moduli as,

$$\begin{aligned}\varepsilon_1&=[\sigma_1-\bar{\nu}(\sigma_2+\sigma_3)]/\bar{E}\\ \varepsilon_2&\equiv[\sigma_2-\bar{\nu}(\sigma_1+\sigma_3)]/\bar{E}\\ \varepsilon_3&=0\end{aligned} \tag{6.4}$$

Consequently, by substituting equation (6.1) into equation (6.4), the strains become

$$\begin{aligned}e_1&=s_1\frac{1-(k+k')\nu(1+\gamma-Bs_1)}{1+\gamma-Bs_1}\\ e_2&=s_2\frac{1+(1+k'/k)\nu(1+\gamma-Bs_2/k)}{1+\gamma-Bs_2/k}\\ e_3&=0\end{aligned} \tag{6.5a}$$

where

$$\begin{aligned}s_i&=\sigma_i/\sigma_R\\ e_i&=\varepsilon_i(1+\nu)/\Delta\alpha\Delta T\\ k&=\sigma_2/\sigma_1\\ k'&=\sigma_3/\sigma_1=\bar{\nu}(\sigma_1+\sigma_2)/\sigma_1=(1+k)\bar{\nu}\end{aligned} \tag{6.5b}$$

Some numerical results obtained from equation (6.5) are shown in Fig. 6.2. It is apparent that, during loading ($\partial\sigma/\partial\varepsilon>0$) above the microcracking threshold ($\sigma_1>\sigma_a^c$), the stress/strain behavior is nonlinear. During unloading ($\partial\sigma/\partial\varepsilon<0$), the microcrack density maintains the value N_p obtained at the loading peak σ_p. Therefore, the stress/strain curve is linear in the unloading stage, as characterized by $\bar{E}_p$ and $\bar{\nu}_p$ obtained at σ_p. Hence, in the absence of unloading transients, the stress/strain trajectory exhibits clock-wise hysteresis (Fig. 6.3). The area enclosed by the hysteresis equals the strain energy dissipation of the external load, as the medium is completely unloaded. Hence, the first loading cycle is an irreversible process.

6.3. Mechanics of Microcrack Toughening

The macrocrack tip stress field induces microcracking at nearby grain facets to form a microcrack zone around the macrocrack. Because of the non-linear characteristic and stress/strain hysteresis of the microcrack zone, the fracture resistance is modified, giving rise to microcrack toughening.

The model used here to describe microcrack toughening comprises a solid medium composed of anisotropic grains of uniform size, with a semi-infinite crack under plane-strain mode I loading (Fig. 6.4). The crack tip stress field prior to microcrack zone formation can be expressed in terms of its principal components as

$$\sigma_1 = \frac{K_I}{\sqrt{2\pi r}} \cos\frac{\vartheta}{2}\left(1+\sin\frac{\vartheta}{2}\right)$$
$$\sigma_2 = \frac{K_I}{\sqrt{2\pi r}} \cos\frac{\vartheta}{2}\left(1-\sin\frac{\vartheta}{2}\right) \qquad (6.6)$$
$$\sigma_3 = \frac{K_I}{\sqrt{2\pi r}} 2\nu\cos\frac{\vartheta}{2}$$

where K_I is the stress intensity factor and r, ϑ are the polar coordinates.

The microcrack zone structure and the mechanics of toughening are dependent upon the history of macrocrack evolution. Suppose the macrocrack is originally in a medium free of microcracks. As the load is gradually applied, a frontal microcrack zone is induced in a region ahead of the crack tip where the stress field concentrates. In turn, the microcrack zone modifies the crack tip stress field. When K_I exceeds the apparent toughness, crack propagation initiates and a microcrack zone wake forms (Fig. 6.5), in which the volume elements are gradually unloaded ($\partial\sigma/\partial a < 0$). Due to the hysteresis behavior associated with these elements, the stress and strain fields are further modified, such that K_I must be increased to sustain the crack propagation, thus giving rise to R-curve behavior. In this study, we focus on two distinctive crack propagation stages: initiation of crack propagation and steady-state crack propaga-

tion (Fig. 6.1).

6.3.1. Initiation of Crack Propagation

The configuration of the system at the initiation stage is shown schematically in Fig. 6.6. The macrocrack is originally in a microcrack-free medium and gradually loaded to the crack propagation point ($K_I=K_c^s$). The microcrack zone is enclosed by the boundary on which the maximum principal stress σ_1 equals the critical stress σ_a^c for microcrack induction. Close to the crack tip, the stress field varies rapidly and the microcrack density is expected to reach a saturation value N_s in a zone around the macrocrack tip (Fig. 6.6).

The fracture toughness K_c^s is modified by the microcrack zone in two aspects. First, the microcracks adjacent to the crack tip deteriorate the load-bearing ability of the local medium and reduce the fracture toughness. The amount of deterioration can be approximated as [16,30]

$$K_c^0 \approx K_c^i(1-N_s/g) \tag{6.7}$$

where K_c^i is the intrinsic toughness of a microcrack-free medium, K_c^0 is the degraded toughness (which also characterizes the crack tip stress field) and N_s/g is the fraction of facets microcracked in the saturation zone.

Meanwhile, the stress and strain fields are modified by the presence of the microcrack zone. Since the material response is linear both in the unmicrocracked region outside the microcrack zone and in the saturation zone where the microcrack density is constant, stress intensity factors can be defined in each region (Fig. 6.6). The stress intensity K_I^s, which chacterizes the linear field in the unmicrocracked region remote from the crack tip, is the stress intensity factor applied on the system. Meanwhile, K_I^{tip} (in the saturation zone) is experienced by the crack tip and dictates crack propagation ($K_I^{tip}=K_c^0$). As each volume element in this system has experienced an increasing strain, the path independent J-integral [21] can be applied.

$$J=\int_{\Gamma}(Wn_x-\sigma_{ij}n_j u_{i,x})dS \tag{6.8}$$

where

$$W=\int_0^{\varepsilon}\sigma_{ij}\,d\,\varepsilon_{ij} \tag{6.9}$$

$\vec{u}$ is the displacement vector and $\vec{n}$ is the unit normal to the contour Γ encircling the crack tip. If Γ is chosen in the unmicrocracked region,

$$J=(1-\nu^2)(K_I^s)^2/E \tag{6.10}$$

Whereas in the saturation zone,

$$J=(1-\bar{\nu}_s^2)(K_I^{tip})^2/\bar{E}_s \tag{6.11}$$

where $\bar{E}_s$ and $\bar{\nu}_s$ are the elastic moduli pertinent to the saturation zone, which can be obtained from equation (3.17) with $N\alpha^3$ replaced by $N_s l^3/8$. Since J is independent of path, equations (6.10) and (6.11) can be combined. At the crack propagation condition, $K_I^{tip}=K_c^0$ and K_c^s is related to K_c^0 by

$$K_c^s=H(\nu,N_s,l)K_c^0 \tag{6.12}$$

where

$$H(\nu,N_s,l)\equiv\frac{1-(1-2N_s l^3/9)^2\nu^2}{(1-\nu^2)(1-2N_s l^3/9)}$$

Combining equations (6.7) and (6.12), the observed toughness K_c^s can be obtained as

$$K_c^s=H(1-N_s/g)K_c^i \tag{6.13}$$

or, in terms of fracture energies*

$$G_c^s=H^2(1-N_s/g)^2\,G_c^i \tag{6.14}$$

The grain size dependence of the fracture energy G_c^s at the initiation stage may be obtained if the unknown parameters are estimated as follows. The structure of the saturation zone is not well known. From the analysis in section 5, it is believed that, at the fracture instability ($K=K_c$), only those facets adja-

---

*$G=(1-\nu^2)K^2/E$

cent to the macrocrack tip subject to residual tension are susceptible to discrete microcracking. Adjacent facets subject to residual compression remain intact until fractured by the extension of the macrocrack. Thus, the microcrack density adjacent to the macrocrack tip is expected to saturate at $N_s \sim g/2$. Moreover, since the saturation zone consists of microcracks on adjacent facets, the saturation zone size h_s is expected to be approximately equal to the facet size l. Poisson's ratio ν of the unmicrocracked medium is taken to be $\nu=1/4$, representative of most ceramics. From section 3, the effective microcrack density N* is expected to be larger than predicted with N=0.5g where $g \sim 3/l^3$. Thus, an estimated $N^* \sim 0.5g^* = 9/4l^3$ is taken. Replacing these estimations into equation (6.13), it is seen that the toughening effect at this stage is quite small,

$$G_c^s \approx 1.1\, G_c^i \tag{6.15}$$

It is also noted that the toughening is independent of the grain size R, a result which is not influenced by the estimations adopted.

6.3.2. Steady-State Crack Propagation

In the steady-state crack propagation stage, the crack is imagined to have propagated extensively such that the fracture energy required to maintain the propagation has reached a steady-state value G_c^{ss}, pertinent to the asymptote in the R-curve (Fig. 6.1). The configuration of the system is also in steady-state, such that the microcrack zone wake and the saturation zone wake extend to $x=-\infty$, each with constant height (Fig. 6.7). The microcrack zone front is defined by $\partial\sigma_1/\partial a > 0$*, and the boundary is given by $\sigma_1 = \sigma_a^c$. The microcrack zone wake, defined by $\partial\sigma/\partial a < 0$, has a constant half height h_m dictated by the conditions,

$$\sigma_1 = \sigma_a^c \quad \text{and} \quad \partial\sigma_1/\partial a = 0 \tag{6.16}$$

The microcrack density in the wake maintains the maximum value obtained at

*Under quasi-static crack propagation, $\partial\sigma/\partial a = -\partial\sigma/\partial x$.

the peak of $\sigma_1 = \sigma_p$.

Differences in fracture energy between the initiation stage and the steady-state stage, due to the presence of the semi-infinite microcrack zone wake, can be calculated from energy balance considerations. In the steady-state, as the crack tip propagates forward by an increment da, the stress and strain fields translate in unison. This translation is equivalent to the creation of an extra region of microcrack zone, of width da, at x=-∞, which has been completely unloaded. A strain energy dissipation is associated with this process. From the energy balance relation given by Budiansky et al [18], the apparent fracture energy G_c^{ss} in the steady-state is

$$G_c^{ss} = G_c^{tip} + 2\int_0^{h_m} U(y)dy \tag{6.17}$$

where G_c^{tip} is the fracture resistance of the crack tip,

$$G_c^{tip} = \frac{(1-\bar{\nu}_s^2)(K_c^{tip})^2}{\bar{E}_s} = G_c^s \tag{6.18}$$

and U(y) is the residual energy density (the energy dissipation associated with the hysteresis in the volume elements at height y and x=-∞). In the unmicrocracked region remote from the macrocrack,

$$G_c^{ss} = (1-\nu^2)(K_c^{ss})^2 / E \tag{6.19}$$

where K_c^{ss} is the apparent toughness, characterizing the remote stress field.

As the nonlinear stress and strain fields in the microcrack zone are unknown at present, the microcrack zone height is estimated using two bounds. First, the nonlinear stress field in the zone is assumed to be bounded by two linear elastic stress fields, one characterized by the applied stress intensity factor K^{ss} and the other characterized by the crack tip stress intensity factor K^{tip} (Fig. 6.7)*. The normalized principal stresse sup tip at height y from x=-∞

The studies of Budiansky et al [18] reveal that, for the transformation problem, the zone height is dictated by the intermediate stress intensity factor, $K=K^{tip}+(K^{ss}-K^{tip})/2$

to x=+∞ are shown in Fig. 6.8. The maximum in the curve σ_p corresponds to the peak load experienced by the volume element at height y and x=-∞;

$$\sigma_p \approx K/2\sqrt{y} \tag{6.20}$$

where K can be either K^{ss} or K^{tip}.

Furthermore, from Fig. 6.8, it is seen that the ratio $k=\sigma_2/\sigma_1$ varies from k~1 at x=+∞ to k~1/3 at x~y/5 (where $\sigma_1=\sigma_p$). To simplify the calculation of U(y), k is assumed to be constant, whereupon the upper bound of U(y) is calculated with $K=K^{ss}$ and k=1 and the lower bound of U(y) is calculated with $K=K^{s}$ and k=1/3. Under plane strain and constant k conditions, the principal strains ε_1 and ε_2 are given in equation (6.5). The strain energy density U(y) consists of two components: one from the interaction between σ_1 and ε_1 and the other from σ_2 and ε_2*; thus,

$$U(y)=U_1(y)+U_2(y) \tag{6.21}$$

where

$$U_i(y)=\int \sigma_i \, d\varepsilon_i$$

and $U_1(y)$, $U_2(y)$ represent the areas enclosed by the hysteresis loop (Fig. 6.3). Replacing the curve between σ_a^c and σ_p in the hysteresis with a straight line, U(y) can be approximated as a triangular area. From equations (6.5) and (6.21), it follows that

$$U(y)=\frac{1+k}{2E}\sigma_a^c\sigma_p\left[\frac{1}{1+\gamma-\gamma\sigma_p/\sigma_a^c}\right. \tag{6.22}$$
$$\left.+2\nu^2\gamma(\sigma_p/\sigma_a^c)-1-2\nu^2\gamma\right]$$

The total strain energy dissipation involves the saturation zone and the microcrack zone;

$$2\int_0^{h_m} U(y)dy = 2\int_0^{h_s} U(y)dy + 2\int_{h_s}^{h_m} U(y)dy \tag{6.23}$$

*No shear components are involved since the stress field is given in principal components.

The strain energy dissipation in the saturation zone is simply,

$$2\int_0^{h_s} U(y)dy \approx 2U(h_s)h_s \tag{6.24}$$

since the saturation zone should be small. Replacing y in equation (6.20) by h_s and inserting σ_p in equation (6.22), the total strain energy becomes

$$2\int_0^{h_m} U(y)dy = \frac{1-\nu^2}{E}K^2\left[\frac{1+k}{4(1-\nu^2)}Q(\gamma,\upsilon,\nu)\right] \tag{6.25}$$

where

$$\upsilon = \frac{2\sigma_a^c\sqrt{h_s}}{K} \tag{6.26}$$

and

$$Q(\gamma,\upsilon,\nu) \equiv \frac{\gamma}{1+\gamma-\gamma/\upsilon} + 2\nu^2\gamma(1-2ln\ \upsilon) + \frac{2(1-\upsilon)}{1+\gamma} - \frac{2\gamma}{(1+\gamma)^2}\ln\left[(1+\gamma)\upsilon-\gamma\right] - (1-2\nu^2\gamma)(2-\upsilon) \tag{6.27}$$

Thus, the upper bound of the apparent fracture energy $(G_c^{ss})_U$ is given by combining equations (6.17), (6.18) and (6.25) with K=K^{ss} and k=1 as

$$(G_c^{ss})_U = (1-\frac{N_s}{g})^2H^2\left[\frac{Q}{2(1-\nu^2)}\right]^{-1}G_c^i \tag{6.28}$$

Similarly, the lower bound of the apparent fracture energy $(G_c^{ss})_L$ is obtained with K=K^{tip} and k=1/3 as

$$(G_c^{ss})_L = (1-\frac{N_s}{g})^2\left[H^2+\frac{Q}{3(1-\nu^2)}\right]G_c^i \tag{6.29}$$

The grain size dependence of the steady-state fracture energy G_c^{ss} may be obtained with the following estimations. From section 4, the parameter B is expected to be larger than predicted (B~2/3). Thus, an estimated B~1-2 is taken. From equation (6.3), γ can be expressed as a function of R/R_c^s;

$$\gamma = B(\sqrt{R_c^s/R}-1) \tag{6.30}$$

The parameter v can also be obtained as a function of R/R_c^s. From previous discussion, it may be assumed that the saturation zone size h_s is related to the

facet size l as

$$h_s = wl \tag{6.31}$$

At the threshold facet size l_c of microcrack zone formation ($l_c = 0.4 l_c^s$), the microcrack zone is expected to coincide with the saturation zone, so that

$$h_s = h_m = wl \tag{6.32}$$

From equation (6.20), it follows that

$$\frac{2\sigma_a^c \sqrt{h_m}}{K} = \frac{2\sigma_a^c \sqrt{wl_c}}{K} = 1 \tag{6.33}$$

Interting equation (4.6), w should satisfy

$$\frac{2\sigma_R \sqrt{w}}{K} = \frac{1}{\sqrt{l_c^s} - \sqrt{l_c}} \approx 2.7 \tag{6.34}$$

and v in equation (6.26) is obtained as

$$v \approx 2.7(1 - \sqrt{R/R_c^s}) \tag{6.35}$$

Inserting these estimates into equations (6.28) and (6.29), the upper and lower bounds of $_c^{ss}$ can be obtained as a function of R/R_c^s, as plotted in Fig. 6.9.

6.4. Discussion

The calculation of the fracture energies at the two extreme stages in the R-curve can be correlated with the experimental data of fracture energy, in several single phase noncubic ceramics; especially the grain size dependence. The correlation not only substantiates the present model and analysis, but also clarifies controversies about the exact grain size dependence of the fracture energy of noncubic ceramics, arising from data obtained with different tests (e.g. notch beam, double cantilever beam). The correlation is conducted only for $R < R_c^s$, since spontaneous microcracking is not considered in the present analysis. Furthermore, it is noticed that the formation of the microcrack zone is fully suppressed if $R < 0.4 R_c^s$* and the microcrack toughening mechanism is no

*see section 5

longer operative.

The fracture energy at the initiation of crack propagation as given in equation (6.15) is expected to conform to the experimental data obtained with most NB tests [22-27] where fracture instability is monitored at the initiation of fracture from a sawn notch (i.e. a frontal microcrack zone only). The general observation in these tests is that the toughening is not detected as seen from the Al_2O_3 data summarized [12] in Fig. 6.10. These results confirm the prediction of equation (6.15).

Meanwhile, the trends in the steady-state fracture energy with grain size plotted in Fig. 6.9 should conform to experimental data obtained with most DCB tests [22,23,28,29] which monitor the equilibrium of a crack after extensive quasi-static propagation (i.e. an extended microcrack zone), such as the data summarized [10] in Fig. 6.11. Comparison of these data with the predicted behavior in Fig. 6.9 shows that a good conformation is obtained (especially the unique features distinctive in the steady-state cracking stage). The toughening is quite significant (~100% enhancement) in the grain size range where toughening is expected ($0.4<R/R_c^s<1.0$). No toughening is observed at $R=R_c^s$ and $R=0.4R_c^s$. Furthermore, the experimental data lie closer to the predicted upperbound of G_c^{ss}, indicating that the linear stress field characterized by K^{ss} is a better approximation of the actual non-linear stress field.

It is substantiated that microcrack toughening derives from the nonlinear characteristic of the microcrack zone, and inherent in this process is an R-curve behavior arising from the stress/strain hysteresis in the microcracking medium (which dissipates additional strain energy when a microcrack zone wake gradually forms during crack propagation). Consequently, experimental measurements of fracture energy of microcracking materials using tests like NB, DCB, which monitor fracture instability at different stages during crack

propagation, are expected to vary. Moreover, chacteristics of the grain size dependence of the fracture energy of such materials can vary significantly if "fracture energy" is confined in a certain stage in the R-curve. For instance, the fracture energy at the initiation of the R-curve, as usually measured with the NB test, would exhibit no grain size dependence. Conversely, the fracture energy at the asymptote of the R-curve, as usually measured with DCB test, shows a pronounced toughening effect between $0.4R_c^s$ and R_c^s. Differences among tests should be discriminated accordingly. Ideally, it is appropriate to measure the complete R-curve. DCB tests which allow stepwise measurement of the fracture energy thus appear more desirable.

A continuum mechanics approach to analyse the microcrack toughening process has been presented which enables the calculation of the fracture energies at two extreme stages in the R-curve. Semi-quantitatively, the results reveal the dependence on various microstructural parameters, e.g. R, $\Delta\alpha$, ΔT, etc.. The analysis can be extended to incorporate a more accurate solution of the nonlinear stress and strain fields pertinent to the nonlinear microcracking medium. The nature of the saturation zone also needs to be studied. Moreover, analyses which incorporate the permanent strain effects associated with microcracking (e.g. higher strain energy dissipation in hysteresis) are expected to yield more toughening effect in the steady-state cracking stage.

REFERENCES

1. A. G. Evans, A. H. Heuer and D. L. Porter, "Fracture '77", vol.1, pp.529, edited by D. M. R. Taplin, Univ. of Waterloo Press, Waterloo, Ontario, Canada (1977).
2. R. G. Hoagland, C. W. Marschall, A. R. Rosenfield, G. Hollenberg and R. Ruh, Mater. Sci. Eng., 15, 1, 51 (1974).
3. C. C. Wu, S. W. Freiman, R. W. Rice and J. J. Mecholsky, J. Mater. Sci., 13, 12, 2659 (1978).
4. R. G. Hoagland, G. T. Hahn and A. R. Rosenfield, Rock Mech., 5, 2, 77 (1973).
5. R. G. Hoagland, J. D. Embury and D. J. Green, Scr. Metall., 9, 9, 907 (1975).
6. A. G. Evans, ibid., 10, 1, 93 (1976).
7. F. E. Buresch, "Fracture Mechanics of Ceramics", vol.4, pp.835, edited by R. C. Bradt, D. P. H. Hasselman and F. F. Lange, Plenum Press, N.Y. (1978).
8. W. Kreher and W. Pompe, J. Mater. Sci., 16, 3, 694 (1981).
9. R. G. Hoagland and J. D. Embury, J. Am. Ceram. Soc., 63, 7, 404 (1980).
10. R. W. Rice, S. W. Freiman and P. F. Becher, ibid., 64, 6, 345 (1981).
11. A. G. Evans and K. T. Faber, ibid., 64, 7, 394 (1981).
12. N. Claussen, B. Mussler and M. V. Swain, ibid., 65, 1, C-14 (1982).
13. B. Musller, M. V. Swain and N. Claussen, ibid., 65, 11, 566 (1982).
14. H. Hubner and J. Jillek, J. Mater. Sci., 12, 117 (1977).
15. R. Knehans and R. Steinbrech, J. Mater. Sci. Letters, 1, 327 (1982).
16. Y. Fu and A. G. Evans, Acta Met., 30, 1619 (1982).
17. R. M. McMeeking and A. G. Evans, J. Am. Ceram. Soc., 65, 5, 242 (1982).

18. B. Budiansky, J. Hutchinson and J. Lambropolous, Int. J. Solids & Structure, 19, 337 (1983).

19. A. G. Evans and A. H. Heuer, J. Am. Ceram. Soc., 63, 241 (1980).

20. F. F. Lange, J. Mater. Sci., 17, 225 (1982).

21. J. R. Rice, "Fracture", vol.2, pp.191, edited by H. Liebowitz, Academic Press, N.Y. (1968).

22. L. A. Simpson, J. Am. Ceram. Soc., 56, 11, 610 (1973).

23. B. J. Dalgleish, P. L. Pratt and J. Sanford, "Science of Ceramics", vol.8, pp.659, edited by P. Popper, The British Ceramic Soc., Stoke-on-Trent, England (1976).

24. P. L. Pratt,"Fracture '77", vol.3, pp.909, edited by D. M. R. Taplin, Univ. of Waterloo Press, Waterloo, Canada (1977).

25. A. G. Evans and G Tappin, Proc. Br. Ceram. Soc., 20, 275 (1972).

26. N. Claussen, P. Pabst and C. P. Lahmann, ibid., 25, 139 (1975).

27. R. F. Pabst, "Fracture Mechanics of Ceramics", vol.2, pp.556, edited by R. C. Bradt, D. P. H. Hasselman and F. F. Lange, Plenum Press, N.Y. (1974).

28. G. D. Swanson, J. Am. Ceram. Soc., 55, 1, 48 (1972).

29. S. W. Freiman, K. R. McKinney and H. L. Smith, pp.659 in Ref. 27.

30. J. Zwissler and A. Adams, "Fracture Mechanics of Ceramics", edited by R. C. Bradt, D. P. H. Hasselman, F. F. Lange and A. G. Evans, Plenum Press, N.Y. (1982). In press.

FIGURE CAPTIONS

6.1. Schematic of R-curve characteristic and microcrack zone configuration at different stages of crack propagation.

6.2. Nonlinear stress/strain curve of a microcracking medium subject to plane-strain biaxial loading.

6.3. Schematic illustrating the nonlinear characteristic and unloading hysteresis of the microcrack zone.

6.4. Schematic of the stress field around a semi-infinite crack.

6.5. Schematic illustrating the evolution of the microcrack zone configuration during crack propagation.

6.6. Schematics of (a) frontal microcrack zone and saturation zone, (b) the nonlinear stress field ahead of the crack tip, at the initiation of crack propagation.

6.7. Schematics of (a) extended microcrack zone and saturation zone, (b) the nonlinear stress field ahead of the crack tip, at the steady-state of crack propagation.

6.8. Distribution of principal components of a linear stress field around a crack.

6.9. Plot of the grain size dependence of fracture energies at the steady-state crack propagation stage.

6.10. NB values of fracture energy of Al_2O_3 vs grain size (after Ref. 12).

6.11. DCB values of fracture energy vs grain size for Al_2O_3, TiO_2 and Nb_2O_5 (after Ref. 10).

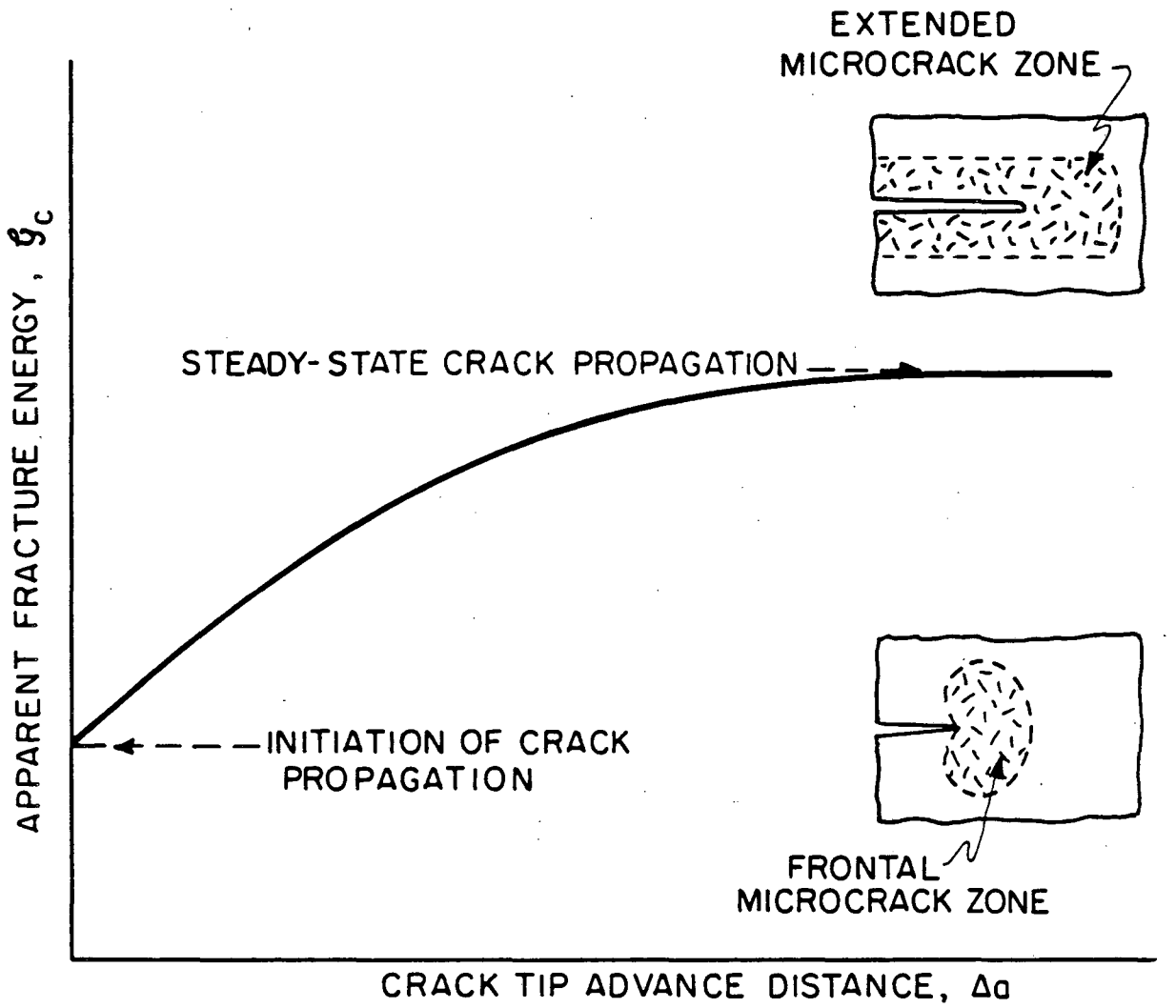
EXTENDED
MICROCRACK ZONE
STEADY-STATE CRACK PROPAGATION
APPARENT FRACTURE ENERGY, $\mathcal{G}_c$
INITIATION OF CRACK
PROPAGATION
FRONTAL
MICROCRACK ZONE
CRACK TIP ADVANCE DISTANCE, Δa
XBL 839-6339

Fig.6.1

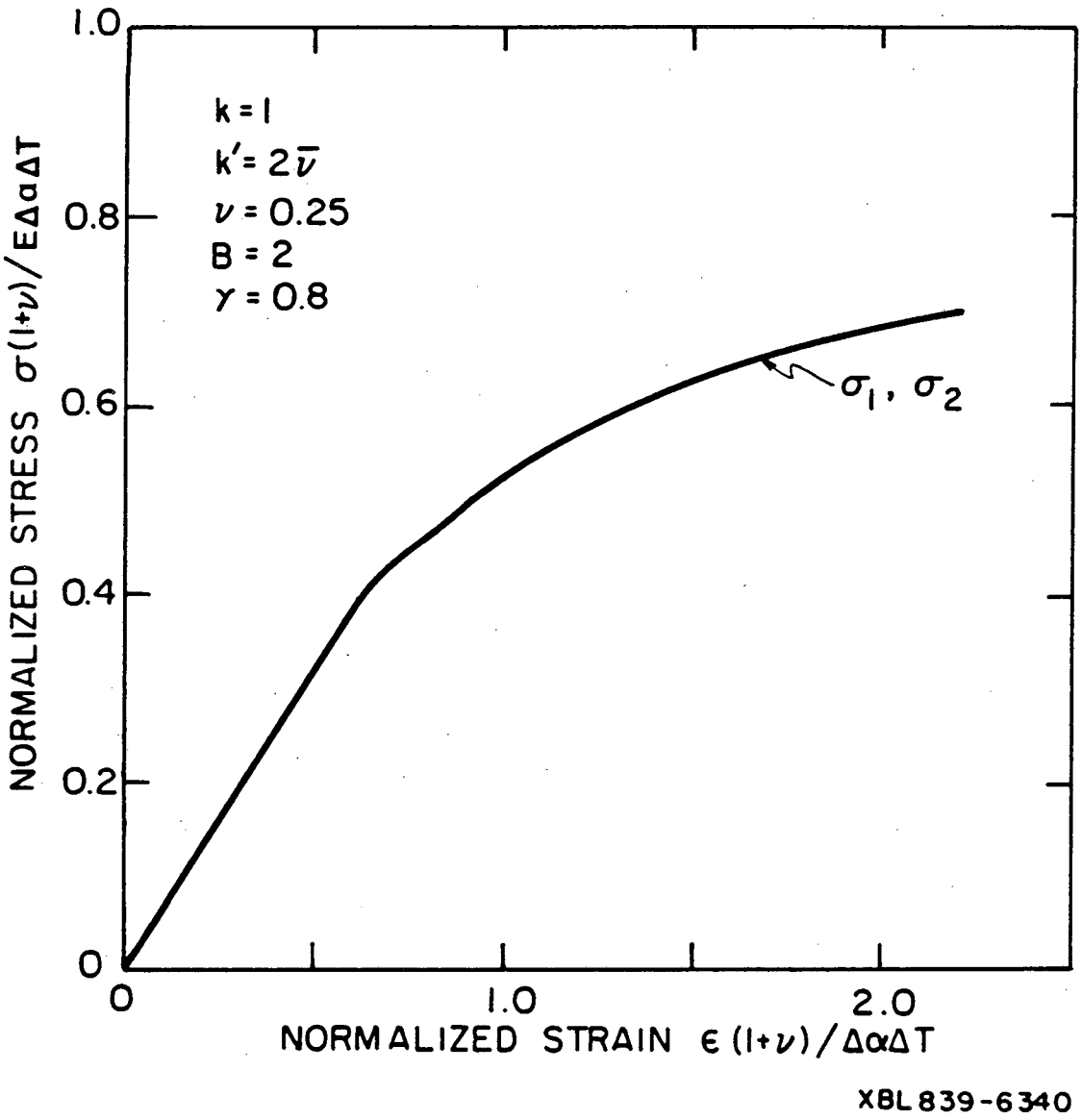
1.0
0.8
0.6
0.4
0.2
0
0
1.0
2.0
k = 1
k' = 2ν̄
ν = 0.25
B = 2
γ = 0.8
σ1, σ2
NORMALIZED STRESS σ(1+ν)/EΔαΔT
NORMALIZED STRAIN ε(1+ν)/ΔαΔT
XBL839-6340

Fig.6.2

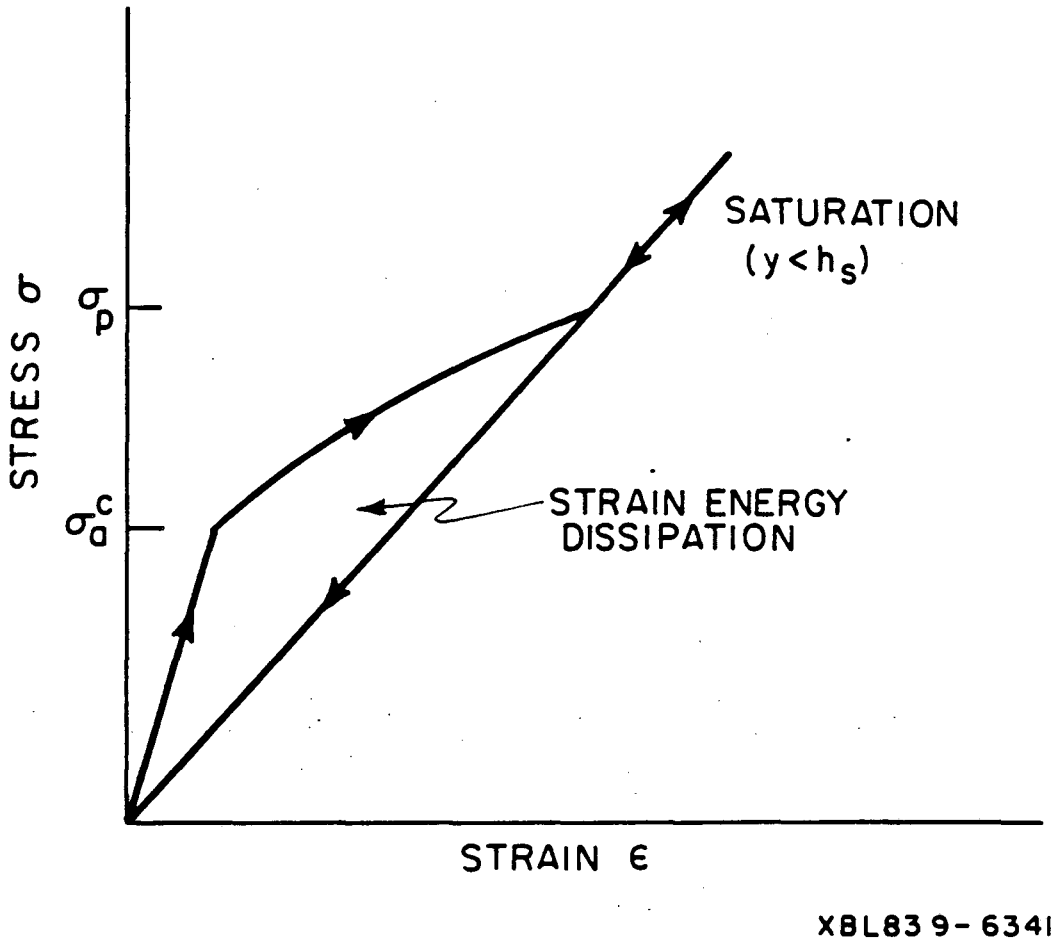
STRESS σ
q_p
q_a^c
SATURATION
(y < h_s)
STRAIN ENERGY
DISSIPATION
STRAIN ε
XBL839-6341

Fig.6.3

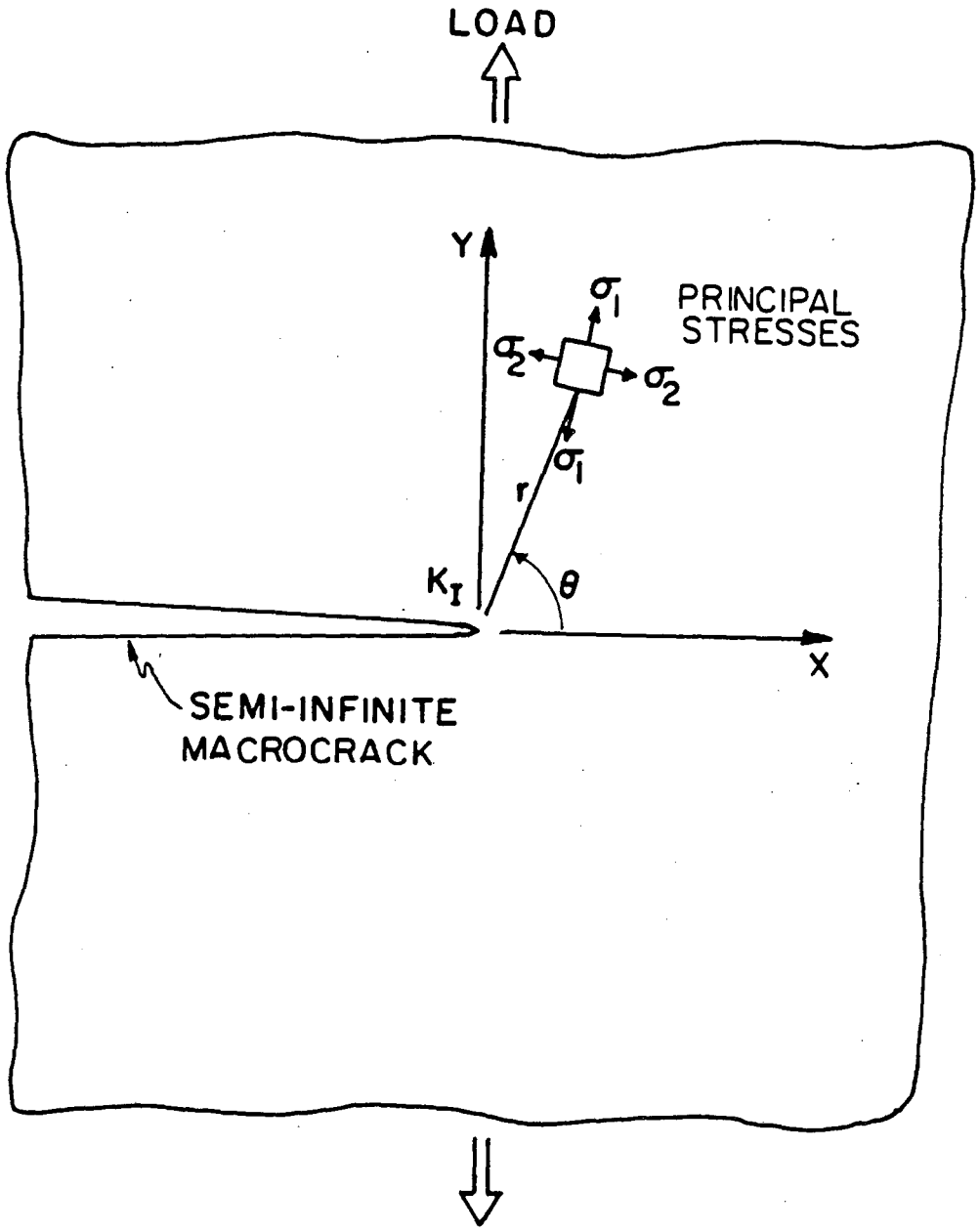

XBL839-6342

Fig.6.4

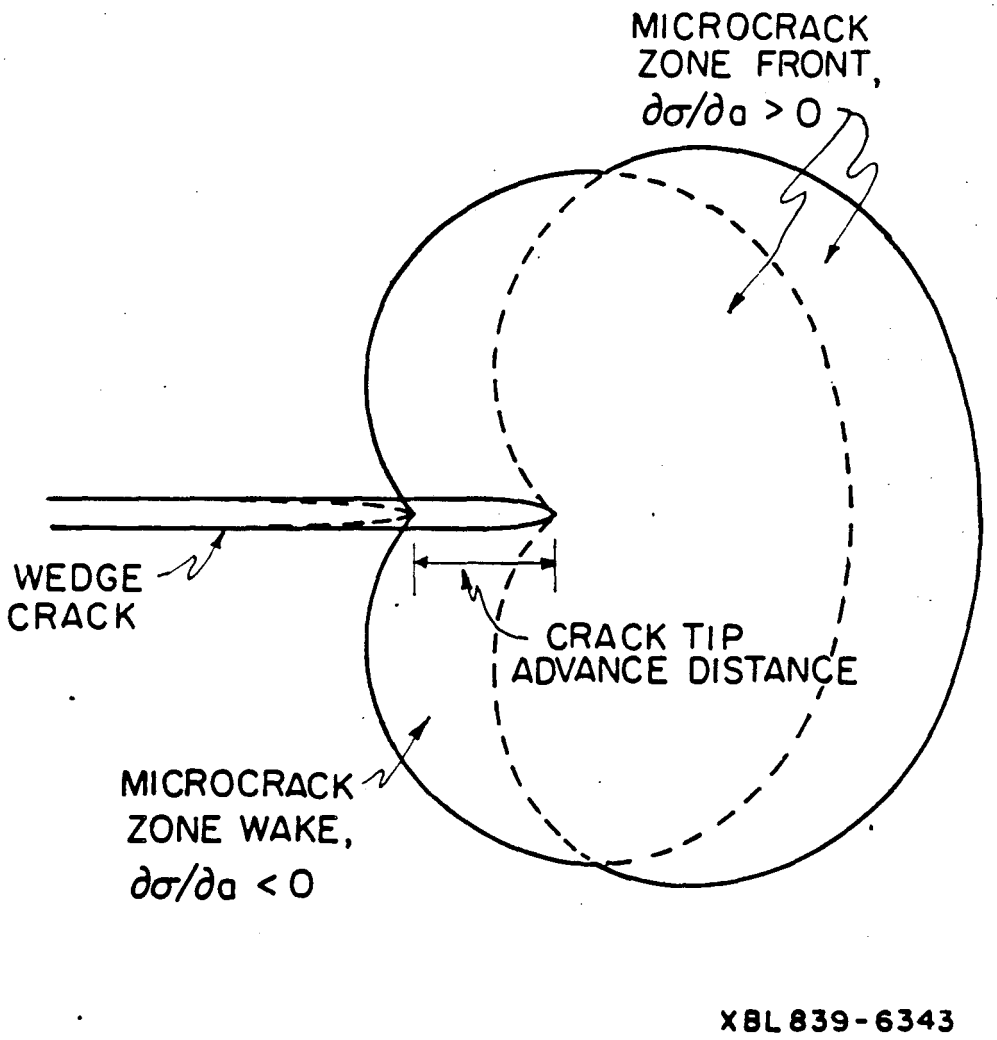

XBL 839-6343

Fig.6.5

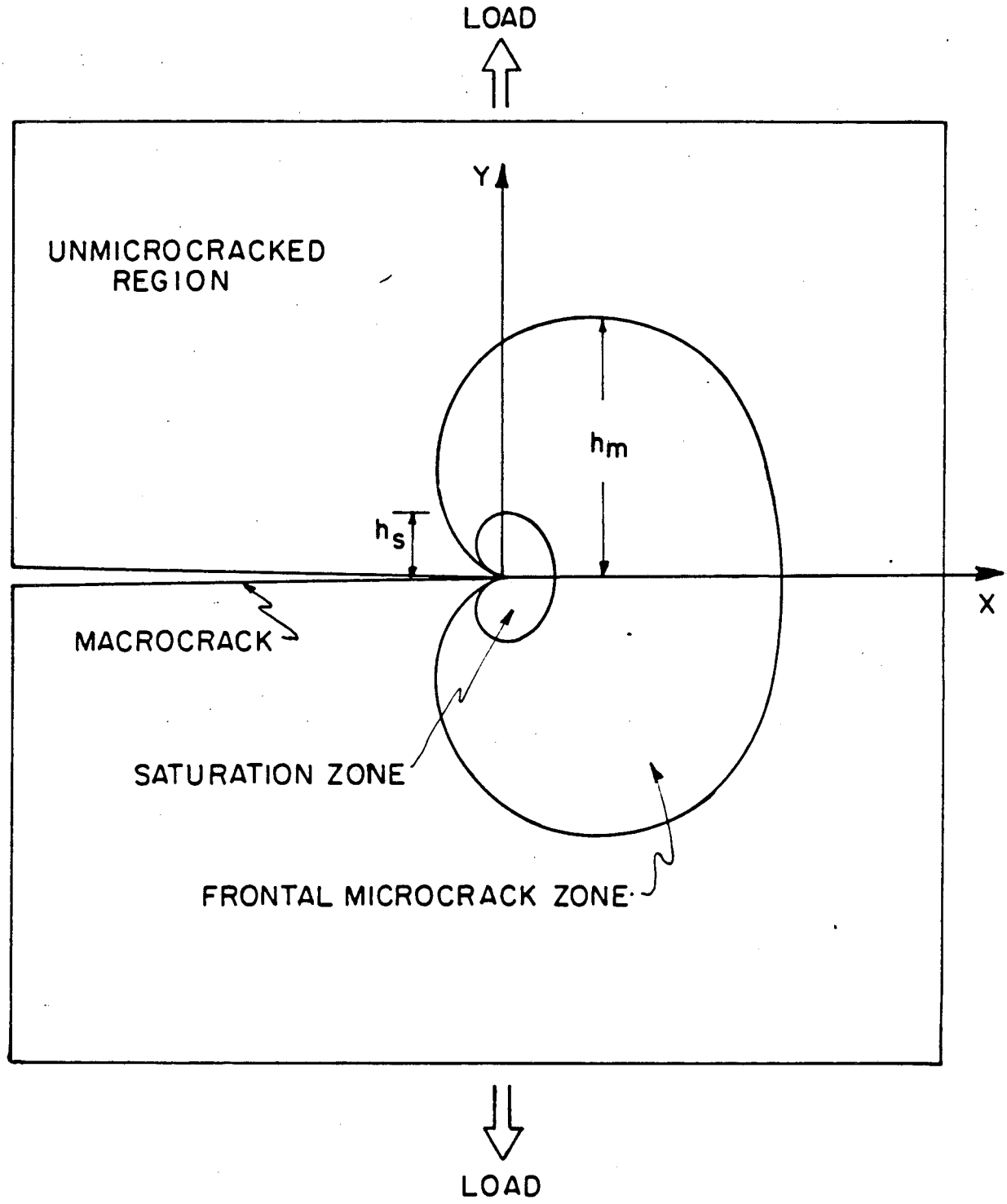

XBL 839-6349

Fig6.6a

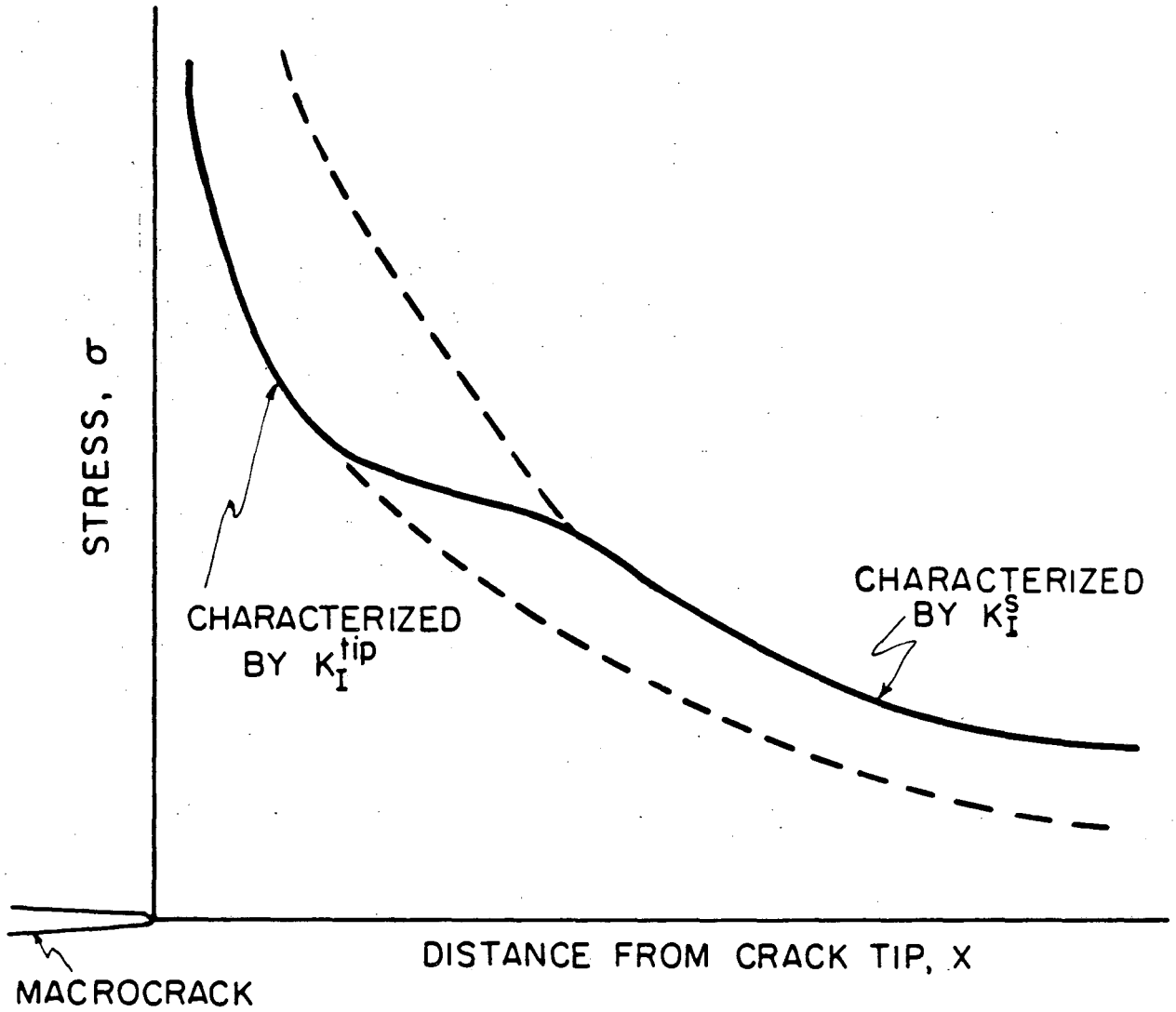
STRESS, σ
CHARACTERIZED BY K_I^{tip}
CHARACTERIZED BY K_I^S
DISTANCE FROM CRACK TIP, X
MACROCRACK
XBL839-6344

Fig.6.6b

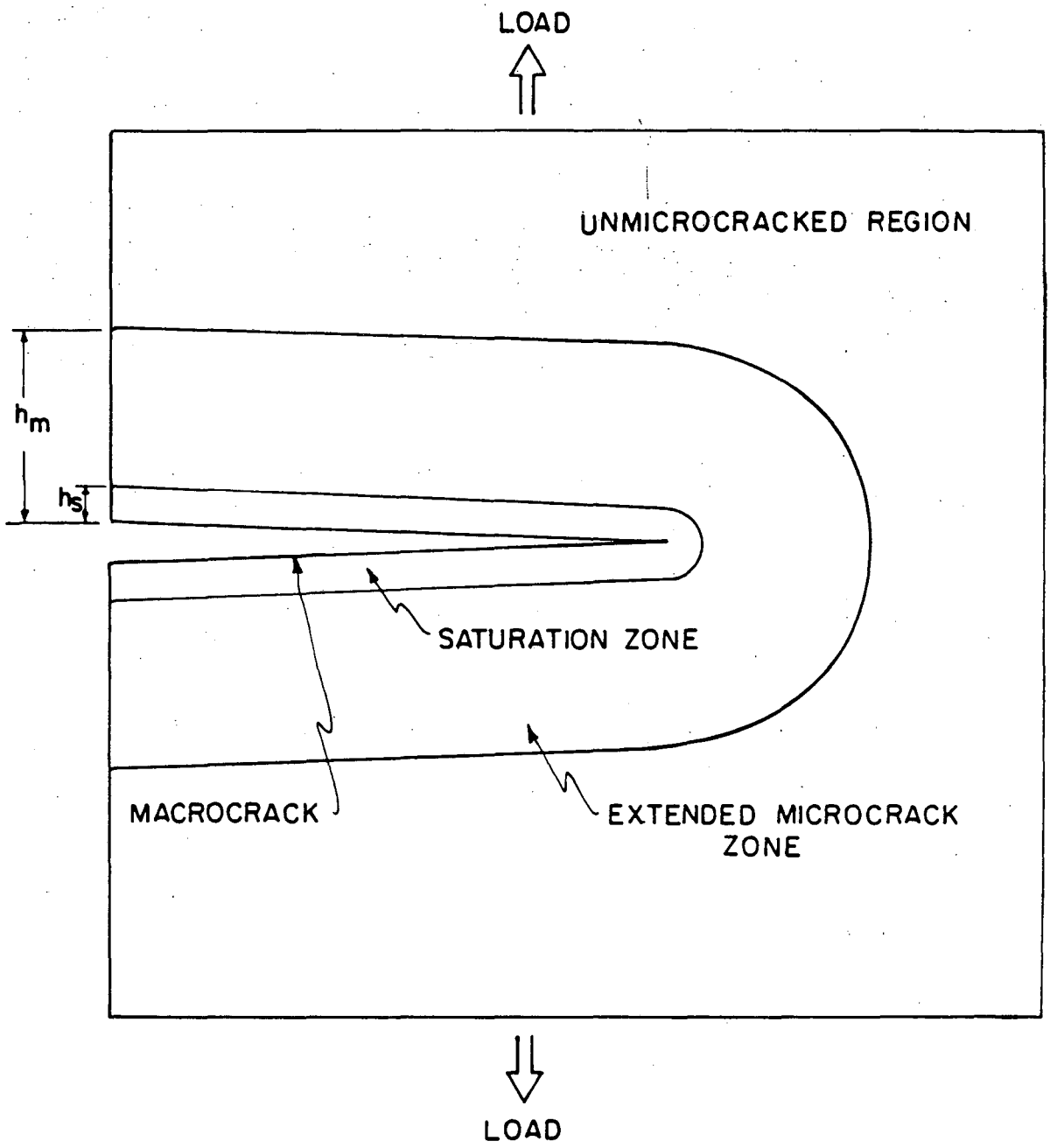

XBL 839-6350

Fig.6.7a

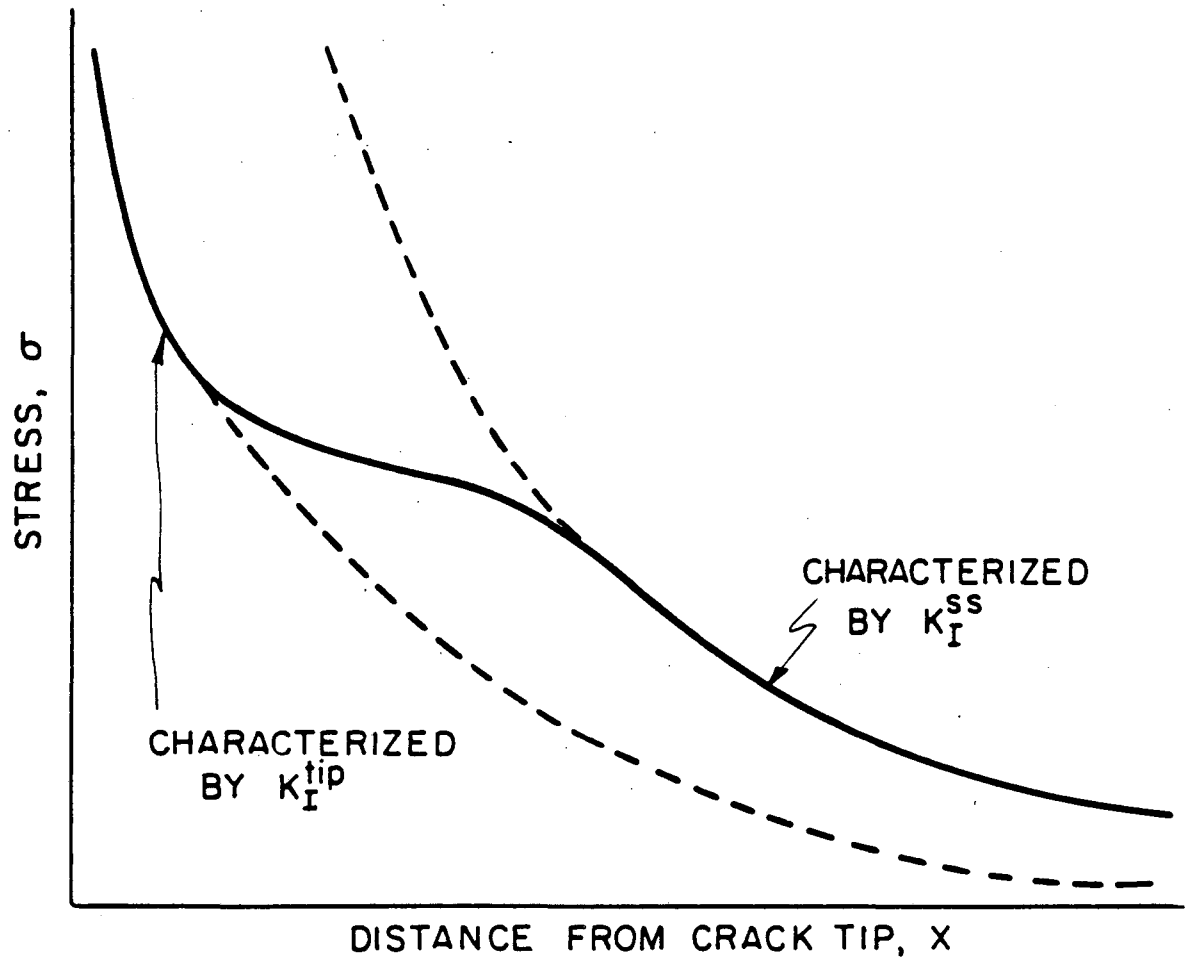
STRESS, σ
CHARACTERIZED BY K_I^{ss}
CHARACTERIZED BY K_I^{tip}
DISTANCE FROM CRACK TIP, X
XBL 839-6345

Fig.6.7b

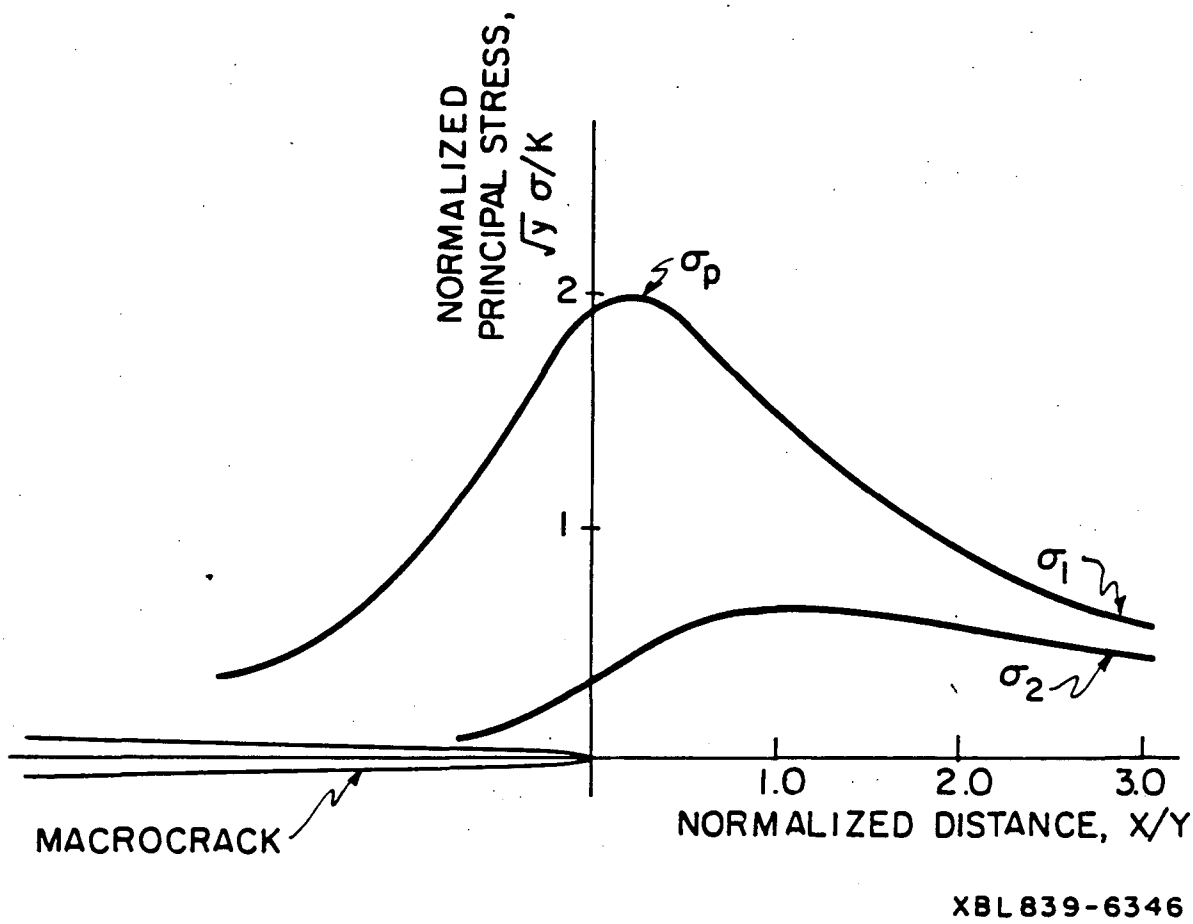
NORMALIZED PRINCIPAL STRESS, $\sqrt{y}\,\sigma/K$
2
1
σ_p
σ_1
σ_2
MACROCRACK
1.0
2.0
3.0
NORMALIZED DISTANCE, X/Y
XBL839-6346

Fig.6.8

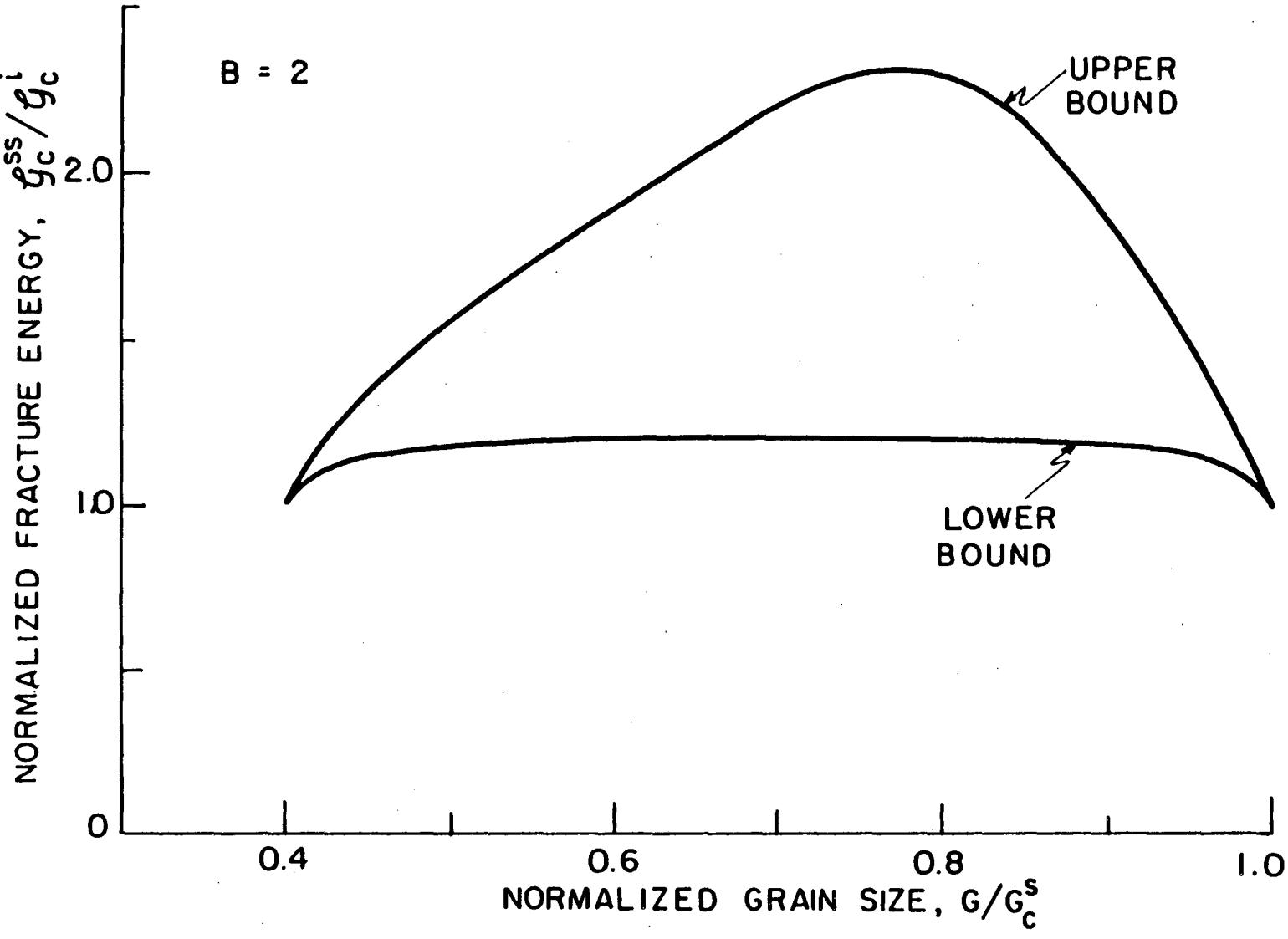
B = 2
UPPER BOUND
LOWER BOUND
NORMALIZED FRACTURE ENERGY, $\mathcal{G}_c^{ss}/\mathcal{G}_c^i$
2.0
1.0
0
0.4
0.6
0.8
1.0
NORMALIZED GRAIN SIZE, G/G_c^s
XBL 839-6347

Fig.6.9

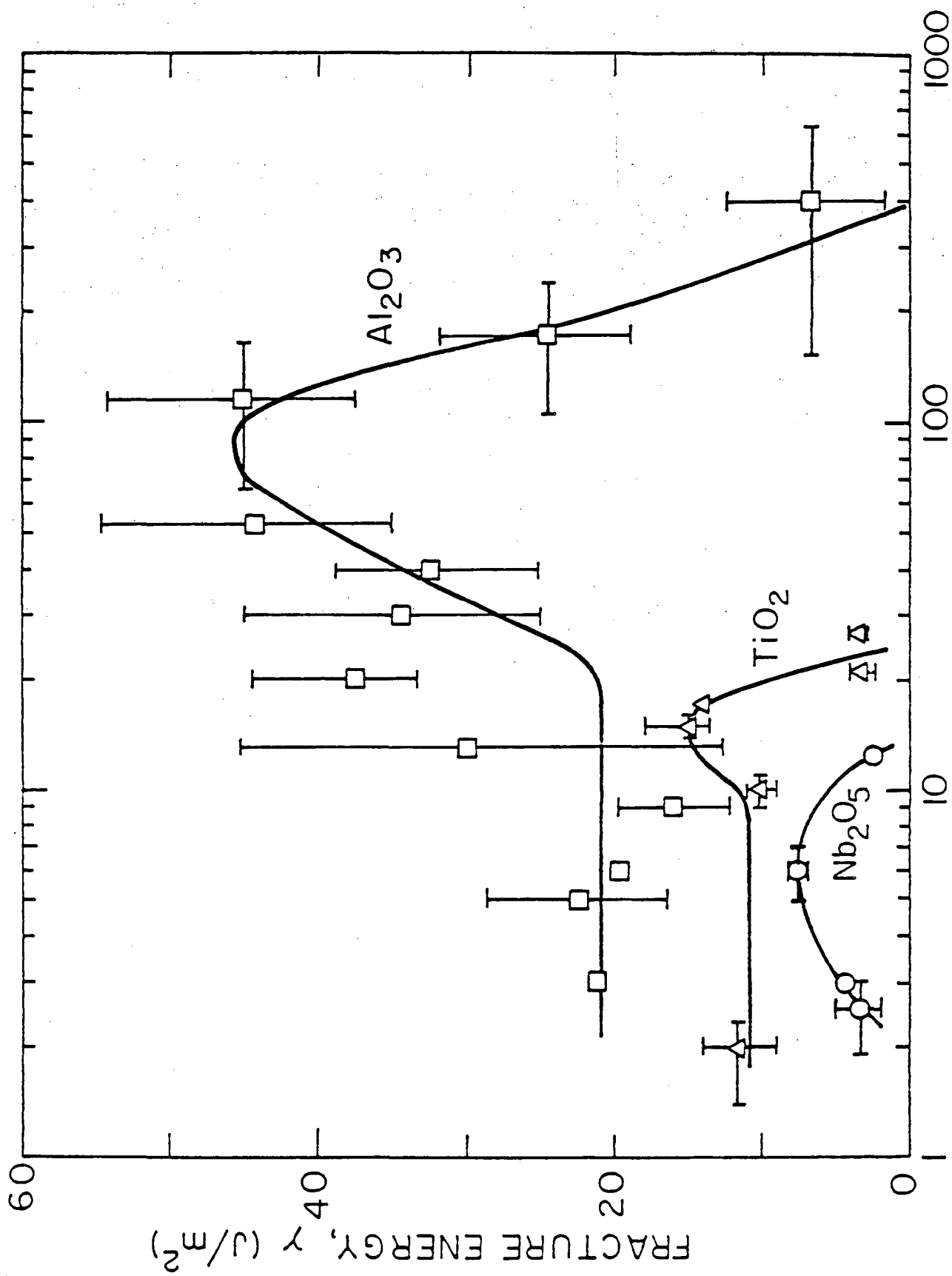

XBL8111-6951

Fig.6.11

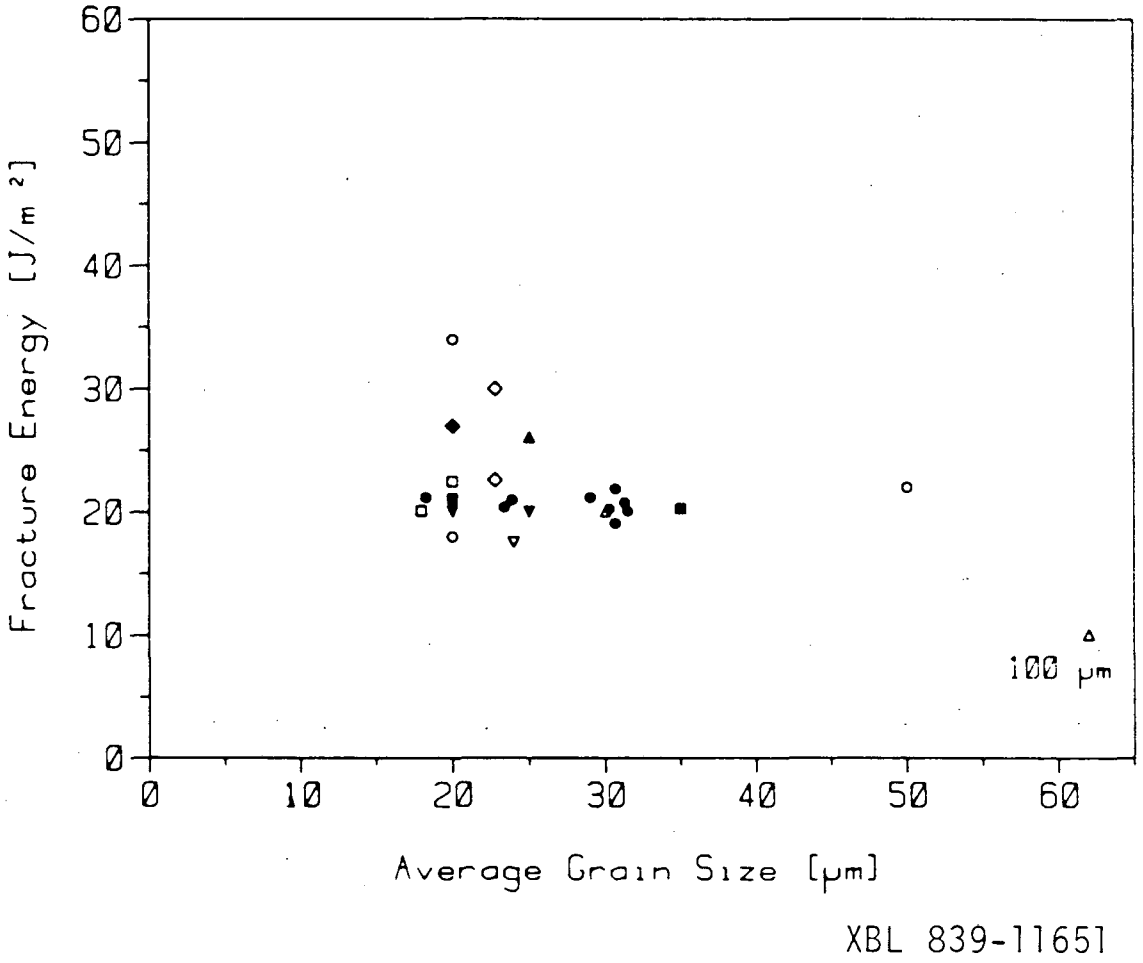

XBL 839-11651

Fig.6.10

7. Conclusion

Whereas specific results, implications relevent to the topic of each section have been presented in separate discussions, the general conclusions pertinent to the primary topic of this work are:

1) A continuum mechanics description of the microcrack toughening process can be constructed. The constitutive behavior of the microcrack zone is based on the overall strain response of a microcracking medium subject to a uniform stress field.

2) A generalized microcracking criterion has be constructed for microcracking at facets subject to general stresses.

3) The effective microcrack density causing elastic moduli decrease is larger than calculated based on a two-dimensional analysis and other simplifications.

4) Induced microcracking is initiated at a threshold load. Above the threshold, the stress/strain behavior becomes nonlinear. During unloading, linearity resumes and a hysteresis is present corresponding to dissipation of strain energy.

5) The stress/strain characteristics resemble those of hardening materials and mertensitic transformation composites. Hence, similarities in process zone toughening effects are also expected.

6) There is a grain size threshold, $R=0.4R_c^s$ for the onset of microcrack zone formation, deriving from the microstructural requirements for nucleating discrete microcracks. At $R=0.4R_c^s$, the microcrack zone coincides with the saturation zone and no toughening is observable.

7) The fracture energy of a microcracking material is described by an R-curve, which derives from the gradual unloading of the microcrack

zone wake irreversible to the loading stage such that additional strain energies are dissipated in the hysteresis.

8) At the initiation stage of crack propagation, the toughening effect originates from the nonlinear strain response of the frontal microcrack zone, counteracted by an detoughening effect due to induced microcracks adjacent to the macrocrack tip. The overall toughening effect is quite small.

9) At the steady-state of crack propagation, additional toughening derives from the extened microcrack zone wake. At $R=R_c^s$, spontaneous microcracking initiates, the hysteresis is greatly reduced no appreciable toughening is observable.

10) Characteristics of the grain size dependence of the fracture energy limited in a certain region in the R-curve can vary significantly. At initiation stage, no grain size dependence is observable. At steady-state, a pronounced toughness enhancement may be observed between $0.4R_c^s$ and R_c^s.

11) Usually, NB tests monitor the fracture energy at initiation cracking stage; whereas DCB tests monitor it at steady-state cracking stage.

This report was done with support from the Department of Energy. Any conclusions or opinions expressed in this report represent solely those of the author(s) and not necessarily those of The Regents of the University of California, the Lawrence Berkeley Laboratory or the Department of Energy.

Reference to a company or product name does not imply approval or recommendation of the product by the University of California or the U.S. Department of Energy to the exclusion of others that may be suitable.

TECHNICAL INFORMATION DEPARTMENT
LAWRENCE BERKELEY LABORATORY
UNIVERSITY OF CALIFORNIA
BERKELEY, CALIFORNIA 94720